Check for updates

The peculiar effect of water on ionic liquids and deep eutectic solvents

Chunyan Ma, [ab] Aatto Laaksonen, [bcde] Chang Liu, [b] Xiaohua Lu [*b] and Xiaoyan Ji [*ab]

Ionic liquids (ILs) and deep eutectic solvents (DESs) have been suggested as eco-friendly alternatives to organic solvents. A trace amount of water is often unavoidable as impurity, and water is also added on purpose to reduce their problematically high viscosity and lower their high price. Understanding the distinct effects of water on the properties of ILs/DESs is highly important. In this review, we collect published experimental and theoretical results for IL/DES–H_2O systems at varied water concentrations and analyze them. Results from mechanistic studies, thermodynamic modelling and advanced experiments are collected and critically discussed. Six commonly studied IL/DES–H_2O systems were selected to map experimental observations onto microscopic results obtained in mechanistic studies. A great variety of distinct contours of the excess properties can be observed over the entire compositional range, indicating that the properties of IL/DES–H_2O systems are highly unpredictable. Mechanistic studies clearly demonstrate that the added H_2O rapidly changes the heterogeneous 3D structures of pure ILs/DESs, leading to very different properties and behaviour. There are similarities between aqueous electrolytes and IL/DES solutions but the bulky and asymmetric organic cations in ILs/DESs do not conform to the standard salt dissolution and hydration concepts. Thermodynamic modelling previously assumes ILs/DESs to be either a neutral ion-pair or completely dissociated ions, neglecting specific ion hydration effects. A new conceptual framework is suggested for thermodynamic modelling of IL/DES–H_2O binary systems to enable new technologies for their practical applications.

[a] Energy Engineering, Division of Energy Science, Luleå University of Technology, Luleå, 971 87, Sweden. E-mail: xiaoyan.ji@ltu.se; Tel: +46-725393298
[b] State Key Laboratory of Material-Oriented Chemical Engineering, Nanjing Tech University, Nanjing, 210009, P. R. China. E-mail: xhlu@njtech.edu.cn
[c] Department of Materials and Environmental Chemistry, Arrhenius Laboratory, Stockholm University, Stockholm, SE-106 91, Sweden
[d] Department of Chemistry-Ångström Laboratory, Uppsala University, Box 538, SE-75121 Uppsala, Sweden
[e] Centre of Advanced Research in Bionanoconjugates and Biopolymers, Petru Poni Institute of Macromolecular Chemistry Aleea Grigore Ghica-Voda, 41A, 700487 Iasi, Romania

Chunyan Ma obtained her MSc degree from Nanjing Tech University. She is currently a PhD candidate at Luleå University of Technology under the supervision of Prof. Xiaoyan Ji and Prof. Xiaohua Lu. Her research focuses on thermodynamic modelling and process simulation for ILs/DESs-based technologies for CO_2 separation.

Chunyan Ma

Aatto Laaksonen is a Professor in Physical Chemistry at Stockholm University; BSc in Mathematics, at Stockholm University; PhD in Physical Chemistry, at Stockholm University 1981. He masters virtually all computer modelling and simulation methods used in materials and bio-sciences. His group has developed many novel methods and computational schemes and in particular, a hierarchical multiscale tool to connect length and time scales from first-principles simulations to the mesoscopic modelling of soft matter and beyond. He has studied IL systems in the last decade. His group has developed unique methods and computational schemes suitable to study ILs under various conditions.

Aatto Laaksonen

This journal is © The Royal Society of Chemistry 2018

Chem. Soc. Rev., 2018, 47, 8685–8720 | 8685

1. Introduction

Even though ionic liquids (ILs) were discovered more than a century ago, it is only over the last several decades that they have become promising alternative replacements to the volatile and hazardous organic solvents. This is due to the unique properties of ILs, which include negligible vapor pressure, high thermal stability, non-flammability, the ability to dissolve both organic and inorganic compounds, and so on.[1,2] Deep eutectic solvents (DESs) are eutectic mixtures of two or more components, and have been identified as either a new class of ILs or IL analogues.[3] DESs share many characteristics and properties with ILs, although these two are different types of solvents based on their molecular structures.[3] Fig. 1 demonstrates that IL is composed primarily of an anion and a cation. In contrast, DES is typically formed with a hydrogen-bond acceptor (HBA), for example a quaternary ammonium halide salt, and a hydrogen-bond
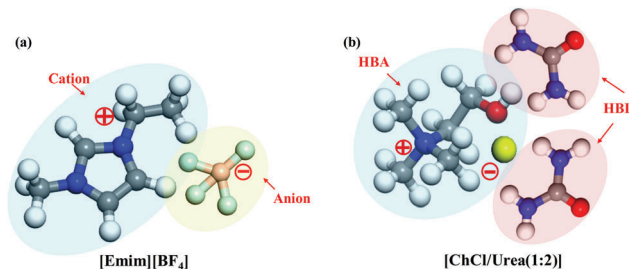

Fig. 1 (a) Typical IL; (b) typical DES.

donor (HBD), which can be a variety of species. It has been suggested that ILs and/or DESs may revolutionize various industrial processes in the future, and much research has been carried out with regard to certain applications. Examples include CO_2 capture and separation,[4–6] lubrication and tribology,[7–9] biomass dissolution[10–16] and absorption heat transformers.[17,18] Herein, we briefly introduce some of these applications.

Blanchard *et al.*[4] first reported the use of ILs as promising absorbents for CO_2 separation in 1999. Since then, developing ILs for CO_2 capture and separation has become an intense research area because of the significant solubility of CO_2 in these solvents and their high selectivity, as well as the low energy demand for solvent regeneration compared with current technologies, such as those based on aqueous amine solutions. Recently, task-specific ILs (TSILs) have been proposed to further increase the CO_2 absorption capacity. The first TSIL was reported by Bates *et al.*[19] A review by Cui *et al.*[20] stresses that the presence of strong CO_2-philic reactive sites is essential for the development of ILs capable of capturing CO_2 from post-combustion flue gases *via* chemisorption. DESs have also been widely developed for CO_2 separation because of their many appealing properties compared with conventional ILs, such as low cost, biodegradability and simple preparation processes.[21] Because both ILs and DESs are highly tunable, it is possible to incorporate CO_2-philic

Dr Chang Liu is a professor in the college of chemical engineering at Nanjing Tech University in China. He received his PhD in Chemical Engineering from Nanjing University of Technology in 2003. His expertise is on material thermodynamics. In the past ten years, he worked on the development of thermodynamic and kinetic model of layered titanate nanomaterials and achieved a large scale preparation of this material. Recently

Chang Liu

his research interest focuses on thermodynamic properties of IL aqueous solutions and its application in CO_2 capture.

Dr Xiaohua Lu is a professor in Chemical Engineering at Nanjing Tech University; PhD in Chemical Engineering at Nanjing University of Chemical Technology 1988. He has been a leader in the development of fundamentally based models and theories of the thermodynamic behavior of complex fluids. In particular, he proposed and developed the concept of the "ion hydration factor" for ionic solutions, which enabled the development of the

Xiaohua Lu

Lu-Maurer model to calculate chemical potential gradients for nonideal, non-equilibrium complex fluids. He also pioneered the extension of non-equilibrium statistical mechanics to interfaces. Up to now, he has published 300+ journal articles.

Dr Xiaoyan Ji is a professor in the division of Energy Science/Energy Engineering at Luleå University of Technology in Sweden. She received her PhD in Chemical Engineering from Nanjing University of Chemical Technology in 2000. Her expertise is on applied thermodynamics focused on fundamental theoretical modelling and experimental measurements for complex fluids with interfaces. Since 2008, the research has been focusing on developing

Xiaoyan Ji

novel IL/DES-based technologies for CO_2 capture and separation. Up to now, as a first author or main contributor, she has published 95+ journal articles and 5 books/book chapters.

8686 | *Chem. Soc. Rev.*, 2018, **47**, 8685–8720

This journal is © The Royal Society of Chemistry 2018
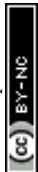
functional groups into these substances to promote their CO_2 absorption capacity, and functionalized ILs have been found to be as efficient as alkanolamine solvents in terms of CO_2 absorption capacity, while being much more energy efficient.[22] In addition, some ILs and DESs exhibit high physisorption capacities.[23] However, the CO_2 absorption rate of ILs/DESs is generally low because of their high viscosities, and the costs associated with the large-scale manufacturing of these substances are still too high.

Using ILs as lubricants was first proposed by Ye et al.[7] in 2001. Since then, ILs have attracted considerable attention in the field of tribology because of their remarkable lubrication and anti-wear properties compared with those of fossil-based and synthetic lubricants.[9] In addition, many new materials (that is, other than metal surfaces) require new types of lubricants, and ILs have been found to be better alternatives for such novel surfaces. Because of their high price, however, ILs are primarily used as additives to conventional lubrication oils at present.[9] The number of publications, including both journal papers and patents, regarding this topic has increased dramatically, even though ILs remain too expensive for industrial applications. In the case of DESs, many reports have noted that their lubrication properties are superior to those of mineral oils.[24,25]

Biomasses are typically dissolved by conventional techniques such as cooking in strong alkaline or acidic solutions, which is both expensive and polluting. In 2002, Rogers and co-workers first reported that cellulose, which is insoluble in water and in most organic solvents, can be dissolved in ILs to form a solution of cellulose at concentrations greater than 10 wt%, providing a new platform for the efficient utilization of this resource (Swatloski et al.[10]). In fact, both ILs and DESs have been shown to be excellent solvents for dissolving and further processing of biomass and cellulose in particular.[11–16] However, again, ILs are expensive and difficult to synthesize on a large scale, making their practical use on an industrial scale difficult at the moment. In contrast, DESs are usually less expensive than ILs and have also been tested as an alternative solvent for the extraction of cellulose from biomass and for further processing to generate fuels or plastic substitutes.[12–15] The use of either ILs or DESs is expected to provide environmentally sustainable chemical processes giving biodegradable products; however, their high cost remains an obstacle to practical applications.

ILs can also be used as absorbents when combined with H_2O to formulate new working pairs that may replace currently-used working fluids, such as lithium bromide–H_2O or ammonia–H_2O, in absorption cycles meant to recover waste heat and utilize low-grade energy.[17,18,26,27] Since Kim et al.[26] proposed working pairs composed of imidazolium-based ILs in 2004, much research has been carried out to identify new IL–H_2O working pairs. As such, developing novel and suitable ILs has lately become one of the most active research topics in the field of cooling technology.[17,18,27] DESs have also been assessed for use in absorption refrigeration systems in combination with the widely used hydrofluorocarbon refrigerant R134a to develop more energy-efficient refrigeration (or heat pump) systems.[28]

Although emerging ILs/DESs-based technologies are promising in many applications, the drawbacks of high cost and/or high viscosity are still impediments to further development and implementation.[29,30] Adding suitable co-solvents has been proposed as one of the most promising options to developing IL/DES-based processes. Among the potential co-solvents, H_2O is both environmentally friendly and has low viscosity. H_2O is also a common impurity in various CO_2-enriched gas streams, and has been used as a physical absorbent for the removal of CO_2 from biogas during biogas upgrading.[31] H_2O is also an important component of biomass. Additionally, in tribology, H_2O can serve as a lubricant with very low friction, while, in absorption cycles, H_2O is frequently used as one component in working pairs.[17] The addition of H_2O could, therefore, be a viable approach to developing IL/DES-based technologies for practical applications.[32] For this reason, it is crucial to study the properties of IL/DES–H_2O systems.

The addition of H_2O can drastically alter the properties of ILs/DESs, as can be seen from the large amount of experimental data reported for such systems. As an example, the viscosities of ILs/DESs can be decreased significantly by the addition of only a trace amount of water.[33] The mixing of water with ILs/DESs can be either endothermic, exothermic or both, depending on the water content.[34] In addition, the excess volume can be either positive, negative or both, thus generating an S-shaped curve.[35] It is, therefore, evident that mixture of H_2O and ILs/DESs can be very different from ordinary binary solvent mixtures. ILs are molten salts and thus similar to electrolytes, but are still liquids over a wide range of temperatures below 373 K. DESs also contain cations and anions,[25] and so again are similar to electrolytes, although they are more complex because they contain at least one additional neutral compound. The electrical conductivity of IL/DES–H_2O systems generally shows a maximum value at a relatively low IL/DES concentration.[36] All these observations imply that IL/DES–H_2O systems are unique compared with either organic solvent mixtures or aqueous electrolyte solutions. However, no attempts have been made to systematically assess the extent to which these systems differ from binary solvent mixtures or aqueous electrolyte solutions by comprehensively summarizing the available literature.

It has been pointed out that it would be desirable to develop theoretical models to describe the properties of IL/DES–H_2O systems. It should be possible to determine empirical correlations based on experimental work and the corresponding results from high-quality computational studies. Such work could lead to the development of empirical models describing, for example, densities and viscosities at various temperatures and concentrations. However, interestingly, we have found no attempts to summarize and rationalize the available experimental results as a means of obtaining new insights into mechanistic studies and, ultimately, devising predictive models.

Mechanistic studies of IL/DES–H_2O systems on the microscopic level are crucial to gaining an understanding of the effects of adding H_2O to ILs/DESs. Such studies are also important in terms of further developing an appropriate model that describes and predicts the properties of such systems over

the entire compositional range from a pure IL/DES to an infinitely dilute IL/DES solution. To study the mechanisms of IL/DES–H$_2$O systems, both molecular simulations and advanced experiments have been conducted for more than a decade, the majority of which have examined imidazolium-based ILs.[37,38]

Several review articles have been published focusing on the importance of ILs/DESs to future process development in the field of chemical engineering as well as their industrial and environmental significance. Although DESs and ILs are two different types of solvents considering their molecular structures, their thermophysical properties are similar. Nearly all of these concentrate on the properties and applications of pure ILs,[1,2,39–52] and DESs are usually not included. There have been some reviews only regarding pure DESs.[3,53–61] For IL/DES–H$_2$O systems, only a handful of reviews have been published with the focus on a single property and/or only a limited number of ILs.[35,48,62] Tariq et al.[62] discussed the surface tension of ILs and IL solutions, with regard to the effects of temperature, the addition of water or other impurities, and the IL structure on the surface tension. Bahadur et al.[35] assessed the excess molar volumes of binary IL–H$_2$O mixtures, using approximately 50 ILs. Podgorsek et al.[48] focused on the mixing enthalpies of binary mixtures containing ILs and proposed that thermodynamic quantities of mixing could provide valuable insights into molecular interactions and microscopic structures in such mixtures. However, summarizing the research work on both experimental observations and mechanistic studies of various types of IL/DES–H$_2$O systems is virtually nonexistent.

The purpose of the present review is to summarize the state-of-the-art research of IL/DES–H$_2$O systems. This review covers both experimental and mechanistic studies concerning various types of ILs/DESs to present a broad picture of the present body of knowledge. The experimental data for IL/DES–H$_2$O systems, primarily consisting of density, viscosity, electrical conductivity and excess/mixing enthalpy values, is surveyed and analyzed. In addition, mechanistic studies of IL/DES–H$_2$O systems using molecular simulations, quantum-chemical calculations or thermodynamic analysis are addressed, and relationships between the experimental data on the macroscopic properties and mechanistic phenomena on the microscopic molecular structure are discussed. The properties and mechanisms of various IL/DES–H$_2$O systems are compared with one another as well as with those of common aqueous electrolyte solutions. Furthermore, current developments in theoretical modelling are discussed. Finally, a framework for developing new theoretical models is proposed to study the macroscopic properties and phase equilibria for IL/DES–H$_2$O systems, as a means of developing practical applications in clean process technologies and designing new eco-friendly solvents.

2. A survey of experimental data for IL/DES–H$_2$O systems

Considering the increasing technological and scientific importance of IL/DES–H$_2$O systems, much research and development work has been carried out during recent years, as reflected in the steadily increasing number of publications. The density, viscosity, electrical conductivity, excess/mixing enthalpy, surface tension and interfacial tension of IL/DES–H$_2$O systems have all been extensively studied experimentally. In this section, we report and discuss the available data regarding the physicochemical properties for a wide variety of such systems.

2.1 Density ρ

Density is one of the fundamental properties and often plays a key role in understanding the behaviour of ILs/DESs in the presence of water. It is easy to measure so that extensive amounts of experimental data can be found in the literature on the IL/DES–H$_2$O systems. Mostly, the densities ρ and the excess molar volumes V^E are reported simultaneously to analyze the mixing of ILs/DESs and H$_2$O. The V^E is calculated from the density according to the following equation:

$$V^E = \frac{x_1 M_1 + x_2 M_2}{\rho_{mix}} - \frac{x_1 M_1}{\rho_1^*} - \frac{x_2 M_2}{\rho_2^*} \tag{1}$$

where x_1 and x_2 are the mole fractions, M_1 and M_2 are the molecular weights, and ρ_1^*, ρ_2^* and ρ_{mix} are the densities of component 1, component 2 and their mixture, respectively.

In total, 700+ articles have been published until August 2018 reporting the density of IL/DES–H$_2$O binary systems based on the databases including Scopus, Web of science and the database on ionic liquid properties (NIST Standard Reference Database no. 147, or so-called IL Thermo v2.0). Some of the reported results cover the densities in a wide compositional range or even the whole compositional range of IL/DES–H$_2$O systems, and some results focus on an infinitely dilute IL/DES solution[63,64] or an IL/DES with a trace amount of water.[65–67] The studied ILs cover both conventional ILs and TSILs. To the best of our knowledge, only one review article has been published summarizing the excess molar volumes V^E of about 50 ILs.[35] In this work, the experimental results for both the ILs and DESs (excluding those have been summarized in the review by Bahadur et al.[35]) are collected in Table 1. Also, it should be mentioned that the information on the data over the infinitely dilute IL/DES solutions or the IL/DES with a trace amount of water is excluded in Table 1.

The characteristic features of V^E within the whole compositional range (i.e. from 0 to 1) can be very different for different ILs/DESs. According to the reported experimental data from literatures, the V^E plotted against the mole fraction for an IL/DES–H$_2$O binary mixture can be positive,[68] negative,[69] or both,[70] and the shapes of the curves (V^E–x) can display a single hump,[69,71] positive double humps,[72] negative double humps[73] or be sinusoidal (S-shape)[70,74] as shown in Fig. 2.

Further analysis of the available experimental data shows that most of the densities were measured at atmospheric pressure. The magnitude, sign and shape of V^E depend on the anion, cation and other physical parameters such as temperature. In general, the values of V^E increase with increasing temperature for the studied systems, that is, with the increase of temperature, the absolute value of V^E decreases when V^E is negative, whereas it increases when V^E is positive. However, for the ammonium-based ILs,

8688 | Chem. Soc. Rev., 2018, 47, 8685–8720

This journal is © The Royal Society of Chemistry 2018

Table 1 Excess molar volumes V^E of IL/DES−H_2O binary systems

At atmospheric pressure

ILs & DESs	T/K	Shape^a (V^E–$x_{IL/DES}$)	V^E/cm^3 mol^{-1} at $x_{IL/DES}$ = extreme position	$(\partial|V^E|/\partial T)_{P,x}$/ range ($x_{IL/DES}$)	Ref.
DESs					
ChCl/urea (1:2)	298.15–333.15	u	[−0.20, −0.12] at $x_{DES} \sim 0.3$	<0/(0–1)	71
ChCl/urea (1:2)	293.15–363.15	u	[−0.16, −0.11] at $x_{DES} \sim 0.3$	<0/(0–1)	78
ChCl/urea (1:2)	303.15	—	—	(0–1)	79
ChCl/urea (1:2)	293.15–323.15	u	[−0.18, −0.15] at $x_{DES} \sim 0.3$	<0/(0–1)	80
ChCl/TG (1:2)	303.15–353.15	u	[−0.90, −0.70] at $x_{DES} \sim 0.3$	<0/(0–1)	73
ChCl/Gluc (2:1)	303.15–353.15	w	[−0.75, −0.70] at $x_{DES} \sim 0.7$; [−0.60, −0.58] at $x_{DES} \sim 0.3$	<0/(0–1)	73
ChCl/EG (1:2)	283.15–363.15	u	[−0.33, −0.25] at $x_{DES} \sim 0.4$	<0/(0–1)	81
ChCl/EG (1:2)	298.15–333.15	u	[−0.33, −0.25] at $x_{DES} \sim 0.4$	<0/(0–1)	82
ChCl/EG (1:2)	303.15–323.15	—	—	—	83
ChCl/EG (1:2)	303.15–313.15	—	—	(0.17–1)	84
ChCl/MA (1:1)	303.15–313.15	—	—	(0.13–1)	84
ChCl/MA (1:2)	283.15–363.15	u	—	<0/(0–1)	81
ChCl/MA (1:2)	303.15–323.15	—	—	—	83
ChCl/Gly (1:2)	283.15–363.15	u	[−0.35, −0.30] at $x_{DES} \sim 0.35$	<0/(0–1)	85
ChCl/Gly (1:2)	298.15–333.15	u	[−0.35, −0.30] at $x_{DES} \sim 0.4$	<0/(0–1)	82
ChCl/Gly (1:2)	303.15–313.15	—	—	(0.19–1)	84
ChCl/Gly (1:2)	283.15–343.15	u	[−0.4, −0.30] at $x_{DES} \sim 0.4$	<0/(0–1)	86
ChCl/LA (1:2)	298.15–363.15	—	—	(0.68–1)	87
CrCl$_3$/ChCl (1:2.5)	298.15–353.15	—	—	(0.053–0.143)	88
CrCl$_3$/ChCl (1:2)	298.15–353.15	—	—	(0.053–0.143)	89
DEAC/Gly (1:2)	298.15–343.15	u	[−0.45, −0.40] at $x_{DES} \sim 0.4$	<0/(0–1)	90
DEAC/EG (1:2)	298.15–343.15	u	[−0.54, −0.45] at $x_{DES} \sim 0.4$	<0/(0–1)	90
ATPPB/DEG (1:4)	293.15–343.15	w	[−0.72, −0.44] at $x_{DES} \sim 0.25$	<0/(0–1)	91
ATPPB/DEG (1:10)	293.15–343.15	u	[−0.66, −0.44] at $x_{DES} \sim 0.3$	<0/(0–1)	91
ATPPB/DEG (1:16)	293.15–343.15	u	[−0.74, −0.53] at $x_{DES} \sim 0.3$	<0/(0–1)	91
Imidazolium-based ILs					
[C$_4$C$_2$im][Br]	293.15–323.15	u	[−0.6, −0.5] at $x_{IL} \sim 0.4$–0.5	<0/(0–1)	92
[Mmim][DMP]	298.15	—	—	(0.252–1)	93
[Mmim][MeSO$_4$]	298.15–328.15	s	[−0.11, −0.047] at $x_{IL} \sim 0.4$–0.5; [0.07, 0.122] at $x_{IL} \sim 0.05$	<0/(0.32–1); >0/(0–0.32)	94
[Emim][BuSO$_4$]	288–318	u	[−0.42, −0.23] at $x_{IL} \sim 0.3$–0.4	<0/(0–1)	95
[Emim][HexSO$_4$]	288–318	u/s	[−0.16, −0.087] at $x_{IL} \sim 0.58$; [0.028, 0.042] at $x_{IL} \sim 0.93$	<0/(0–0.85); >0/(0.85–0.1)	95
[Emim][OcSO$_4$]	298–318	u/s	[−0.11, −0.10] at $x_{IL} \sim 0.39$–0.74; 0.045 at $x_{IL} \sim 0.1$	<0/(0–1); —	95
[Emim][TFA]	278.15–348.15	u	[−0.76, −0.3] at $x_{IL} \sim 0.25$–0.35	<0/(0–1)	96
[Emim][TCM]	298.15	s	$x_{IL} \sim 0.45$; $x_{IL} \sim 0.013$	>0/(0–0.05); <0/(0.05–1)	97
[Emim][Ac]	298.15–343.15	u	[−1.57, −1.49] at $x_{IL} \sim 0.39$	<0/(0–1)	98
[Emim][Ac]	293.15–353.15	—	—	(0.347–0.705)	99
[Emim][Ac]	298.15–353.15	u	—	(0.665–0.955)	33
[Emim][DCA]	298.15–343.15	m	[0.21, 0.41] at $x_{IL} \sim 0.46$; [0.18, 0.43] at $x_{IL} \sim 0.26$	>0/(0–1)	98
[Emim][L-lactate]	298.15	n	1.3 at $x_{IL} \sim 0.5$	—	100
[Emim][Glyci]	300	u	−2.6 at $x_{IL} \sim 0.2$	(0–1)	101
[Emim][DMP]	293.15–333.15	u	[−1.6, −1.5] at $x_{IL} \sim 0.3$–0.4	(0–1)	102
[Emim][Et$_2$PO$_4$]	293.15–373.15	u	[−1.75, −1.3] at $x_{IL} \sim 0.24$	(0–1)	103
[Bmim][DMP]	293.15–333.15	u	[−1.4, −1.17] at $x_{IL} \sim 0.3$	<0/(0–1)	102
[Bmim][L-lactate]	298.15–318.15	n	[0.72, 1.1] at $x_{IL} \sim 0.40$	<0/(0–1)	104
[HDBU][IM]	293.15–313.15	u	[−1.61, −1.50] at $x_{IL} \sim 0.3$	<0/(0–1)	105
[BDBU][IM]	293.15–313.15	u	[−1.36, −1.21] at $x_{IL} \sim 0.3$	<0/(0–1)	105
[TMG][IM]	293.15–313.15	u	[−1.5, −1.4] at $x_{IL} \sim 0.3$	<0/(0–1)	106
[Amim][Cl]	298.15	—	—	(0–1)	107
[Amim][Cl]	298.15–353.15	u	—	(0.665–0.955)	33
Pyrrolidinium-based ILs					
[Pyrr][HCOO]	298.15	u	−0.5 at $x_{IL} \sim 0.19$	—	68
[Pyrr][NO$_3$]	298.15–333.15	n	[2.33, 2.48] at $x_{IL} \sim 0.12$	>0/(0.4–1)	68
[Pyrr][HSO$_4$]	298.15	n	3.90 at $x_{IL} \sim 0.096$	—	68
[Empyr][EtSO$_4$]	298.15–343.15	s	[−0.42, −0.08] at $x_{IL} \sim 0.4$; [0.033, 0.40] at $x_{IL} \sim 0.89$	<0/(0–0.4); >0/(0.4–1)	108
[Epmpyr][Cl]	293.15–313.15	u	[−1.1, −0.70] at $x_{IL} \sim 0.4$	<0/(0–1)	109
[Epmpyr][Ac]	288–313.15	u	[−1.15, −1.0] at $x_{IL} \sim 0.3$	<0/(0–1)	110
[Epmpyr][SAL]	293.15–313.15	u	[−1.3, −0.70] at $x_{IL} \sim 0.3$	<0/(0–1)	111
[Empyr][Glyc]	298.15–348.15	u	[−1.19, −1.0] at $x_{IL} \sim 0.29$–0.35	<0/(0–1)	112

This journal is © The Royal Society of Chemistry 2018

Chem. Soc. Rev., 2018, 47, 8685–8720 | 8689

Table 1 (continued)

At atmospheric pressure

ILs & DESs	T/K	Shape[a] (V^E–$x_{IL/DES}$)	V^E/cm^3 mol^{-1} at $x_{IL/DES}$ = extreme position	$(\partial|V^E|/\partial T)_{P,x}$/ range ($x_{IL/DES}$)	Ref.
[Empyr][Ac]	298.15–348.15	u	[−1.15, −0.97] at $x_{IL} \sim$ 0.32–0.41	<0/(0–1)	112
Piperidinium-based ILs					
[Empip][EtSO$_4$]	298.15–343.15	u	[−0.69, −0.45] at $x_{IL} \sim$ 0.26–0.36	<0/(0–1)	108
Piperazinium-based ILs					
[(OH)$_2$C$_2$pi][EtCOO]	293.15–323.15	—	—	(0–0.12)	36
[MP][Glyci]	300	u	−3 at $x_{IL} \sim$ 0.25	(0–1)	101
Guanidinium-based ILs					
[(C$_2$)$_2$^{2}(C$_1$)^2(C$_1$)$_2$^{3}gu][EtSO$_4$]	293.15–323.15	u	[−0.6, −0.2] at $x_{IL} \sim$ 0.2	<0/(0–1)	113
[TMG][BEN]	298.15	—	—	(0–0.224)	114
[TMG][SAL]	298.15	—	—	(0–0.224)	114
[TMG][Lac]	303.15–328.15	u	[−1.2, −1.0] at $x_{IL} \sim$ 0.3	<0/(0–1)	115
Morpholinium-based ILs					
[Emmor][EtSO$_4$]	298.15–343.15	u	[−0.26, −0.12] at $x_{IL} \sim$ 0.32–0.44	<0/(0–1)	108
[Emmor][Ac]	298.15–348.15	u	[−1.1, −1.0] at $x_{IL} \sim$ 0.3	<0/(0–1)	116
[Emmor][Pro]	298.15–348.15	u	[−1.2, −1.0] at $x_{IL} \sim$ 0.3	<0/(0–1)	116
[Emmor][Glyc]	298.15–348.15	u	[−0.86, −0.66] at $x_{IL} \sim$ 0.29	<0/(0–1)	112
Collidinium-based ILs					
[Col][HCOO]	298.15	u	−2.8 at $x_{IL} \sim$ 0.3	—	68
Cholinium-based ILs					
[Cho][Lac]	293.15	u	−1.2 at $x_{IL} \sim$ 0.25	—	117
[Cho][Prop]	293.15	u	−1.28 at $x_{IL} \sim$ 0.25	—	117
[Cho][Mal]	293.15	u	−0.8 at $x_{IL} \sim$ 0.2	—	117
[Cho][Glyci]	300	u	−2.3 at $x_{IL} \sim$ 0.25	(0–1)	101
Ammonium-based ILs					
TMEAC	293.15–323.15	w	[−0.75, −0.35] at $x_{IL} \sim$ 0.16; [−0.50, −0.10] at $x_{IL} \sim$ 0.02–0.46	>0/(0–1)	118
[DEMA][MeSO$_3$]	293.15–353.15	—	—	(0.347–0.705)	99
[DEMA][OTf]	293.15–353.15	—	—	(0–0.964)	119
PAF	293.15–333.15	u	[−1.34, −1.26] at $x_{IL} \sim$ 0.4	<0/(0–1)	120
3HPAF	293.15–333.15	s	[−0.48, −0.42] at $x_{IL} \sim$ 0.19; [1.20, 1.38] at $x_{IL} \sim$ 0.91	<0/(0–0.4); >0/(0.4–1)	120
3HPATFAc	293.15–333.15	u	[−7.0, −6.86] at $x_{IL} \sim$ 0.8	>0/(0–1)	120
PAAc	293.15–333.15	u	[−1.69, −1.67] at $x_{IL} \sim$ 0.5	<0/(0–1)	120
3HPAAc	293.15–333.15	u	[−1.18, −1.13] at $x_{IL} \sim$ 0.3	<0/(0–1)	120
[PN][NO$_3$]	298.15	u	−0.6 at $x_{IL} \sim$ 0.3	—	69
2-HEAB	298.15/323.15	u	−1.2 at $x_{IL} \sim$ 0.22	—	121
2-HEAP	298.15/323.15	u	−1.1 at $x_{IL} \sim$ 0.30	—	121
2-HEAH	298.15/323.15	u	$x_{IL} \sim$ 0.29	—	121
2-HDEAH	298.15/323.15	u	$x_{IL} \sim$ 0.18	—	121
[DIPEA][HCOO]	298.15	u	−0.80 at $x_{IL} \sim$ 0.37	—	68
M2HEAPr	293.15–343.15	u	[−1.23, −1.20] at $x_{IL} \sim$ 0.4	>0/(0–1)	122
BHEAC	303.15–353.15	u	[−1.23, −1.20] at $x_{IL} \sim$ 0.32	<0, T < 333.15; >0, T < 333.15/(0–1)	123
[CyN$_{1,1}$PrSO$_3$H][Tos]	303.15–328.15				124
Phosphonium-based ILs					
[aP$_{4443}$][Ala]	298.15–343.15		—	(0.25–1)	125
[aP$_{4443}$][Val]	298.15–343.15		—	(0.25–1)	125
[aP$_{4443}$][Leu]	298.15–343.15		—	(0.25–1)	125
[P$_{2444}$][DEP]	298.15–348.15		[−0.781, −1.17] at $x_{IL} \sim$ 0.2	<0/(0–1)	126

At elevated pressures

DESs	T/K, P/MPa	Shape (V^E–$x_{IL/DES}$)	x_{DES} = extreme position	$(\partial|V^E|/\partial P)_{T,x}$/range ($x_{DES}$)	Ref.
ChCl/EG (1:2)	298.15–323.15, 0.1–50	u	[−0.34, −0.24] at $x_{DES} \sim$ 0.4	<0/(0–1)	76
ChCl/urea (1:2)	298.15–323.15, 0.1–50	u	[−0.16, −0.08] at $x_{DES} \sim$ 0.3	<0/(0–1)	75
ChCl/Gly (1:2)	298.15–323.15, 0.1–50	u	[−0.33, −0.24] at $x_{DES} \sim$ 0.4	<0/(0–1)	77

[a] 'u': negative single hump, 'n': positive single hump, 'm': double hump, 'w': negative double hump, and 's': sinusoidal or S-shape.
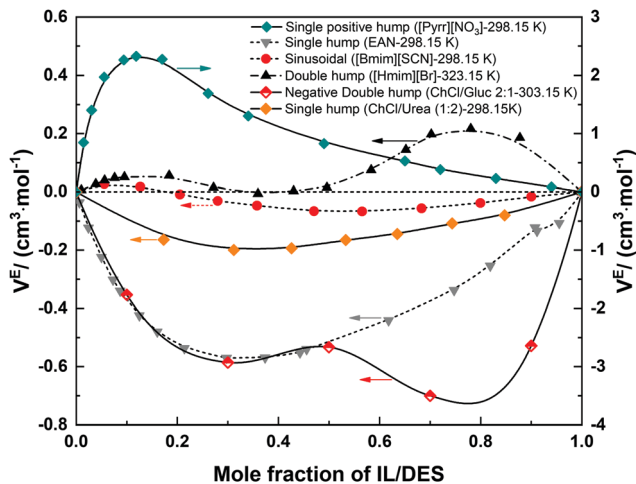
8690 | Chem. Soc. Rev., 2018, 47, 8685–8720

This journal is © The Royal Society of Chemistry 2018

Fig. 2 The V^E–$x_{IL/DES}$ curves.

the temperature only exhibits a weak effect on the overall V^E, and the value of V^E for some ammonium-based ILs, *e.g.* TMEAC, becomes more negative with the increase of temperature, which is opposite to most conventional ILs. By increasing the alkyl chain length of cation, V^E also increases for the ILs with the same anion for all the studied systems. The type of the alkyl group attached to the cation only shows a slight effect on V^E, whereas when the alkyl group is replaced with a polar or hydrophilic group, a more significant effect can be observed.[35] The anion is dominant in determining the magnitude, shape and sign of V^E–x_{IL} based on the reported experimental data for the ILs with the cations being imidazolium, pyridinium, pyrrolidinium, piperidinium and ammonium.[35] The ILs with the anion with many oxygen atoms result in negative V^E values. The absolute value of V^E for the ammonium-based ILs is much greater compared with those for other ILs. The typical maxima of V^E are smaller than 2 cm^3 mol^{-1}, but there are some exceptions, such as those for [Pyrr][NO$_3$], [Pyrr][HSO$_4$] and 3HPATFAc (Table 1).

Based on the results listed in Table 1, we can see that, for all the studied DESs, the extreme positions of V^E–x_{DES} are almost the same. Their values of V^E are always negative, and the absolute value decreases with increasing temperature ($(\partial|V^E|/\partial T)_{P,x} < 0$). Over the entire compositional range, it can be divided into two regions: the H$_2$O-rich ($x_{DES} < 0.5$) and DES-rich ($x_{DES} > 0.5$) regions. Almost for all the studied DESs, there is an extreme point near the H$_2$O-rich region.

Only very few research groups have investigated the volumetric properties (density or molar volume) at high pressures, and all of them are for DESs. For example, Leron *et al.*[75–77] reported the volumetric properties of dry/aqueous DESs at pressures up to 50 MPa. From the results, we can find that pressure has a more significant influence on the magnitude of V^E than temperature for the studied DESs, and the magnitude of V^E increases with increasing pressure.

2.2 Viscosity η

Viscosity η (*i.e.* dynamic viscosity, also known as absolute viscosity) is an important transport property as it is directly

related to the mass transfer rate.[127] Among the factors affecting viscosity, temperature is an important one, and viscosity should be always given at the measured (or calculated) temperature to make any sense. For most fluids, the viscosity can vary nonlinearly many orders of magnitude with changes in temperature. The explanation on the molecular level to the decrease of viscosity with increasing temperature in a fluid is that: the temperature of a substance is directly proportional to the average velocity of the molecules consisting the substance, and the molecules require more free space around them when their velocities increase. As a result, the fluid density decreases, and the intermolecular interactions become weaker due to the increase of mutual distances between the molecules.

Concerning the viscosities of ILs, we should remember that ILs are often complicate to synthesize, and their purities can be rather poor even for the commercially purchased samples. For most ILs/DESs, the most serious problem is that they are hygroscopic and absorb moisture as soon as they are exposed to atmosphere in the experiments with a variety of viscometers. This problem has been recently highlighted by Diogo *et al.*[128] Significantly different experimental values for viscosities were reported for the same pure IL/DES from different laboratories,[71,78] in fact, deviating much more than the reported experimental uncertainties. These large discrepancies imply not only the difficulty in measuring the viscosity of ILs/DESs accurately but also the special nature of ILs/DESs.

The relatively high viscosity of ILs/DESs generally results in the difficulty in their practical applications for different industrial processes, especially in those with traditional mass transfer units. The addition of H$_2$O can change the viscosity significantly, sometimes, even with orders of magnitude. To further illustrate the effect of water on the viscosity, excess viscosity η^E (*i.e.* viscosity deviation $\Delta\eta$) or excess logarithm viscosity $(\ln\eta)^E$ can be calculated from the measured experimental data of viscosity.[78,85] η^E, $\Delta\eta$, and $(\ln\eta)^E$ are calculated as following:

$$\eta^E = \Delta\eta = \eta_{mix} - x_1\eta_1{}^* - x_2\eta_2{}^*$$
$$(\ln\eta)^E = \ln\eta_{mix} - x_1\ln\eta_1{}^* - x_2\ln\eta_2{}^* \qquad (2)$$

where $\eta_1{}^*$, $\eta_2{}^*$ and η_{mix} are the viscosities of component 1, component 2 and their mixture, respectively.

Similar to V^E, the magnitude and sign of $\Delta\eta$ or $(\ln\eta)^E$ can be positive, negative, or both, and the shape of the curve ($\Delta\eta$–x or $(\ln\eta)^E$–x) can be single hump or sinusoidal (S-shape),[78,85,129] reflecting the non-ideal behaviour of these binary systems (Fig. 3). The extreme position shows the water content having the largest effect on the transport properties of these systems. Similar to density, the viscosity of IL/DES–H$_2$O is also a subject with extensive research efforts. Until August 2018, more than 550 articles have been published reporting the viscosity of ILs/DESs with H$_2$O. Most of them focus on the effect of water as a trace impurity[130,131] or on the water-saturated ILs/DESs,[65,132] and only around 60 articles studied the viscosity of IL/DES–H$_2$O systems over a wide compositional range even up to the entire compositional range. The reported results show that the
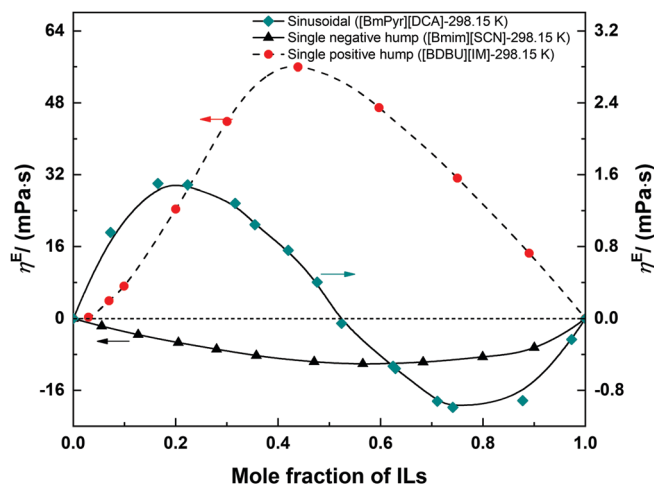
This journal is © The Royal Society of Chemistry 2018

Chem. Soc. Rev., 2018, **47**, 8685–8720 | 8691

Fig. 3 The different shapes of the (η^E–x_{IL}) curves.

presence of H$_2$O in ILs/DESs can decrease the viscosity greatly.[71] No review articles have been published previously to summarize all these experimental viscosity results. In Table 2, we summarize all, up to date, available experimental data on the viscosity of IL/DES–H$_2$O systems over a wide compositional range, the values of $\Delta\eta$ or $(\ln\eta)^E$, the extreme positions and the shapes of the curve ($\Delta\eta$–x or $(\ln\eta)^E$–x), as well as the changes of $\Delta\eta$ or $(\ln\eta)^E$ with temperature, i.e. $(\partial|Y^E|/\partial T)_{P,x}$. Since the viscosity of IL/DES–H$_2$O over a wide compositional range, even up to the entire compositional range, is the main focus here, the effects of possible impurities including a trace amount of water on the viscosity are not included.

All the available data was measured at atmospheric pressure, and no data was found available at the pressure higher than 1 bar. For most of the IL/DES–H$_2$O systems, the shapes of the curves ($\Delta\eta$–x or $(\ln\eta)^E$–x) show a single hump (positive or negative). Only 6 IL/DES–H$_2$O systems with the ILs/DESs of ChCl/urea (1:2), [Emim][Ac], [Bmim][Ac], [Emim][TFA], [Emim][DMP] and [BmPyr][DCA] show sinusoidal or S-shaped curve, and the S-shaped curve for the former 5 ILs/DESs can only be observed in a certain temperature range. $\Delta\eta(\eta^E)$ is more widely used than $(\ln\eta)^E$ for analyzing the viscosity of IL/DES–H$_2$O binary systems. In general, the absolute value of $\Delta\eta$ shown in Table 2 decreases with increasing temperature for the studied ILs/DESs except ChCl/urea (1:2)[78] and [Emim][TFA].[96] Most of the reported data is for the imidazolium-based ILs. From the results listed in Table 2, the excess viscosity is negative for most of the studied ILs/DESs, and the corresponding extreme point is near the IL/DES-rich region ($x_{IL/DES} > 0.5$). This phenomenon implies that the viscosity decreases rapidly in the IL/DES-rich region and thus the presence of water expands the volume of the fluids and favors the diffusion of molecules.

As discussed in the previous section, a trace amount of water for the hygroscopic IL/DES and the other impurities of ILs will significantly affect the viscosity of IL/DES. This is essential for determining a reliable viscosity of pure ILs/DESs or ILs/DESs with a trace amount of water accurately, while such effect is not

so crucial for studying the viscosity of IL/DES–H$_2$O system over the wide/entire compositional range.

2.3 Electrical conductivity Λ

Electrical conductivity Λ is another important transport property, and it provides the information on the mobility of ions or charged molecules in systems. There are mainly two kinds of electrical conductivity data for IL/DES–H$_2$O binary systems. One is the electrical conductivity Λ for the IL/DES–H$_2$O binary systems over a wide compositional range, and the other is that for the dilute IL/DES solution. Analyzing the Λ of the dilute IL/DES solution can reflect the ionic association behaviour in water, i.e. can obtain the ion association constants k_A and provide insight on the specific microstructures. Besides, some investigations on the Λ for the ILs/DESs with a trace amount of water have been conducted,[157] but are excluded in this review. In Table 3, the data of the Λ over the wide compositional range and the reported ion association constants k_A is summarized.

According to the results listed in Table 3, the most studied ILs are imidazolium-based. The electrical conductivity of IL/DES–H$_2$O binary systems shows, in general, a maximum value at a relatively low IL/DES concentration ($x_{IL/DES} \sim 0.03 – 0.1$), which is unique and different when compared with the aqueous solutions with common electrolytes (e.g. NaCl, Na$_2$SO$_4$) or other solvents (e.g. CH$_3$COOH). The further comparison of the electrical conductivity for the IL/DES–H$_2$O binary systems, the aqueous electrolyte (i.e. NaCl, Na$_2$SO$_4$) solutions and the aqueous CH$_3$COOH solution, depicted in Fig. 4, shows that Λ of aqueous electrolyte solutions increases linearly with the increase of solute concentration (i.e. electrolyte) in mole fraction. While for the IL/DES–H$_2$O binary solutions, it initially increases whereas it thereafter decreases with increasing solute concentration (i.e. IL/DES) in mole fraction. Meanwhile, the values of Λ for the IL/DES–H$_2$O binary systems are lower than those for aqueous solutions with strong electrolytes (i.e. NaCl, Na$_2$SO$_4$) but higher than those for aqueous solutions with CH$_3$COOH. This implies that aqueous IL solutions are very different from other aqueous solutions.

For the dilute IL solutions, the ILs with the [Bmim]$^+$ were mostly investigated, and their k_A values in H$_2$O were reported. The values of k_A obtained from different research groups show considerable discrepancies. For example, k_A of [Hmim][Br] from Wang et al.[158] is 71, while that from Shekaari et al.[159] is only 4.9. These discrepancies may be caused by choosing the experimental data in different compositional ranges. Therefore, a reliable and standard method still needs to be developed to obtain reliable k_A values.

Most of the reported k_A values range from 0.014 to 113. There is only one exception for [Bmim][EtCOO] with a negative k_A.[158] The unreasonably negative k_A was obtained when 3 parameters (i.e. k_A, the limiting molar conductivity and the ion distance parameter) were iteratively fitted to a non-linear least square expression without considering the physical meaning of these parameters.

The anions affect the value of k_A greatly. For the ILs with the same cation [Bmim]$^+$, the values of k_A follow the order: [PF$_6$]$^-$ > [BF$_4$]$^-$ > [Br]$^-$ > [Cl]$^-$ > [HCOO]$^-$ > [MeCOO]$^-$ > [EtCOO]$^-$.

8692 | Chem. Soc. Rev., 2018, 47, 8685–8720

This journal is © The Royal Society of Chemistry 2018

Table 2 Excess viscosities $\Delta\eta$ or η^E or $(\ln\eta)^E$ of IL/DES–H$_2$O at atmospheric pressure

ILs & DESs	T/K	Range $(x_{IL/DES})$	$\Delta\eta$ or η^E or $(\ln\eta)^E$ $(\partial\|Y^E\|^b/\partial T)_{P,x}$	Shape^a $(Y^E-x_{IL/DES})/x_{IL/DES} =$ extreme position	Ref.
DESs					
ChCl/urea (1:2)	293.15–323.15	0–1	$\Delta\eta < 0/(\partial\|Y^E\|/\partial T)_{P,x} < 0$	u/x_{DES} = 0.8	80
ChCl/urea (1:2)	298.15–333.15	0–1	$\Delta\eta < 0/(\partial\|Y^E\|/\partial T)_{P,x} < 0$	u/x_{DES} = 0.8	71
ChCl/urea (1:2)	293.15–363.15	0–1	$(\ln\eta)^E < 0/(\partial\|Y^E\|/\partial T)_{P,x} < 0$; $(\ln\eta)^E > 0/(\partial\|Y^E\|/\partial T)_{P,x} > 0$	u/x_{DES} = 0.6 ($T < 343.15$); s/x_{DES} = 0.3 and 0.7 ($T = 343.15$); n/x_{DES} = 0.4 ($T > 343.15$)	78
ChCl/Gly (1:2)	283.15–363.15	0–1	$(\ln\eta)^E > 0/(\partial\|Y^E\|/\partial T)_{P,x} < 0$	n/x_{DES} = 0.4	85
DEAC/Gly (1:2)	298.15–343.15	0–1	—	u/x_{DES} = 0.5	90
DEAC/EG (1:2)	298.15–343.15	0–1	—	u/x_{DES} = 0.3	90
Imidazolium-based ILs					
[Mmim][DMP]	298.15	0.252–1	—	—	93
[Emim][DMP]	298.15–333.15	0–1	$\Delta\eta < 0/(\partial\|Y^E\|/\partial T)_{P,x} < 0$; $\Delta\eta < 0/\Delta\eta > 0$	u/x_{IL} = 0.4 ($T > 298.15$); s/x_{IL} = 0.3 and 0.8 ($T = 298.15$)	102
[Emim][EtSO$_4$]	298.15	0.4–1	$\Delta\eta < 0$	—	133
[Emim][EtSO$_4$]	288.15–343.15	0–1	$\Delta\eta < 0/(\partial\|Y^E\|/\partial T)_{P,x} < 0$	u/x_{IL} = 0.6	134
[Emim][EtSO$_4$]	278.15–348.15	0–1	$\Delta\eta < 0/(\partial\|Y^E\|/\partial T)_{P,x} < 0$	u/x_{IL} = 0.6	96
[Emim][MeSO$_4$]	303.15–343.15	0–1	$\Delta\eta < 0/(\partial\|Y^E\|/\partial T)_{P,x} < 0$	u/x_{IL} = 0.5	135
[Emim][Ac]	298.15	0–1	—	u/x_{IL} = 0.65	136
[Emim][Ac]	298.15–353.15	0.665–0.955	—	—	33
[Emim][Ac]	298.15–343.15	0–1	$\Delta\eta < 0/(\partial\|Y^E\|/\partial T)_{P,x} < 0$	u/x_{IL} = 0.6 ($T \leq 313.15$); w/x_{IL} = 0.2 and 0.9 ($T = 328.15$); s/x_{IL} = 0.1 and 0.6 ($T = 343.15$)	98
[Emim][Ac]	293.15–353.15	0.295–0.653	—	—	99
[Emim][SCN]	288.15–318.15	0–1	$\Delta\eta < 0/(\partial\|Y^E\|/\partial T)_{P,x} < 0$	u/x_{IL} = 0.6	137
[Emim][DCA]	288.15–318.15	0–1	$\Delta\eta < 0/(\partial\|Y^E\|/\partial T)_{P,x} < 0$	u/x_{IL} = 0.65	137
[Emim][DCA]	298.15–343.15	0–1	$\Delta\eta < 0/(\partial\|Y^E\|/\partial T)_{P,x} < 0$	u/x_{IL} = 0.77 ($T \leq 343.15$); n/x_{IL} = 0.3 and 0.9 ($T = 343.15$);	98
[Emim][Cl]	373	0.8–1	—	—	138
[Emim][OTf]	278.15–348.15	0–1	$\Delta\eta < 0/(\partial\|Y^E\|/\partial T)_{P,x} < 0$	u/x_{IL} = 0.7	96
[Emim][TCM]	298.15	0–1	$\Delta\eta < 0$	u/x_{IL} = 0.6	97
[Emim][TFA]	278.15–348.15	0–1	$\Delta\eta < 0/(\partial\|Y^E\|/\partial T)_{P,x} < 0$; $\Delta\eta > 0/(\partial\|Y^E\|/\partial T)_{P,x} > 0$	u/x_{IL} = 0.5 ($T = 278.15$); s/x_{IL} = 0.1 and 0.5 ($T > 278.15$); n/x_{IL} = 0.25 ($T > 328.15$)	96
[Emim][NTf$_2$]		0.75–1	$(\ln\eta)^E > 0$	—	139
[Emim][NTf$_2$]	293	0.8–1	—	—	140
[Emim][BF$_4$]	293.15	0–1	$\Delta\eta < 0$	u/x_{IL} = 0.6	141
[Bmim][HSO$_4$]	303.15–343.15	0–1	$\Delta\eta < 0/(\partial\|Y^E\|/\partial T)_{P,x} < 0$	u/x_{IL} = 0.6–0.7	135
[Bmim][MeSO$_3$]	298.15–343.15	0.025–0.441	—	—	142
[Bmim][MeSO$_4$]	303.15–343.15	0–1	$\Delta\eta < 0/(\partial\|Y^E\|/\partial T)_{P,x} < 0$	u/x_{IL} = 0.5–0.6	135
[Bmim][PF$_6$]		0.75–1	$(\ln\eta)^E > 0$		139
[Bmim][DCA]	278.15–363.15	0.52–1	—	—	143
[Bmim][TCM]	278.15–363.15	0.52–1	—	—	143
[Bmim][Ac]	298.15	0–1	—	s/x_{IL} = 0.75 and 0.64	136
[Bmim][SCN]	298.15–348.15	0–1	$\Delta\eta < 0/(\partial\|Y^E\|/\partial T)_{P,x} < 0$	u/x_{IL} = 0.57	70
[Bmim][BF$_4$]	303.15–353.15	0–1	$\Delta\eta < 0/(\partial\|Y^E\|/\partial T)_{P,x} < 0$	u/x_{IL} = 0.7	144
[Bmim][BF$_4$]	293.15	0–1	$\Delta\eta < 0$	u/x_{IL} = 0.65	141
[Bmim][BF$_4$]	298.15	0–1	$\Delta\eta < 0$	u/x_{IL} = 0.7	145
[Bmim][BF$_4$]	283.15–373.15	0.6–1	$(\ln\eta)^E > 0$	—	146
[Bmim][NTf$_2$]		0.75–1	$(\ln\eta)^E > 0$	—	139
[Bmim][I]	298.15	0.1–1	$\Delta\eta < 0$	u/x_{IL} = 0.7	147
[Bmim][DMP]	298.15–333.15	0–1	$\Delta\eta < 0/(\partial\|Y^E\|/\partial T)_{P,x} < 0$	u/x_{IL} = 0.4	102
[Bdmim][BF$_4$]	298.15	0–1	$\Delta\eta < 0$	u/x_{IL} = 0.7	145
[Amim][Cl]	293.15–333.15	0.2–1	—	—	148
[Amim][Cl]	298.15	0–1	—	u/x_{IL} = 0.5	107
[Amim][Cl]	298.15–353.15	0.665–0.955	—	—	33
[Hmim][Cl]	298.15–343.15	0–1	$\Delta\eta < 0/(\partial\|Y^E\|/\partial T)_{P,x} < 0$	u/x_{IL} = 0.8	149
[Hmim][Br]	293.15–333.15	0–1	$\Delta\eta < 0/(\partial\|Y^E\|/\partial T)_{P,x} < 0$	u/x_{IL} = 0.7	72
[Omim][Cl]	298.15–343.15	0–1	$\Delta\eta < 0/(\partial\|Y^E\|/\partial T)_{P,x} < 0$	u/x_{IL} = 0.7	149
[HDBU][IM]	293.15–313.15	0–1	$\Delta\eta > 0/(\partial\|Y^E\|/\partial T)_{P,x} < 0$	n/x_{IL} = 0.45	105
[BDBU][IM]	293.15-313.15	0–1	$\Delta\eta > 0/(\partial\|Y^E\|/\partial T)_{P,x} < 0$	n/x_{IL} = 0.45	105
[TMG][IM]	293.15–313.15	0–1	$\Delta\eta > 0/(\partial\|Y^E\|/\partial T)_{P,x} < 0$	n/x_{IL} = 0.45	106
Pyridinium-based ILs					
[B$_4$mPy][SCN]	298.15–348.15	0–1	$\Delta\eta < 0/(\partial\|Y^E\|/\partial T)_{P,x} < 0$	u/x_{IL} = 0.54	70
[PPy][BF$_4$]	293.15–323.15	0–1	$\Delta\eta < 0/(\partial\|Y^E\|/\partial T)_{P,x} < 0$	u/x_{IL} = 0.7	150
[BPy][BF$_4$]	293.15–323.15	0–1	$\Delta\eta < 0/(\partial\|Y^E\|/\partial T)_{P,x} < 0$	u/x_{IL} = 0.7	150
[BPy][BF$_4$]	283.15–348.15	0.144–0.89	$\Delta\eta < 0/(\partial\|Y^E\|/\partial T)_{P,x} < 0$	u/x_{IL} = 0.7	151
[OcPy][BF$_4$]	283.15–348.15	0.144–0.89	$\Delta\eta < 0/(\partial\|Y^E\|/\partial T)_{P,x} < 0$	u/x_{IL} = 0.7	151

Table 2 (continued)

ILs & DESs	T/K	Range ($x_{IL/DES}$)	$\Delta\eta$ or η^E or $(\ln\eta)^E$ $(\partial|Y^E|^b/\partial T)_{P,x}$	Shape^a $(Y^E - x_{IL/DES})/x_{IL/DES} =$ extreme position	Ref.
Cholinium-based ILs					
[Cho][Glyc]	293.15–323.15	0.063–0.634	—	—	152
[Cho][Lac]	293.15–323.15	0.059–0.9728	—	—	152
Ammonium-based ILs					
TMEAC	293.15–323.15	0–1	$(\ln\eta)^E > 0/(\partial|Y^E|/\partial T)_{P,x} < 0$	n/x_{IL} = 0.16	118
[MTEOA][MeSO$_4$]	298.15	0–1	$\Delta\eta > 0$	n/x_{IL} = 0.4	153
[DEMA][MeSO$_4$]	293.15–353.15	0.295–0.653	—	—	99
[BA][Ac]	293.15–313.15	0.031–1	$\Delta\eta < 0/(\partial|Y^E|/\partial T)_{P,x} < 0$	u/x_{IL} = 0.6	154
[BA][NO$_3$]	293.15–313.15	0.1–1	$\Delta\eta < 0/(\partial|Y^E|/\partial T)_{P,x} < 0$	u/x_{IL} = 0.65	154
[EA][NO$_3$]	293.15–318.15	0–1	$\eta^E < 0/(\partial|Y^E|/\partial T)_{P,x} < 0$	u/x_{IL} = 0.74	74
Phosphonium-based ILs					
[aP$_{4443}$][Ala]	298.15–343.15	0.25–1	—	—	125
[aP$_{4443}$][Val]	298.15–343.15	0.25–1	—	—	125
[aP$_{4443}$][Leu]	298.15–343.15	0.25–1	—	—	125
Piperidinium-based ILs					
[Bmpip][SCN]	298.15–348.15	0–1	$\Delta\eta < 0/(\partial|Y^E|/\partial T)_{P,x} < 0$	u/x_{IL} = 0.63	70
[Bmpip][DCA]	298.15–343.15	0–1	$\Delta\eta < 0/(\partial|Y^E|/\partial T)_{P,x} < 0$	u/x_{IL} = 0.62	129
[Empip][EtSO$_4$]	298.15–343.15	0–1	$\Delta\eta < 0/(\partial|Y^E|/\partial T)_{P,x} < 0$	u/x_{IL} = 0.7	108
Piperazinium-based ILs					
[(OH)$_2$C$_2$pi][C$_2$CO$_2$]	293.15–323.15	0–0.12			36
Guanidinium-based ILs					
[(C$_2$)$_2$^{2}(C$_1$)^2(C$_1$)$_2$^{3}gu][EtSO$_4$]	293.15–323.15	0–1	$\Delta\eta < 0/(\partial|Y^E|/\partial T)_{P,x} < 0$	u/x_{IL} = 0.6	113
[TMG][Lac]	303.15–328.15	0–1	$\Delta\eta < 0/(\partial|Y^E|/\partial T)_{P,x} < 0$	u/x_{IL} = 0.3	115
[TMG][BEN]	298.15	0–0.224	—	—	114
[TMG][SAL]	298.15	0–0.224	—	—	114
Morpholinium-based ILs					
[Emmor][EtSO$_4$]	298.15–343.15	0–1	$\Delta\eta < 0/(\partial|Y^E|/\partial T)_{P,x} < 0$	u/x_{IL} = 0.7	108
[Emmor][Ac]	338.15–348.15	0–0.7155	$\Delta\eta < 0/(\partial|Y^E|/\partial T)_{P,x} < 0$	u/x_{IL} = 0.7	116
[Emmor][Pro]	343.15, 348.15	0–0.7436	$\Delta\eta < 0/(\partial|Y^E|/\partial T)_{P,x} < 0$	u/x_{IL} = 0.7	116
Pyrrolidinium-based ILs					
[Pyrr][C$_7$CO$_2$]	293.15–313.15	0–1	$\eta^E > 0/(\partial|Y^E|/\partial T)_{P,x} < 0$	n/x_{IL} = 0.4	155
[P$_3$myrr][Br]	298.15–343.15	0–0.3535	—	—	156
[Pe$_5$myrr][Br]	298.15–343.15	0–0.3254	—	—	
[B$_4$mPyr][Br]	298.15–343.15	0–0.4450	—	—	156
[BmPyr][SCN]	298.15–348.15	0–1	$\Delta\eta < 0/(\partial|Y^E|/\partial T)_{P,x} < 0$	u/x_{IL} = 0.47	70
[BmPyr][DCA]	298.15–343.15	0–1	$\Delta\eta < 0/(\partial|Y^E|/\partial T)_{P,x} < 0$; $\Delta\eta > 0/(\partial|Y^E|/\partial T)_{P,x} < 0$	s/x_{IL} = 0.8; x_{IL} = 0.2	129
[Empyr][EtSO$_4$]	298.15–343.15	0–1	$\Delta\eta < 0/(\partial|Y^E|/\partial T)_{P,x} < 0$	u/x_{IL} = 0.5	108

^{a} 'u': negative single hump, 'n': positive single hump, and 's': sinusoidal. ^{b} Y: $\Delta\eta$ or η^E or $(\ln\eta)^E$.

Except the imidazolium-based ILs, only few results on Λ have been reported for the phosphonium-, ammonium-, and piperazinium-based ILs as well as DESs.

2.4 Excess/mixing enthalpy H_m

Energetic properties of IL/DES–H$_2$O mixtures are relevant both in fundamental and application contexts.[34] At the fundamental level, it is closely related to the nature of molecular or ionic interactions and to the microscopic structure of mixtures.[34] In applications, it may concern the contributions from thermodynamics and thermochemistry to other scientific disciplines such as chemistry, materials science, chemical engineering, and so on.[34]

Although the mixing enthalpy H_m is important, the reported experimental data for IL/DES–H$_2$O binary systems is quite

limited compared with other properties, such as density and viscosity. Podgorsek et al.[34] has reviewed the H_m of binary mixtures containing ILs (IL-associating compounds (i.e. H$_2$O and alcohols), IL-non-associative compounds (i.e. acetone, 1-butanone, and 3-pentanone) and IL-IL) until 2015. They state that the thermodynamic quantities of mixing could provide valuable insight into molecular interactions and microscopic structures in such mixtures. Combined with the new results after 2015, the updated experimental results are summarized in this work, and the available IL/DES–H$_2$O binary systems over the wide compositional range are listed in Table 4. With the increase of IL/DES content, both the magnitude and sign of mixing enthalpy (H_m) are changed. The H_m can be positive or negative, and the shapes of H_m–$x_{IL/DES}$ for most of the ILs/DESs show a single hump. For [Emim][SCN], [HiQuin][SCN], [C$_8$iQuin][SCN],

Table 3 Electrical conductivities of IL/DES−H$_2$O at atmospheric pressure

ILs & DESs	T/K	Range $x_{\text{IL/DES}}$ or $\Phi_{\text{IL/DES}}$ or $m_{\text{IL/DES}}$[a]	Λ/s m^{-1} ($x_{\text{IL/DES}}$ or $\Phi_{\text{IL/DES}}$ or $m_{\text{IL/DES}}$ = extreme position)	Ref.
Wide compositional range				
Imidazolium-based ILs				
[Bmim][PF$_6$]	288.15–308.15	x_{IL} = 0.2	—	160
[Bmim][BF$_4$]	298.15	Φ_{IL} = 0–1	∼5 (Φ_{IL} ∼ 0.4) max	161
[Bmim][BF$_4$]	298.15	m_{IL} = 0–5.1812	∼4.7 (m_{IL} ∼ 2.45) max	162
[Bmim][BF$_4$]	293.15–323.15	x_{IL} = 0.0256–0.8986	4.41–8.710 (x_{IL} ∼ 0.078) max	163
[Bmim][DCA]	298.15	Φ_{IL} = 0–1	∼4.8 (Φ_{IL} ∼ 0.6) max	161
[Bmim][MeSO$_4$]	298.15–343.14	x_{IL} = 0–0.5	4.059 (x_{IL} ∼ 0.049) max	142
[Bmim][MeSO$_4$]	298.15	x_{IL} = 0–1	3.416 (x_{IL} ∼ 0.0563) max	164
[Bmim][I]	—	x_{IL} = 0–1	1.5 (x_{IL} ∼ 0.05) max	165
[Bmim][I]	—	x_{IL} = 0.1–1	—	147
[Bmim][Br]	298.15	m_{IL} = 0.019–5.396	∼7.07 (m_{IL} ∼ 2.29) max	162
[Bmim][Cl]	298.15	m_{IL} = 0.0–5.502	∼6.68 (m_{IL} ∼ 2.345) max	162
[Bmim][Cl]	298.15	x_{IL} = 0–0.5018	5.98 (x_{IL} ∼ 0.0498) max	166
[Emim][Br]	298.15	m_{IL} = 0.0195–6.903	∼8.86 (m_{IL} ∼ 2.318) max	162
[Emim][BF$_4$]	298.15	Φ_{IL} = 0–1	∼9 (Φ_{IL} ∼ 0.5) max	161
[Emim][BF$_4$]	298.15	x_{IL} = 0–1	8.52 (x_{IL} ∼ 0.175) max	167
[Emim][MeSO$_4$]	298.15	x_{IL} = 0–1	6.232 (x_{IL} ∼ 0.075) max	164
[Emim][EtSO$_4$]	298.15	Φ_{IL} = 0–1	∼4.5 (Φ_{IL} ∼ 0.5) max	161
[Emim][EtSO$_4$]	298.15	x_{IL} = 0–1	4.11 (x_{IL} ∼ 0.0554) max	168
[Emim][EtSO$_4$]	298.15	x_{IL} = 0–1	4.45 (x_{IL} ∼ 0.0709) max	167
[Emim][BuSO$_4$]	298.15	x_{IL} = 0–1	3.09 (x_{IL} ∼ 0.0773) max	168
[Emim][HeSO$_4$]	298.15	x_{IL} = 0–1	2.48 (x_{IL} ∼ 0.0282) max	168
[Emim][NTf$_2$]	303.15	x_{IL} = 0.5–1	—	169
[Ehim][NTf$_2$]	303.15	x_{IL} = 0.5–1	—	169
[Emim][OTf]	303.15	x_{IL} = 0.5–1	—	169
[Ehim][OTf]	303.15	x_{IL} = 0.5–1	—	169
[Mmim][Cl]	450	x_{IL} = 0.25–1	—	170
[Amim][Cl]	293.15–333.15	x_{IL} = 0.2–1	—	148
[Amim][Cl]	298.15	x_{IL} = 0.000171–1	7.922 (x_{IL} ∼ 0.0665) max	107
[TMG][IM]	293.15–313.15	0–1	4.0 (x_{IL} ∼ 0.05) max	106
Phosphonium-based ILs				
[aP$_{4443}$][Ala]	298.15–343.15	x_{IL} = 0.25–1	—	125
[aP$_{4443}$][Val]	298.15–343.15	x_{IL} = 0.25–1	—	125
[aP$_{4443}$][Leu]	298.15–343.15	x_{IL} = 0.25–1	—	125
Ammonium-based ILs				
CPL-TBAF	293.15–333.15	x_{IL} = 0.00183–0.171	0.765–0.64 (x_{IL} ∼ 0.0505) max	171
CPL-TBABr	308.15–328.15	x_{IL} = 0.0505	0.78–0.64 (x_{IL} ∼ 0.0505) max	171
CPL-TBACl	293.15–333.15	x_{IL} = 0.00183–0.171	0.8–0.74 (x_{IL} ∼ 0.0505) max	171
[BA][NO$_3$]	298.15	x_{IL} = 0–1	3.7 (x_{IL} ∼ 0.109) max	154
[BA][Ac]	298.15	x_{IL} = 0–1	1.727 (x_{IL} ∼ 0.0579) max	154
Choline-based ILs				
[Cho][H$_2$Prop]	298.15–333.15	x_{IL} = 0.004–0.1657	2.834–3.356 (x_{IL} ∼ 0.04) max	172
Pyridinium-based ILs				
[EPy][MeSO$_3$]	298.15–333.15	x_{IL} = 0.0039–0.383	4.672–4.995 (x_{IL} ∼ 0.05) max	172
Piperazinium-based ILs				
[(OH)$_2$C$_2$pi][EtCOO]	293.15–323.15	x_{IL} = 0–0.12	3.75 (x_{IL} ∼ 0.0291) max	36
DESs				
DEAC/Gly (1:2)	298.15–343.15	x_{DES} = 0.1002–0.9018	—	173
DEAC/EG (1:2)	298.15–343.15	x_{DES} = 0.1–0.9	—	173
ChCl/urea (1:2)	293.15–363.15	x_{DES} = 0–1	5.97 (x_{DES} ∼ 0.1) max	79

ILs	T/K	Range $m_{\text{IL/DES}}$ (mol m^{-3})	k_{A} (dm^3 mol^{-1})	Ref.
Dilute solutions of ILs				
Imidazolium-based ILs				
[Bmim][BF$_4$]	298.15	50–1000	—	174
[Bmim][BF$_4$]	303.2–323.2	4.2–55.3	—	175
[Bmim][BF$_4$]	298.15	0.1–1.4	105	158
[Bmim][PF$_6$]	303.2–323.2	3–5.6	—	175
[Bmim][PF$_6$]	298.15	0.1–1.4	113	158
[Bmim][MeSO$_4$]	303.2–323.2	5–16.3	—	175
[Bmim][OTf]	303.2–323.2	4–21.1	—	175

Table 3 (continued)

ILs	T/K	Range $m_{IL/DES}$ (mol m^{-3})	k_A (dm^3 mol^{-1})	Ref.
[Bmim][Br]	298.15	0.1–1.4	66	158
[Bmim][Cl]	278.15–313.15	6	7.2–4.5	176
[Bmim][Cl]	298.15	0.4734–2.099	4.04	177
[Bmim][Cl]	298.15	0.4833–1.681	8.56	178
[Bmim][HCOO]	298.15		2.25	179
[Bmim][Ac]	298.15		0.37	179
[Bmim][EtCOO]	298.15		−0.24	179
[Emim][EtSO$_4$]	278.15–313.15	0.25–5	0.014–0.7	180
[Hmim][Cl]	298.15	0.1239–1.927	5.36	177
[Hmim][Cl]	293.15–303.15	0.0009–0.0841	2.4–7.8	181
[Hmim][Cl]	298.15	0.2349–1.62	4.78	178
[Hmim][Br]	283.15–303.15	0.6–63.84	2.94–4.93	159
[Hmim][Br]	298.15	0.1–1.4	71	158
[Omim][Cl]	298.15	0.3264–1.863	2.51	177
[Omim][Cl]	298.15	0.2751–1.631	1.54	178
[Omim][Br]	298.15	0.1–1.4	79	158
[C$_{10}$mim][Cl]	298.15	0.1226–1.530	4.53	177
[C$_{10}$mim][Cl]	298.15	0.3586–1.878	25.86	178
[C$_{10}$mim][Br]	298.15	0.1–1.4	84	158
[C$_{12}$mim][Br]	298.15	0.1–1.4	96	158
Others				
[C$_3$C$_1$pyr][PF$_6$]	288.15–318.15	0–1.4^b	—	182
[C$_3$C$_1$pip][PF$_6$]	288.15–318.15	0–1.4^b	—	182
[N$_{4444}$][PF$_6$]	288.15–318.15	0–0.25^b	—	182
[P$_{4444}$][PF$_6$]	288.15–318.15	0–0.25^b	—	182

^{a} $x_{IL/DES}$, $\Phi_{IL/DES}$ and $m_{IL/DES}$ are the mole fraction, volumetric fraction and molarity of IL/DES (mol m^{-3}), respectively. ^{b} Unit: g L^{-1}.
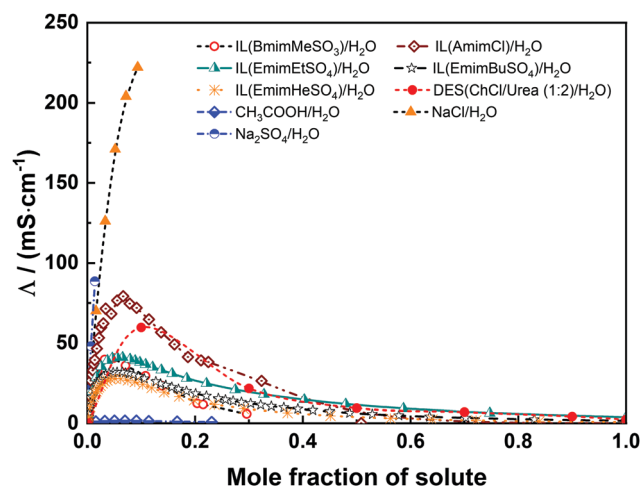

Fig. 4 The electrical conductivity Λ of aqueous solutions with selected electrolytes, organic solvent and ILs/DESs.

ChCl/MA (1:1), ChCl/urea (1:2) and ChCl/urea (1:1.5), the values of H_m show an S-shaped curve as depicted in Fig. 5. For these 6 binary systems, the values of H_m are always positive in the H$_2$O-rich region (0 < $x_{IL/DES}$ < 0.5) and then change to negative with an increase of the mole fraction of IL/DES. This observation implies that the mixing process is initially endothermic and then changes to exothermic with increasing the content of IL/DES. The turnover points depend on the type of ILs/DESs.

2.5 Other important properties – surface and interfacial tensions

Other properties such as surface and interfacial tensions are also of importance in industrial applications although they

have not been investigated as widely as the other properties discussed above.[62] The surface and interfacial tensions reflect the properties on the liquid–gas/vapor surface and liquid–liquid phase boundary, respectively. The surface tension is an important property in studies of physics and chemistry at the free surface because it affects the transfer rates of gas absorption, for example, where a gas–liquid interface exists.[204] Although some work has been conducted on the surface tension of IL/DES–H$_2$O binary systems, the experimental data over a whole compositional range at different temperatures is still scarce.[62] For the interfacial tension,[205] only few results were published.

2.6 Summing-up

A large amount of experimental investigations has been carried out to study the physicochemical properties of IL/DES–H$_2$O binary systems including density, viscosity, electrical conductivity, excess/mixing enthalpy and so on. Density and viscosity are the most widely studied properties. The electrical conductivity and excess/mixing enthalpy both have much attention but the number of investigated ILs is still small. Studies of surface and interfacial tensions over a whole compositional range at different temperatures are still scarce. The electrical conductivity of IL/DES–H$_2$O binary systems over a wide compositional range generally shows a maximum value at a relatively low IL/DES concentration. The excess volume and viscosity and mixing enthalpy are often used as a measure of non-ideal behaviour of IL/DES–H$_2$O binary system, and the shape depends on the cations and anions, as well as the physical conditions, *i.e.* temperature and pressure. This implies that the properties of the mixtures are truly unique and at the same time largely unpredictable. To understand the IL/DES–H$_2$O binary systems deeper,

8696 | *Chem. Soc. Rev.*, 2018, **47**, 8685–8720

This journal is © The Royal Society of Chemistry 2018

Table 4 Mixing enthalpies of IL/DES–H$_2$O binary systems

ILs & DESs	T, K	$x_{IL/DES}/H_{m,min}{}^{a}$	$x_{IL/DES}/H_{m,max}{}^{a}$	$x_{IL/DES}$, $H_m = 0$	Shape/$H_m{}^{a}$	$(\partial \lvert H_m \rvert / \partial T)_{P,x}$	Ref.
DESs							
ChCl/EG (1:2)	298.15/308.15	0.4/[−1.08, −1.06]	—	—	u/<0	>0	183
ChCl/MA (1:1)	298.15/308.15	0.4/∼ −0.6	0.05/∼0.1	0.1	s/(<0, >0)	>0, H_m < 0; >0, H_m > 0	183
ChCl/Gly (1:2)	298.15/308.15	0.4/∼ −0.9	—	—	u/<0	>0	183
ChCl/urea (1:2)	308.15/318.15	0.7/∼ −0.07	0.14/∼0.2	0.3	s/(<0, >0)	>0, H_m < 0; <0, H_m > 0	184
ChCl/urea (1:1.5)	308.15/318.15	0.5/[−0.3, −0.2]	0.05/∼0.15	0.2	s/(<0, >0)	>0, H_m < 0; <0, H_m > 0	184
ChCl/urea (1:2.5)	308.15/318.15		0.16/∼0.28	—	n/>0	<0	184
Imidazolium-based ILs							
[Emim][SCN]	313.14–348.13	0.61/∼ −0.45	0.10/[0.2, 0.37]	0.32	s/(<0, >0)	<0, H_m < 0; >0, H_m > 0	185
[Emim][MeSO$_3$]	313.14–348.14	0.25/∼ −2.73	—	—	u/<0	>0	186
[Emim][HSO$_4$]	313.14	0.5/∼ −2.55	—	—	u/<0	—	186
[Emim][MeSO$_4$]	313.14	0.25/∼ −1.14	—	—	u/<0	—	187
[Emim][DEP]	313.13–348.12	0.38/∼ −6	—	—	u/<0	<0	185
[Emim][EtSO$_4$]	313.14–348.12	0.25/[−0.834, −0.975]	—	—	u/<0	<0	188
[Emim][EtSO$_4$]	298.15	0.2/−0.991	—	—	u/<0	—	189
[Emim][OTf]	313.13–348.12	—	0.5/[1.127, 1.244]	—	n/>0	>0	188
[Emim][TFA]	313.04–348.06	0.5/[−2.14, −2.0]	—	—	u/<0	<0	188
[Emim][TCM]	288.15–318.15	—	0.5/∼1.6	—	n/>0	—	97
[Emim][BF$_4$]	298.15	—	0.57/0.483	—	n/>0	—	190
[Emim][EtSO$_4$]	363.15	0.39/−0.814	—	—	u/<0	—	191
[Emim][EtSO$_4$]	303.15	0.2/−0.986	—	—	u/<0	—	187
[Emim][MeSO$_4$]	303.15	0.3/−0.537	—	—	u/<0	—	187
[Emim][OTf]	303.15	—	0.40/1.071	—	n/>0	—	187
[Emim][DMP]	298.15	0.3/−6.25	—	—	u/<0	—	192
[Emim][DMP]	298.15	0.3/−6.3	—	—	u/<0	—	193
[Bmim][BF$_4$]	278.15–333.15	—	0.33/[2.05–2.35]	—	u/>0	>0	194
[Bmim][Cl]	303.15/318.15	—	—	—	u/<0	<0	195
[Bmim][OTf]	303.15	—	0.40/1.389	—	n/>0	—	187
[Hmim][OTf]	313.12–347.85	—	0.38/[1.6, 2.1]	—	n/>0	>0	185
[Mmim][DMP]	298.15	0.3/−6.5	—	—	u/<0	—	93
[OHemim][TFA]	323.13–384.14	0.32/∼ −1.25	—	—	u/<0	<0	186
Phosphonium-based ILs							
[P$_{2444}$][DEP]	313.13–348.12	0.3/[−2.5, −3]	—	—	u/<0	<0	185
[P$_{2444}$][DEP]	298.15	0.3/−1.76	—	—	u/<0	—	1, 2, 126 and 196
Pyridinium-based ILs							
[B$_3$mpy][BF$_4$]	298.15/318.15		0.30/[1.635–2.099]		n/>0	>0	197
[B$_4$mpy][BF$_4$]	298.15/318.15		0.33/[1.81–2.245]		n/>0	>0	198
[BPy][BF$_4$]	298.15/318.15		0.31–0.36/[1.78–2.549]		n/>0	>0	199
[B$_2$mpy][BF$_4$]	298.15/318.15		0.33–0.36/[1.49–2.13]		n/>0	>0	200
[B$_3$mpy][BF$_4$]	303.15		0.40/2.319		n/>0	—	187
Choline-based ILs							
[Cho][Glyc]	303.15	0.20/−6	—		u/<0	—	152
[Cho][Lac]	303.15	0.19/−20	—		u/<0	—	152
Ammonium-based ILs							
[EA][NO$_3$]	298.15		0.378/0.6977		n/>0	—	69
[PA][NO$_3$]	298.15		0.34/0.8955		n/>0	—	69
Piperidinium-based ILs							
[Empip][EtSO$_4$]	298.15	0.21/−1.255	—		u/<0	—	201
[Bmpip][DCA]	298.15	0.371/−0.774	—		u/<0	—	129
Morpholinium-based ILs							
[Emmor][EtSO$_4$]	298.15	0.2/−0.675	—		u/<0	—	201
Pyrrolidinium-based ILs							
[Bmpyr][DCA]	298.15	0.3857/−0.953	—		u/<0	—	129
[Empyr][EtSO$_4$]	298.15	0.24/−1.615	—		u/<0	—	201

Table 4 (continued)

ILs & DESs	T, K	$x_{IL/DES}/H_{m,min}{}^a$	$x_{IL/DES}/H_{m,max}{}^a$	$x_{IL/DES}$, $H_m = 0$	Shape/$H_m{}^a$	$(\partial|H_m|/\partial T)_{P,x}$	Ref.
Quinolinium-based ILs							
[HiQuin][SCN]	298.15–308.15	0.68/[−0.29, −0.25]	0.26/[0.33, 0.35]	0.42	s/(<0, >0)	>0, H_m < 0	202
[C₈iQuin][SCN]	298.15–308.15	0.62/∼ −0.5	0.26/[0.1, 0.3]	0.31	s/(<0, >0)	>0, H_m < 0; >0, H_m > 0	203

^{a} The unit for H_m is kJ mol^{-1}.
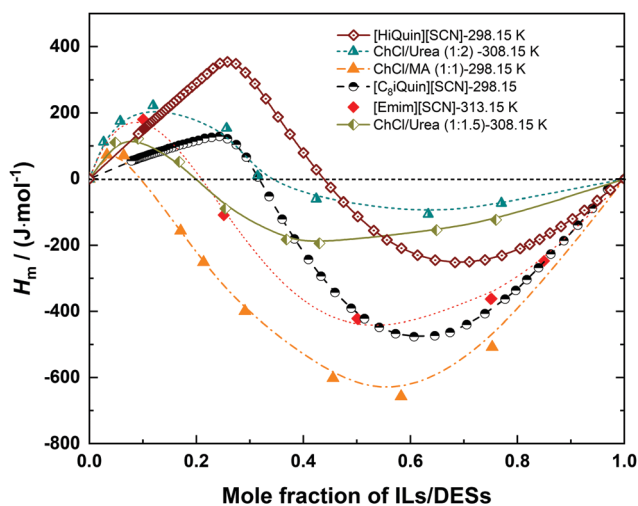
Fig. 5 The IL/DES–H$_2$O systems with an S-shaped curve of H_m–$x_{IL/DES}$.

more experiments of measuring the electrical conductivity and excess/mixing enthalpy should be carried out in order to reflect the non-ideal behavior directly.

3. Mechanistic studies

The physicochemical properties of IL/DES–H$_2$O binary systems are a macroscopic manifestation of the microscopic interactions of ion–ion and ion–solvent (H$_2$O). Understanding how H$_2$O interacts with ILs/DESs and how the properties of ILs/DESs are affected by the presence of H$_2$O is highly important in both scientific research and practical applications. Therefore, in this section, a selection of mechanistic studies on the IL/DES–H$_2$O systems are surveyed.

Considering that as many as 10^{18} ILs/DESs could conceivably be synthesized by combining the possible cations with possible anions, it is crucial to develop theoretical models for the reliable prediction of the properties of these systems. However, it appears that most of the modelling work still empirically correlates the experimental data for a specific system with a specific property. The development of more general theoretical models remains limited. Moreover, there are currently no theoretical models describing the thermodynamic properties over the entire compositional range from pure ILs/DESs to infinitely dilute ILs/DESs solutions. The primary reason for this lack of models is the extremely complex molecular behaviour of ILs/DESs, both in their pure state and combined with water.

Various analyses using X-ray and neutron scattering, NMR spectroscopy and other experimental methods have shown that ILs are highly heterogeneous with long-range structural correlations, while the structures of DESs are more complex. The development of reliable theoretical models for IL/DES–H$_2$O binary systems will require investigations of the molecular behaviour based on mechanistic studies using both experimental and theoretical approaches.

To examine the molecular behaviour of IL/DES–H$_2$O binary systems, much research work has been carried out using different computational methods, including molecular dynamics simulations, Monte Carlo simulations and quantum chemical calculations, and advanced experimental methods including infrared, Raman and NMR spectroscopy, X-ray scattering and neutron scattering as well as thermodynamic analyses. However, reviews that include all these mechanistic analyses are still scarce. Therefore, past investigations of IL/DES–H$_2$O systems are summarized in this section, along with the work concerning aqueous electrolyte solutions to allow comparisons, because of the similarities of ILs/DESs to electrolytes.

3.1 Molecular dynamics or Monte Carlo simulations

Molecular Dynamics (MD) or Monte Carlo (MC) simulations are commonly used to study the microscopic structure and behaviour of molecules in condensed phases and interfaces. MC can provide structural and thermodynamic properties. MD can even be used to study the dynamical and time-dependent phenomena including transport properties. Imidazolium-based ILs with a halide anion (e.g. [Cl]$^-$, [Br]$^-$ or [I]$^-$) are those more frequently studied as we can see from the summary in Table 5.

Aqueous ILs were first investigated using MD simulations by Hanke et al.[38] for [Mmim][Cl]. The simulations were carried out in the range of dilute IL solutions, and the results show a formation of the H$_2$O–Cl complex (hydrated [Cl]$^-$) and then a particular interaction between hydrated-[Cl]$^-$ and the imidazolium ion. After that, Spickermann et al.[206] performed Car–Parrinello MD simulations for a single [Emim][Cl] ion-pair dissolved in 60 H$_2$O molecules. Under their simulation conditions (IL : H$_2$O = 1 : 60, x_{IL} = 0.0164), contact ion-pair still exists, and the hydration is not complete for both the anion and cation. The cation ([Emim]$^+$) shows a stronger connection to the H$_2$O-hydrated-[Cl]$^-$ compared with the H$_2$O-hydrated-metal-ion, facilitating the formation of a joint hydration shell that stabilizes the [Emim][Cl] ion-pair. The MD simulation work conducted by Remsing et al.[207] shows that the dissociated ions from [Bmim][Cl] are completely solvated at low concentrations as a typical electrolyte, but water cannot

8698 | Chem. Soc. Rev., 2018, 47, 8685–8720

This journal is © The Royal Society of Chemistry 2018

Table 5   The MD or MC simulations and QC calculations used to explore the interaction in the IL/DES−H₂O binary systems

Cation	Anion	MD or MC simulation	QC calculation
Imidazolium-based ILs			
[Mim]⁺	[Cl]⁻	—	232
[Mmim]⁺	[Cl]⁻	37 and 38	232
[Mmim]⁺	[PF₆]⁻	—	—
[Mmim]⁺	[DMP]⁻	219	—
[Emim]⁺	[Cl]⁻	206	227 and 232
[Emim]⁺	[Br]⁻	—	227
[Emim]⁺	[BF₄]⁻	—	227
[Emim]⁺	[PF₆]⁻	—	227
[Emim]⁺	[EtSO₄]⁻	209	—
[Emim]⁺	[Ac]⁻	219	—
[Bmim]⁺	[BF₄]⁻	210 and 218	—
[Bmim]⁺	[Cl]⁻	207 and 219	231
[Bmim]⁺	[Br]⁻	—	231
[Bmim]⁺	[I]⁻	147 and 165	—
[Bmim]⁺	[SCN]⁻	—	228 and 231
[Bmim]⁺	[TFA]⁻	—	231
[Bmim]⁺	[OTf]⁻	—	231
[Bmim]⁺	[TOS]⁻	—	231
[Bmim]⁺	[MeSO₃]⁻	—	231
[Bmim]⁺	[DMP]⁻	—	231
[Bmim]⁺	[Ac]⁻	—	231
[Bmim]⁺	[DCA]⁻	—	228
[Bmim]⁺	[TCM]⁻	—	228
[Bmim]⁺	[TCB]⁻	—	228
[Hmim]⁺	[I]⁻	208	—
[Omim]⁺	[NO₃]⁻	217	—
[Omim]⁺	[BF₄]⁻	218	—
[Omim]⁺	[Cl]⁻	218	—
[Pmim]⁺	[Cl]⁻	—	232
[C₄C₁mim]⁺	[Cl]⁻	—	232
[C₇mim]⁺	[Cl]⁻	—	232
[C₁₀mim]⁺	[Cl]⁻	—	232
[Amim]⁺	[Cl]⁻	—	232
[C₂₀H₂₈N₃O]⁺	[NTf₂]⁻	211	—
[C₂₀H₂₈N₃O]⁺	[NO₃]⁻	211	—
Ammonium-based ILs			
[Dema]⁺	[OTf]⁻	212	
[Glyc]⁺, [Ala]⁺, [Val]⁺, [Leu]⁺	[Cl]⁻, [Br]⁻, [BF₄]⁻, [PF₆]⁻	—	233
Phosphonium-based ILs			
[P₆,₆,₆,₁₄]⁺	[BOB]⁻	220 and 221	—
Pyrrolidinium-based ILs			
[Bmpyr]⁺	[Cl]⁻	—	229
Pyridinium-based ILs			
[B₂mPy]⁺	[Cl]⁻	—	229
[B₃mPy]⁺	[Cl]⁻	—	229
[B₄mPy]⁺	[Cl]⁻	—	229
[BPy]⁺	[Cl]⁻	—	229
[Bpy]⁺	[BF₄]⁻	—	229
Piperidinium-based ILs			
[Bmpip]⁺	[Cl]⁻	—	229
DESs			
ChCl/urea (1:2)		79 and 213–215	—
ChCl/Gly (1:2)		213 and 216	—
ChCl/EG (1:2)		213	—

completely disrupt the interaction between ions as ion-pairs still exist even when the mole fraction of water is 0.999.

Recently, D'Angelo et al.[208] studied the molecular structure of [Hmim][I]–H₂O mixture with the molar ratios from 1:1 to 1:200 (i.e. x_{IL} = 0.005–0.5) with MD simulation. Their results show that the H₂O molecules coordinate around the [I]⁻ anion

and the [I]⁻-hydration shell becomes more and more crowded with increasing H₂O content. ILs exist mainly as ion-pairs when the H₂O content is low, while no ion-pairs can be observed in the most diluted IL solutions. Sha et al.[165] studied ion-association from a very dilute [Bmim][I] solution to pure IL. The simulation results show that the cation–anion association is completely

replaced by the anion–water network in the dilute IL solution. When the H_2O content is increased, the anions will be gradually hydrated with more than 7 H_2O molecules in the first anion coordination shell for a very dilute IL solution. By analyzing the interaction energies of cation–cation, anion–H_2O, cation–H_2O and H_2O–H_2O as a function of IL mole fraction (x_{IL}), they found that there is a strong anion hydration effect. When x_{IL} is lower than 0.25, the cage structure of ions will be broken down, and the ion-hydration starts to dominate. The association structure of cation–anion vanishes in the lowest IL mole fraction of 0.003. For [Bmim][I], Nickerson et al.[147] also found that at low concentrations of water, the H_2O molecules get inserted into the ordered cation/anion structure. Hydrogen-bonding (H-bonding) between H_2O and $[I]^-$ was found to be strong and important for the properties of mixtures, particularly leading to the dramatic increase in conductivity at high water concentrations.

Hanke and Lynden-Bell[37] studied the local structure and dynamics for the mixtures of H_2O and IL (either [Mmim][Cl] or [Mmim][PF_6]). They found that the H_2O molecules tend to be isolated from one another in the IL-rich mixtures, and a water percolating network is formed when the molar proportion of water reaches 75%. Bernardes et al.[209] analyzed the structural feature of the [Emim][$EtSO_4$]–H_2O binary system in the entire compositional interval using MD simulations. They found that the size of IL-aggregates decreases with increasing water content. The chain-like IL network is broken down at the point with the mole fraction of water (x_{water}) at 0.95, and then small IL-aggregates or 'icebergs' start to form. For the dilute IL solutions ($x_{water} = 0.996$), only isolated ions and dimers were found and the probability of forming an isolated ion is almost 60%. Therefore, the IL is dissociated mostly under the infinitely dilute IL condition, and water clearly shields the electrostatic interaction energy between the cation and anion, but dimers still exist. Zhong et al.[210] performed MD simulation for the [Bmim][BF_4]–H_2O binary system in the entire compositional range, and they proposed that the local structure is divided into 3 distinct regions ($x_{water} < 0.2$, $0.2 < x_{water} < 0.8$, $0.8 < x_{water}$). When $x_{water} < 0.2$, most of the H_2O molecules are isolated with one another and experience a local environment in the polar network nearly the same as that in pure IL. The polar network of IL is maintained very well until x_{water} reaches 0.8. When $x_{water} > 0.8$, an aggregation is observed and reaches maximum at $0.9 < x_{water} < 0.95$, which means that, in this compositional range, IL starts to dissolve in water and exists in the form of small clusters by the aggregation of cations and anions. Gutiérrez et al.[141] carried out MD simulations for binary systems of [Emim][BF_4] and [Bmim][BF_4] with several molecular solvents (water, ethylene glycol and dimethylformamide) to obtain a microscopic view of structuring and intermolecular forces, H-bonding as well as their relationship with macroscopic behaviour. The results show that the molecular solvents interact preferentially with $[BF_4]^-$ whereas the interaction between the cation and the molecular solvent is less important. When water is used as solvent, stronger interactions and hydration can be observed. The increase of the alkyl-chain length in the cations (i.e. from [Emim]$^+$ to [Bmim]$^+$) does not have a

noticeable effect on the properties of mixtures compared with the change of anions.

Yuvaraj et al.[211] studied the solvation mechanism of two TSILs containing a common L-histidine-derived-imidazolium cation and an anion of $[Br]^-$ or $[NTf_2]^-$, using classical MD simulations and density functional theory (DFT) calculations, and H_2O was chosen as the solvent. On average, 4 H_2O molecules are associated with each anion in these two ILs. The $[Br]^-$ is completely enclosed within the solvation shell, making the $[Br]^-$ fully hydrated. While for the $[NTf_2]^-$-based TSIL, $[NTf_2]^-$ is only partially hydrated and the cation and anion remain coordinated interacting even in the presence of H_2O, which implies that this TSIL may still exist as ion-pairs. Chang et al.[212] studied the structure and dynamics of aqueous ammonium-based IL ([Dema][OTf]) using MD simulations. They observed that the H_2O molecules form a distinct solvation shell around both the cation and anion and thus weaken their mutual association. At low water contents, the H_2O molecules were observed to be isolated from one another while coordinated strongly to the ions. As the water content increases, the ions were found to have more H_2O molecules in their coordination shells, which is more noticeable for the anions. When the water mole fraction is 0.8, the proportion of the anions without any hydrogen-bonds (H-bonds) with water is only 2%. Therefore, the $[OTf]^-$ has a strong affinity for water, and it is easily hydrated by water.

Shah et al.[79] performed MD simulations to analyze the intermolecular interactions in a type-III DES, ChCl/urea (1:2) with the addition of water. The results show that the anion ($[Cl]^-$) becomes preferentially hydrated by water compared with urea or cation, and the effects of water can be classified into 3 regimes based on the mass fraction of H_2O (w_{H_2O}) (i.e. $w_{H_2O} < 5\%$, $5\% < w_{H_2O} < 25\%$, and $w_{H_2O} > 25\%$). In the low water fraction zone ($w_{H_2O} < 5\%$), the number of H-bonds shows a maximum at $w_{H_2O} \approx 2.5\%$. At the intermediate water fraction ($5\% < w_{H_2O} < 25\%$), the components of ChCl/urea (1:2) are hydrated by H_2O, and the anion and urea show a low diffusivity. At the high water fraction ($w_{H_2O} > 25\%$), both anion and urea show high diffusivities. The simulation also shows that there is a strong urea–H_2O interaction, but the $[Cl]^-$ interacts strongly with H_2O compared with urea. Both urea and $[Cl]^-$ can be hydrated by water. Zhekenov et al.[213] studied the formation of three type-III DESs (ChCl/urea (1:2), ChCl/Gly (1:2) and ChCl/EG (1:2)) and the effect of water on the intermolecular interactions by analyzing the number of H-bonds and the diffusion of the constituent species of DESs. A similar behavior was observed for different DESs. Specifically, when water is added in a small amounts ($w_{H_2O} < 5\%$), water gets absorbed in the structure of DES by forming H-bonds with the ions and HBDs; beyond that water amount ($w_{H_2O} > 5\%$), water also dampens the intramolecular interactions in the DES, leading to drastic changes of properties. Fetisov et al.[214] investigated the behaviour of ChCl/urea (1:2) and its equimolar mixture with water ($x_{H_2O} = 0.5$ or $w_{H_2O} = 17\%$) by performing first-principles MD simulation. Their results show that the addition of H_2O breaks the strong H-bonds between the H atoms of urea and $[Cl]^-$ in the pure ChCl/urea (1:2) by preferentially hydrating $[Cl]^-$ and

8700 | Chem. Soc. Rev., 2018, **47**, 8685–8720

This journal is © The Royal Society of Chemistry 2018

forming urea–water H-bonds. Gao *et al.*[215] performed MD simulations to study the properties of ChCl/urea (1 : 2)–H$_2$O mixtures from the pure ChCl/urea (1 : 2) to infinitely dilute ChCl/urea (1 : 2) solutions (x_{H_2O} = 0.999 or w_{H_2O} = 99.5%). The simulation results show that, even at x_{H_2O} = 0.9, neither [Cl]$^-$ nor cation is saturated by water, which means that, at this composition, the ions are only partially hydrated. Moreover, at low water contents, the ion-pairing of cation and anion is dominant, whereas the hydration of ions turns out to be dominant with the increase of water content. The competition between these two interactions (*i.e.* ion-pairing and ions hydration) results in a non-ideal behaviour of properties observed from macroscale. For ChCl/Gly (1 : 2)–H$_2$O binary mixture, Ahmadi *et al.*[216] performed MD simulations at x_{H_2O} = 0.9, three typical distributions for the DES constituents were observed, and ChCl prefers to form H-bonds with water instead of glycerol.

MD simulations have been conducted in order to find the structural regimes with different amounts of water. The simulation from Jiang *et al.*[217] was performed for [Omim][NO$_3$]–H$_2$O mixture at various water concentrations. It reveals that there is a turnover point (x_{water} ≈ 0.75–0.8) for the structural organization of the water network (water–anion–water) and micelle (cation–cation) structure, and water can form liquid-like associated aggregates due to the planar symmetry and strong basicity of [NO$_3$]$^-$. Feng *et al.*[218] investigated the effects of anion and alkyl chain length of cation on the structure and dynamic based on 3 IL–H$_2$O binary systems ([Bmim][BF$_4$]–H$_2$O, [Omim][BF$_4$]–H$_2$O, and [Omim][Cl]–H$_2$O) with the water content from 0.2 to 0.9615 in mole fraction. They found that by increasing the alkyl chain length of cation from [Bmim]$^+$ to [Omim]$^+$, the aggregation of the cations becomes stronger and the diffusion of the anions becomes slower. The H$_2$O molecules are more likely to remain close to the [Cl]$^-$ than the [BF$_4$]$^-$. The diffusion coefficients of anions and water molecules show two recognizable regimes (x_{water} < 0.8 and x_{water} > 0.8). The system may be in a glassy state at x_{water} < 0.8. While when x_{water} > 0.8, the ion-dominated networks will be broken down and changed to water-dominated networks. The MD simulations performed by Niazi *et al.*[219] were used to study the properties of 3 imidazolium-based ILs ([Bmim][Cl], [Emim][Ac] and [Mmim][DMP]) with water at 350 K, ranging from 0 to 99.95% of water in mole fraction (x_{water}), and it was found that a transition takes place from IL–H$_2$O mixed solvents to an aqueous IL solution at around x_{water} = 0.75. Wang *et al.*[220,221] performed atomistic MD simulations for the mixture of a phosphonium-based IL ([P$_{6,6,6,14}$][BOB]) and water to study their volumetric and dynamic properties as well as their local microscopic structures. The results show that the microscopic liquid structure of the pure IL is a connected polar network composed of alkyl chains in the cation and isolated polar domains consisting of the central segments of [P$_{6,6,6,14}$]$^+$ in the cation and [BOB]$^-$, *i.e.* the isolated polar domain is a direct contact ion-pair. When x_{water} is low, the water is embedded into cavities to form solvent-shared ion-pairs through a cation-water-anion triple complex, and no free water can be observed. 4 distinct structural regimes were proposed within the entire compositional range based on x_{water} (0 ≤ x_{water} < 0.50,

0.50 < x_{water} < 0.80, 0.8 < x_{water} < 0.95, 0.95 < x_{water} ≤ 1) concerning the evolution of microscopic liquid structure and the transition of the local ionic organization.

In summary, numerous MD and MC simulations have been conducted to find out the molecular behaviour of the IL/DES–H$_2$O binary systems. The investigated ILs involve both conventional ILs and TSILs. In general, the interaction between the anion and water is stronger than that between cation and water, the anion can be fully hydrated or partially hydrated depending on its size and basicity, and the structural regimes change with the water contents.

It should be mentioned here that, due to the highly complex interaction landscape, ILs are highly challenging to study with molecular mechanical force field based simulations. If the standard force fields that were developed originally for the organic or biomolecular systems are used, it is common that the simulations give too low diffusion and too high viscosity.[222–224] In Car–Parrinello simulations and quantum chemical DFT calculations of ILs, it has been observed that there is a certain degree of charge transfer taking place among the ion-pairs and thus diluting the atomic charges in the vicinity of the charge centers.[225] For example, for the imidazolium-based ILs, the atomic charge gets reduced by a factor roughly 0.85.[226] Scaling the charges down to obtain correct diffusion (and viscosity) has become praxis (although somewhat *ad hoc*) for studying ILs reliably.

3.2 Quantum chemical calculations

Quantum chemical (QC) calculations, including *ab initio* quantum chemistry and DFT, as well as semi-empirical methods, such as the conductor-like screening model for realistic solvents (COSMO-RS), have been used to give insight into the interactions between H$_2$O and IL/DES molecules. Besides, QC calculations become necessary when the information on the electronic structure or molecular properties such as dipole moments, polarizabilities, *etc.* is needed. QC can also be used to obtain interaction energies and new force field parameters often missing for the new IL/DES systems.

Several ILs have been studied as summarized in Table 5. Wang *et al.*[227] performed DFT calculations to investigate the interaction between H$_2$O and the imidazolium-based ILs ([Emim]$^+$) with the anions of [Cl]$^-$, [Br]$^-$, [BF$_4$]$^-$ and [PF$_6$]$^-$. The predicted geometries and interaction energies imply that H$_2$O interacts with the anion ([Cl]$^-$, [Br]$^-$ or [BF$_4$]$^-$) to form X$^-$···W, 2X$^-$···2W, [BF$_4$]$^-$···W, and W···[BF$_4$]$^-$···W complexes where X = Cl or Br and W = H$_2$O. While for [PF$_6$]$^-$, a hydrophobic anion, no stable complex can be formed with water, but either cation or ion-pair can form a complex with the H$_2$O molecules.

Batista *et al.*[228] studied the H$_2$O–IL interaction for the imidazolium-based ILs ([Bmim]$^+$) with the anions of [SCN]$^-$, [DCA]$^-$, [TCM]$^-$ and [TCB]$^-$ with experimental and computational (COSMO-RS) techniques. The [SCN]$^-$- and [DCA]$^-$-based ILs are favorable to interact with the H$_2$O molecules, while the other two ILs indicate weak interactions with H$_2$O. Based on the sigma (screening charge density) profile generated from COSMO-RS,

This journal is © The Royal Society of Chemistry 2018

Chem. Soc. Rev., 2018, **47**, 8685–8720 | 8701

the electronegativity of the anions plays an important role in their interaction with H_2O.

In the work by Khan et al.,[229] the aqueous solutions with the imidazolium-, pyridinium-, pyrrolidinium- and piperidinium-based ILs or cholinium-based ILs were studied. For the aqueous cholinium-based ILs, the results based on the COSMO-RS method show that the H-bonding between H_2O and IL–anion is the dominant interaction, while the electrostatic-misfit interaction and van der Waals forces have minor contributions to the total excess enthalpies.[230] For [Bmim][Cl], the turnover point of the curve H_m–x_{water} is at around x_{water} = 0.75 according to COSMO-RS calculation, which implies that [Cl]$^-$ forms "a complex" with 3 H_2O molecules.[231] The aromaticity of the cation weakens the IL–H_2O interaction.[229] The H_2O–IL interaction is weakened by increasing the alkyl chain length on the imidazolium ring. The excess enthalpies, calculated from COMSO-RS, suggest the formation of complexes between 3 H_2O molecules and one IL molecule for the alkyl-methyl-imidazolium chloride–H_2O binary system.[232]

Zhu et al.[233] conducted a systematic investigation on the interactions of the H_2O molecule with a series of amino acid cations ([Glyc]$^+$, [Ala]$^+$, [Val]$^+$, and [Leu]$^+$), halogen anions ([Cl]$^-$, [Br]$^-$, [BF$_4$]$^-$, and [PF$_6$]$^-$), and clusters (GlyCl)$_n$ (n = 1–5) at the B3LYP-DFT and MP2 levels of theory. Unlike the conventional ILs, the novel GlyCl-type amino acid ILs (AAILs) favour the interaction of its cationic part, rather than its anionic part, with the surrounding H_2O molecules.

Wagle et al.[234] elucidated the molecular interactions, charge transfer interactions, and the thermodynamics associated with three pure DESs by QC calculations. Studies of the effect of water on the DES systems, based on QC calculations are not reported.

3.3 Advanced experimental methods

Experimental methods, such as IR, Raman, NMR, X-ray, UV and neutron scattering, have been carried out to explore the molecular structure and behaviour of IL/DES–H_2O binary systems (Table 6). Again, a major part of the research is on the conventional imidazolium- and pyridinium-based ILs, and some work is on TSILs and DESs.

Zhang et al.[235] applied two-dimensional (2D) IR spectroscopy to investigate the dilution process of [Emim][BF$_4$] in H_2O. It shows that, with the addition of H_2O, the cohesion between cation and anion becomes weak. During the dilution process, the three-dimensional (3D) network structure of pure ILs is gradually destroyed into ion-clusters, the ion-cluster is then further dissociated into ion-pairs surrounded by H_2O, and the ion-pairs surrounded by H_2O become dominant with a relatively high amount of H_2O. Ultimately, the ion-pairs surrounded by H_2O may be dissociated into fully hydrated and separated ions. However, within the investigated compositional range (x_{water} from 0.02 to 0.9), the IL has not been completely dissociated into ions. Mele et al.[236] studied the structure of [Bmim][BF$_4$] with/without trace amount of water by NMR spectroscopy through intermolecular nuclear overhauser enhancements to present a direct experimental evidence of the interactions (i.e. cation–cation, cation–H_2O, and cation–anion interactions). The water content investigated in their work is from 0 to 0.52 in the mole fraction of water. The results show that the presence of water makes the cation–cation association looser and water can act as HBD towards [BF$_4$]$^-$. The IL structure is appreciably changed with the increase of water content, and the IL still exists as tight ion-pairs with small amounts of water. For [Bmim][BF$_4$]–H_2O system, Almásy et al.[237] investigated the structure by small-angle

Table 6 Spectroscopic studies used to explore the interaction in the IL/DES–H_2O binary systems

Cation	Anion	Methods	Ref.
ILs			
[Emim]$^+$	[BF$_4$]$^-$	2-D vibrational spectroscopy	235
[Emim]$^+$	[Cl]$^-$	Small-angle neutron scattering	238
[Bmim]$^+$	[BF$_4$]$^-$, [Br]$^-$	UV absorption spectrophotometry	239
[Omim]$^+$	[Br]$^-$	UV absorption spectrophotometry	239
[Bmim]$^+$	[BF$_4$]$^-$	NMR spectroscopy	236
[Bmim]$^+$	[BF$_4$]$^-$	Small-angle neutron scattering	237
[Bmim]$^+$	[Cl]$^-$, [Br]$^-$, [I]$^-$, [BF$_4$]$^-$	Raman Spectroscopy	244
[Bmim]$^+$	[PF$_6$]$^-$, [SbF$_6$]$^-$[ClO$_4$]$^-$, [(CF$_3$SO$_2$)$_2$N]$^-$, [NO$_3$]$^-$, [CF$_3$CO$_2$]$^-$	ATR-IR spectroscopy	240
[Emim]$^+$	[NTf$_2$]$^-$ and [EtSO$_4$]$^-$	FTIR spectroscopy and DFT	243
[Bmim]$^+$	[NTf$_2$]$^-$	PGSE NMR	242
[Bpy]$^+$	[BF$_4$]$^-$	Infrared spectroscopy and DFT	245
[Cho]$^+$	[Lac]$^-$, [Prop]$^-$ and [Mal]$^-$	^{1}H NMR	246
[TEA]$^+$	[MeSO$_3$]$^-$	FIR spectroscopy and DFT	247
[N$_{0002}$]$^+$	[C$_3$CO$_2$]$^-$	X-ray scattering	248
[Bmim]$^+$,[Emim]$^+$	[MeSO$_4$]$^-$	NMR spectroscopy	164
[DEMA]$^+$	[MeSO$_3$]$^-$	NMR, Raman, Infrared spectroscopy	259
DESs			
ChCl/Gly (1:2), ChCl/EG (1:2), ChCl/urea (1:2)		FTIR absorbance and Raman spectroscopy	249
ChCl/urea (1:2)		Neutron scattering	252
ChCl/Gly (1:2), ChCl/EG (1:2), ChCl/urea (1:2)		PFG-NMR	251
ChCl/EG (1:2)		FTIR and Raman spectroscopy	216

8702 | Chem. Soc. Rev., 2018, 47, 8685–8720

This journal is © The Royal Society of Chemistry 2018

neutron scattering. They strongly suggested that the system is close to phase separation at $x_{IL} \approx 0.075$. For [Emim][Cl]–H$_2$O system, the investigation by using small-angle neutron scattering technique shows that [Emim][Cl] is homogenously dissolved in water, which is mainly caused by a strong hydration of [Cl]$^-$ by water.[238] Zhang et al.[239] investigated the aggregation of the imidazolium-based ILs ([Bmim][BF$_4$], [Bmim][Br] and [Omim][Br]) in water by UV absorption spectrophotometry with x_{IL} from 5.62×10^{-7} to 0.062 (i.e $x_{water} > 0.94$). Three transformations (α, β and γ) at different IL contents occur within the investigated compositional range. In the very dilute IL solutions (x_{IL} from 0 to α), the anions and imidazolium cations are almost "free", and H-bonds are dominant among the hydrated ions. After that, a floating hydrogen-bonded network with 3D structure starts to form, and the association among anions and cations occurs to form ion-pairs. When reaching another transformation point (β), the coulombic and aliphatic interactions become dominant to form IL aggregation. The longer the alkyl-chain length and the smaller the anion, the easier the formation of IL-aggregates in the second transformation region. With a further increase of the IL content, the number of the IL-aggregates increases and, finally, an IL quasi-structure is formed at the γ transformation point.

Using the attenuated total reflection and transmission infrared (ATR-IR) spectroscopy, Cammarata et al.[240] investigated the behaviour of H$_2$O in the ILs with [Bmim]$^+$ and the anions of [PF$_6$]$^-$, [SbF$_6$]$^-$, [BF$_4$]$^-$, [ClO$_4$]$^-$, [(CF$_3$SO$_2$)$_2$N]$^-$, [NO$_3$]$^-$ and [CF$_3$CO$_2$]$^-$. They concluded that the anion is responsible for the interaction between IL and H$_2$O. Besides, for [NO$_3$]$^-$ and [CF$_3$CO$_2$]$^-$, H$_2$O forms aggregates or a kind of associations in the IL–H$_2$O system, similar to hydrated ions in the aqueous electrolyte solutions.[241] Rollet et al.[242] studied the self-diffusion of [Bmim][NTf$_2$] in H$_2$O ranging from 0.03 to 0.3 (saturation) in mole fraction of water using the pulsed gradient spin-echo NMR (PGSE NMR) method. It was found that the anion and cation show comparable self-diffusion coefficients, indicating that the anion and cation are associated with one another strongly and move together largely. The shielding effect of H$_2$O on the electrostatic interactions leads to a decrease of IL cohesion, resulting in a decrease of the viscosity.

Combining FTIR spectroscopy and DFT calculations, Köddermann et al.[243] found that, for [Emim][NTf$_2$] and [Emim][EtSO$_4$], when the mass concentration of water is below 1 wt%, single H$_2$O molecules can be embedded into the IL environment and no H$_2$O clusters exist. This means that the H$_2$O molecules are isolated from one another, interacting only with the IL in the IL-rich region. Singh et al.[244] investigated the ILs with [Bmim]$^+$ and different anions ([Cl]$^-$, [Br]$^-$, [I]$^-$, or [BF$_4$]$^-$) as well as their aqueous mixtures (x_{water} from 0 to 1) with Raman spectroscopy and dispersion-corrected DFT. It was found that, for the ILs with the anions [Cl]$^-$, [Br]$^-$, or [I]$^-$, the structure changes significantly with the increase of water content, while for [Bmim][BF$_4$], no significant change in the structure was observed due to the strong cation–anion interaction. At low IL concentrations, a complete dissociation of IL into cation and anion by the water disruption is indicated. Wang et al.[245]

elucidated the H-bonding between H$_2$O and pyridinium-based IL ([BPy][BF$_4$]) using the IR spectroscopy and DFT calculations, and a strong anion–H$_2$O–anion complex and a new H-bond with the aromatic C–H on [BPy]$^+$ can be formed. While for the imidazolium-based ILs, the strong anion–cation interaction and a steric hindrance from the alkyl chains prevent the H$_2$O molecules forming H-bonds with the aromatic C–H on the cation. The study from Khan et al.[232] indicates that the increase of the molar volume, i.e. increase the alkyl chain length on the cation of ILs, can lead to a decrease of their ability to form H-bonds with H$_2$O based on the experimental observation on the increase of the blue shift in the IR spectra for the alkyl-methyl-imidazolium chloride–H$_2$O binary systems.

For the hydrophobic ILs, for example, [C$_n$mim][NTf$_2$], the water solubility is only up to 1.8 wt%. At the water concentrations below 1 wt%, the H$_2$O molecules are embedded in the IL environment and no water clusters exist.[243] According to the self-diffusion coefficients, Rollet et al.[242] proposed that the hydrophobicity of [NTf$_2$]$^-$ prevents H$_2$O being incorporated into the ILs and then dissociating the ILs into ion-pairs. Meanwhile, H$_2$O is not homogeneously mixed with the IL and thus forms small aggregates (i.e. [Bmim][NTf$_2$] + several H$_2$O molecules or H$_2$O + several [Bmim][NTf$_2$] molecules), and the size of the H$_2$O cluster increases with increasing H$_2$O content.

For the TSILs, Patinha et al.[246] investigated the solvation scheme for 3 cholinium carboxylate IL–H$_2$O binary systems ([Cho][Lac]–H$_2$O, [Cho][Prop]–H$_2$O, [Cho][Mal]–H$_2$O) by performing ^{1}H NMR studies. Both the cation and anion interact with H$_2$O, but the anion does more strongly. For the IL–H$_2$O binary systems with the cholinium cation and the small carboxylate anion, it is feasible to form the domains of hydrophobic clusters. Combining FIR spectroscopy and DFT calculations, Peter et al.[247] studied the ion speciation for [TEA][MeSO$_3$] in water. The results show a significant decrease of contact ion-pairs in the mixture with increasing water concentration. A minimum of 4 water molecules are needed to initiate the transition process from contact ion-pairs to solvent-separated ion-pairs. Salma et al.[248] investigated the effect of water on the nano-structural organization of [N$_{0002}$][C$_3$CO$_2$] (i.e. so-called EAB) using a small- and wide-angle X-ray scattering where the water is from 0 to 0.91 in mole fraction. There are two peaks, i.e. pre-peak and principle peak, for pure EAB. By adding water, the pre-peak moves towards lower transferred-momentum (Q) values, while the principal peak approaches larger Q values. The pre-peak shifting to the lower Q values comes from the strong H-bond interaction between water and the polar ends of IL-cation and -anion, and it indicates that the H-bond interaction between water and EAB ions (i.e. [N$_{0002}$]$^+$ and [C$_3$CO$_2$]$^-$) leads to a progressive disruption of the cation–anion coulombic interaction.

Mechanistic study on DES–H$_2$O system has also been conducted by Pandey et al.[249] who studied the effects of temperature and the addition of H$_2$O on the solvatochromic probe behaviour using the FTIR absorbance and Raman spectroscopy. Compared with the conventional ILs, as more components are involved in DESs, the interactions are more complex. For pure DES, a 3D intermolecular H-bonding network has been confirmed.[250]

This journal is © The Royal Society of Chemistry 2018

Chem. Soc. Rev., 2018, 47, 8685–8720 | 8703

According to the results of Pandey et al.,[249] for ChCl/urea $(1:2)$ or so-called reline, the addition of H_2O definitely helps to form inter-species H-bonding. However, with the addition of H_2O, the overall H-bonding landscape will not alter much. For the different DESs, i.e. ChCl/Gly $(1:2)$ or so-called glyceline, ChCl/EG $(1:2)$ or so-called ethaline, and reline, the H-bonding between H_2O and ethaline or glyceline is more pertinent compared with that between H_2O and reline. For the ethaline- and glyceline-based DESs, the H-bonding among inter-species appears to be important in their aqueous solutions. While for reline, the interstitial accommodation of H_2O appears to be dominant. D'Agostino et al.[251] used the pulsed field gradient (PFG) NMR to probe self-diffusion of molecular and ionic species in the choline chloride (ChCl)-based DESs–H_2O binary systems. The self-diffusion of water in the studied DES–H_2O binary systems is considerably higher than that in the homogeneous bulk liquid water, which strongly suggests that the studied DES–H_2O solutions are not homogeneous but contain distinct microscopic water-rich phases after a significant amount of water is added. In addition, it was also found that when water is added to the solutions, their viscosities decrease but a discontinuity is observed for all the studied systems at the point corresponding to 1:1 mole equivalent of $H_2O:[Cl]^-$. Hammond et al.[252] studied the effect of water on the nano-structure of ChCl/urea $(1:2)$ with neutron scattering and empirical potential structure refinement (EPSR). The results show that the interactions in this DES are weakened by the addition of water, but the solution still remains the nature of pure-DES even at high w_{H_2O} (up to 40.95%). When w_{H_2O} reaches the overcrowding point (50.98%), i.e. $x_{water} = 0.833$, the DES component will be fully solvated by water, and the system changes to an aqueous solution. For a DES–H_2O binary mixture, Ahmadi et al.[216] investigated the character of the ChCl/Gly $(1:2)$ system in the presence of water by combining FTIR and Raman spectroscopy. They found that for this DES, the association of water with DES reaches a maximum at $x_{water} \approx 0.9$, proposing that the DES–H_2O interaction is dominant and over the DES–DES interaction. During the hydration process, the nature of DES is preserved instead of the nature of the constituent (i.e. glycerol), which also implies that the DES–H_2O mixture is unique compared with the organic solvent mixtures.

Several investigations have found that pure ILs can exhibit a nanoscale spatial heterogeneity, i.e. nano-phase separation on the nanoscopic level due to the separation of polar/non-polar domains,[253,254] and such polar/non-polar nano-phase separation can also occur in IL–H_2O mixtures which can be reflected by the observation of the structural regimes with different amounts of water using MD simulation as we mentioned above.[217–221] Based on the MD simulation results, some research groups studied the glass transition for the IL–H_2O systems by analyzing the Differential Thermal Analysis (DTA) trace and Raman spectra.[255–258] For $[DEME][BF_4]$–H_2O system,[255] the glass-transition temperature (T_g) varies with the water content (x_{water}), which implies that this homogeneous solution may separate into a polar-rich phase and a nonpolar-rich phase. Based on the features in the glassy state, it has presumed that the presence of water may

enhance the nano-phase separation and the 'nearly-free state' of H_2O molecules may trigger the transition. The turning point of phase transition for this $[DEME][BF_4]$–H_2O solution is around $x_{water} = 0.96$. Moreover, the glass transition behaviour has also been demonstrated for the $[DEME][I]$–H_2O[256] and $[Bmim][BF_4]$–H_2O.[257] It shows that the glass-formation region depends on the cation and anion of ILs, for example, for $[DEME][I]$–H_2O,[256] the region is $x_{water} < 0.95$, while it is $x_{water} < 0.9$ for $[Bmim][BF_4]$–H_2O.[257] Therefore, as a special solvent, the IL–H_2O homogeneous solutions may behave as different nano-phases on nanoscopic level. The presence of H_2O molecules may in this case enhance the micro-heterogeneity in the IL–H_2O mixtures.

Based on these experimental methods, the molecular structure and behaviour of IL/DES–H_2O binary systems can be explored. In addition, these techniques can also be used to evaluate "ionicity", which is an effective fraction of ions available to participate in conduction and an evaluation of the fraction of free charges at a specific temperature. Andanson et al.[164] studied the ionic association and interactions in ILs ($[Bmim][MeSO_4]$ and $[Emim][MeSO_4]$) with the addition of water. In this work, based on the diffusion coefficients measured by NMR spectroscopy, the molar conductivity was obtained with the Nernst–Einstein equation. The ionicity was quantitatively obtained by calculating the ratio between the molar conductivity based on the results from NMR and those directly measured experimentally. It shows that for these two ILs, their ionicity is around 0.4–0.6, and there is no obvious increase in ionicity with an increase of water content until $x_{water} > 0.8$. From these observations, they concluded that when $x_{water} < 0.8$, there is no major modification of the structure and the ionic association occurs despite of the strong decrease of the viscosity occurs. Yaghini et al.[259] studied how the added water affects the transport properties, the local coordination, and the thermal behaviour of $[DEMA][MeSO_3]$ by NMR, Raman and infrared spectroscopy. The results show that water interacts primarily with the anion and slightly affects the ionicity of IL. The ionicity at $x_{water} \approx 0$–0.57 in their work was measured with the same method as Andanson et al.[164] The changes on the ionicity with the addition of water are limited to 0.55–0.65, and only a slight increase in the ionicity is observed by adding water. In addition, the ionicity can also be assessed qualitatively with the Walden plot of log (molar conductivity) versus log (reciprocal viscosity) by comparing the lines of IL–H_2O mixtures with that of 0.01 M aqueous KCl solution.[166]

3.4 Thermodynamic analysis

Thermodynamic analysis can also be performed to study the interaction in the IL–H_2O binary systems indirectly. Katayangi et al.[260] studied the mixing schemes for IL–H_2O systems and compared with the NaCl–H_2O system by calorimetric analysis at 298.15 K. It was found that at the infinitely dilute solution of IL, the IL molecules break away from their pure environment and settle in the H_2O environment presumably as separated ions. A complete dissociation of ion-pairs only takes place when the content of IL is extremely low, for example, 0.015 (x_{IL}) for $[Bmim][BF_4]$ and 0.013 (x_{IL}) for $[Bmim][I]$. The anion $[I]^-$ in

8704 | Chem. Soc. Rev., 2018, 47, 8685–8720

This journal is © The Royal Society of Chemistry 2018

[Bmim][I] is hydrated by H$_2$O although the hydration is much weaker compared with aqueous NaCl solutions. However, the [BF$_4$]$^-$ in [Bmim][BF$_4$] may not be hydrated by H$_2$O at all or only partially. With increasing the IL concentration, the IL-ions begin to organize themselves, directly or in an H$_2$O-mediated manner. When the x_{IL} is high, such as $x_{IL} = 0.5$–0.6, IL exists as clusters similar to pure ILs. Using the similar method, Miki et al.[261] studied 1-propanol-[Bmim][Cl]–H$_2$O system. They find that the effect of [Bmim]$^+$ is similar when the temperature is increased, which means that the effect of [Bmim]$^+$ is to reduce the global average of the H-bond probability of bulk H$_2$O. They provided circumstantial evidence that the IL is dissociated below a certain threshold. When the IL concentration is higher than this threshold, the IL-ions start to attract one another. They suggested that, in the H$_2$O-rich region, the hydration "structure" is similar to the structure of D-fructose. The net effect of this hydration "structure" is to reduce the probability of forming H-bonds in the bulk H$_2$O away from solutes.

Seddon et al.[262] studied the effects of impurities and additives (e.g. H$_2$O, [Cl]$^-$ and other co-solvents) on the properties of [C$_n$mim]$^+$-based ILs. The [Cl]$^-$ impurities present in ILs can be from the unreacted materials, i.e. dissolved NaCl or AgCl (metathesis), or reactant, i.e. HCl to form acid–base reaction. The results of volumetric properties show that the same pattern is observed at different temperatures although the volumetric expansion from the ideal behaviour increases with increasing temperature. They found that the anion has a primary effect on the H$_2$O miscibility and the cation has a secondary effect. Those so-called hydrophobic ILs are in fact hygroscopic. The interaction between H$_2$O and [Bmim][BF$_4$] was further investigated. It was suggested that H$_2$O is accommodated inside the IL structure in the IL-rich region ($0.5 < x_{IL} < 1$) by forming H-bonds with both cation and anion, leading to a decrease of electrostatic attraction between the anion and cation and thereby a decrease of viscosity. Further addition of H$_2$O ($x_{IL} < 0.5$) may result in completely solvated ions and the appearance of the H$_2$O molecules without H-bonds to the other species (i.e. the so-called "free H$_2$O"[263]).

Gardas et al.[264] measured the density, the speed of sound and the osmotic coefficients for ILs ([Emim][Br], [Emim][Cl]) in the dilute concentration at different temperatures. The volumetric analysis shows that the changes of the apparent molar volume with concentration are different from those for an aqueous solution of alkali halides, but similar to those for aqueous solutions of tetraalkylammonium salts. This implies that the cation has a great effect on the properties of the solutions. The values of the limiting apparent molar volume appear to increase linearly with increasing temperature, indicating the weakening of ion-solvent interactions.[265] By analyzing osmotic and activity data, the hydration numbers for [Emim][Br] and [Emim][Cl] with the values of 1.78 and 2.3, respectively, were obtained, which are smaller compared with the values for alkali halides. They assumed that the decreased hydration number of anions was because the cations do not get hydrated. The estimated excess partial molar entropies within the studied compositional range ($x_{IL} = 0$–0.004) indicate that ion-pair formation is favored over the hydration of ions.

Rumyantsev et al.[266] investigated the peculiarities in the structural organization of DESs based on carboxybetaine (betaine) as a function of water at temperatures from 243 to 360 K by using the activation thermodynamics, IR spectroscopic measurements and QC calculations. The viscosity at different temperatures was used to obtain the activation thermodynamic parameters, such as entropy (ΔS_A), enthalpy (ΔH_A), and free energy (ΔG_A) based on the Frenkel–Eyring–Kobeko relation. The results show that the values of $T \cdot \Delta S_A$ do not change significantly with temperature for the investigated DESs, i.e. the betaine- and choline-based DESs. However, for the betaine-based DES, $T \cdot \Delta S_A$ drops sharply with the increase of w_{H_2O} from 5 to 20% and increases sharply with the increase of w_{H_2O} from 30 to 40%. This observation is peculiar compared with the linear change with w_{H_2O} for the choline-based DES (ChCl/urea (1 : 2)). Combining the QC calculation and IR spectroscopy reveals a formation of strong H-bond complexes between betaine and water.

Reid et al.[267] used the Kirkwood–Buff theory of solutions to quantify the interaction for 6 IL–H$_2$O solutions. The studied ILs are protic ILs (PILs): [DMEtA][Pr] and [DMEtA][NTf$_2$] and aprotic ILs (AILs): [Emim][OTf], [Emim][BF$_4$], [Bmim][BF$_4$], and [Cho][NTf$_2$], and the concentrations of water are from 0 to 0.5 in mole fraction. It shows that at these concentrations, the strength of ion–ion interaction is not significantly affected by the presence of water for the PIL. Although the strong H$_2$O–H$_2$O interactions were observed in the PILs, the solution remains stable as a homogeneous phase other than phase split.

Wang et al.[158] measured the electrical conductivity of 8 ILs in various solvents including H$_2$O and studied their ion association and solvation, and the measurement was performed in the successively diluted solutions. They claimed that the association of [C$_n$mim][Br] in H$_2$O relates to not only the electrostatic interactions between the cation and anion but also the hydration strength of cation. The weak hydration of the cation leads to an enhanced association between the cation and anion (larger k_A). They compared the results for the ILs with the anions of [Br]$^-$, [BF$_4$]$^-$ and [PF$_6$]$^-$, finding that the association constant k_A in H$_2$O is lowest for the ILs with [Br]$^-$ due to the strong hydration of [Br]$^-$. While for the ILs with [BF$_4$]$^-$ and [PF$_6$]$^-$, their association constants k_A in H$_2$O are similar under the vacuum conditions because of the weak or non-existing hydration for these two anions.

To infer the atomistic/molecular properties, the molecular thermodynamic models such as the perturbed chain-statistical associating fluid theory (PC-SAFT) can be used, and the conceptual framework will be useful in order to extend the molecular thermodynamic models to the IL/DES–H$_2$O binary systems. In the next section (3.5), the observed mechanisms from our analysis of the current literature are summarized and used for a new conceptual framework for further modelling work at molecular level.

3.5 Summing-up

Many investigations have been conducted both theoretically and experimentally to study the molecular behaviour of IL/DES–H$_2$O systems, however, most of the work is focused

This journal is © The Royal Society of Chemistry 2018

Chem. Soc. Rev., 2018, 47, 8685–8720 | 8705

on the conventional ILs. For the DESs and novel ILs, such as TSILs and AAILs, the work is still limited. It shows that the mechanisms for DESs and novel ILs are much more complicated due to the highly-complex and heterogeneous liquid structures themselves. More research needs to be carried out to obtain a molecular level picture to rationalize the structure that is formed and the driving forces behind. It is found that, except AAILs, water usually connects more tightly with anions than cations, and the hydration of anions frequently takes place. Usually, small anions (*e.g.* halide ions) are fully hydrated at the infinitely dilute IL/DES solution, large anions (*e.g.* $[BF_4]^-$) are only partially hydrated, and hydrophobic anions (*e.g.* $[NTf_2]^-$) interact with water but do not behave like a normal hydration. For some particular ILs, glass transition has been demonstrated, which means that there is a special phase change in these IL–H_2O binary systems on a nanoscopic level.

Based on the results on conventional IL–H_2O and typical DES–H_2O systems, the observed mechanisms can be summarized in a simplified way as shown in Fig. 6a and b. The general schematic mechanisms of NaCl–H_2O system are depicted in Fig. 6c for comparison. Note that our intention is to illustrate the mechanisms upon the addition of water, and in Fig. 6, both the cation and anion for NaCl are represented as spherical particles with different sizes, while, for IL, each cation is represented as an asymmetric particle concerning their large size and asymmetry, but each anion is still represented as a spherical particle.

As shown in Fig. 6a, the pure IL is a supercluster with three-dimensional structure network (I). Upon the addition of H_2O,

(1) When the amount of H_2O is low, the H_2O molecules mix well with IL with strong interactions (van der Waals, H-bonds, electrostatic, *etc.*), and H_2O is embedded inside and at the periphery of the IL without any H_2O clusters formed (Fig. 6a, region II). This is similar to the mixed solvents.

(2) With a further addition of H_2O, the IL clusters start to dissociate into individual ions or ion-pairs and the dissociated ions are gradually hydrated (Fig. 6a, region III).

(3) When the amount of H_2O becomes very high, the IL structures are completely dissociated as ions (Fig. 6a, region IV). Depending on the size of the IL-ions, some of them are fully hydrated, while some are partially hydrated. This is partially similar to the aqueous electrolyte solutions (*e.g.* aqueous NaCl solution), in which all the ions in a dilute solution are fully hydrated as described in Fig. 6c (region III).

Comparing the conventional IL–H_2O systems with aqueous electrolyte (*e.g.* NaCl) solutions, the main differences are on:

(a) For IL–H_2O systems, IL itself can be a solvent with specific properties, for example, the dielectric constants can be as high as 86,[268] and the content of IL can be in the range of 0–100%; for aqueous NaCl solutions, no pure NaCl solution can exist at all under the same condition, and the concentration of NaCl can only go up to a certain range (saturated solubility $x_{sat.}$), *i.e.* the content of NaCl can be in the range of 0–$x_{sat.}$.

(b) For IL–H_2O systems, the size of the ions are regularly much larger compared with Na^+ or Cl^-. Even in a very dilute solution,
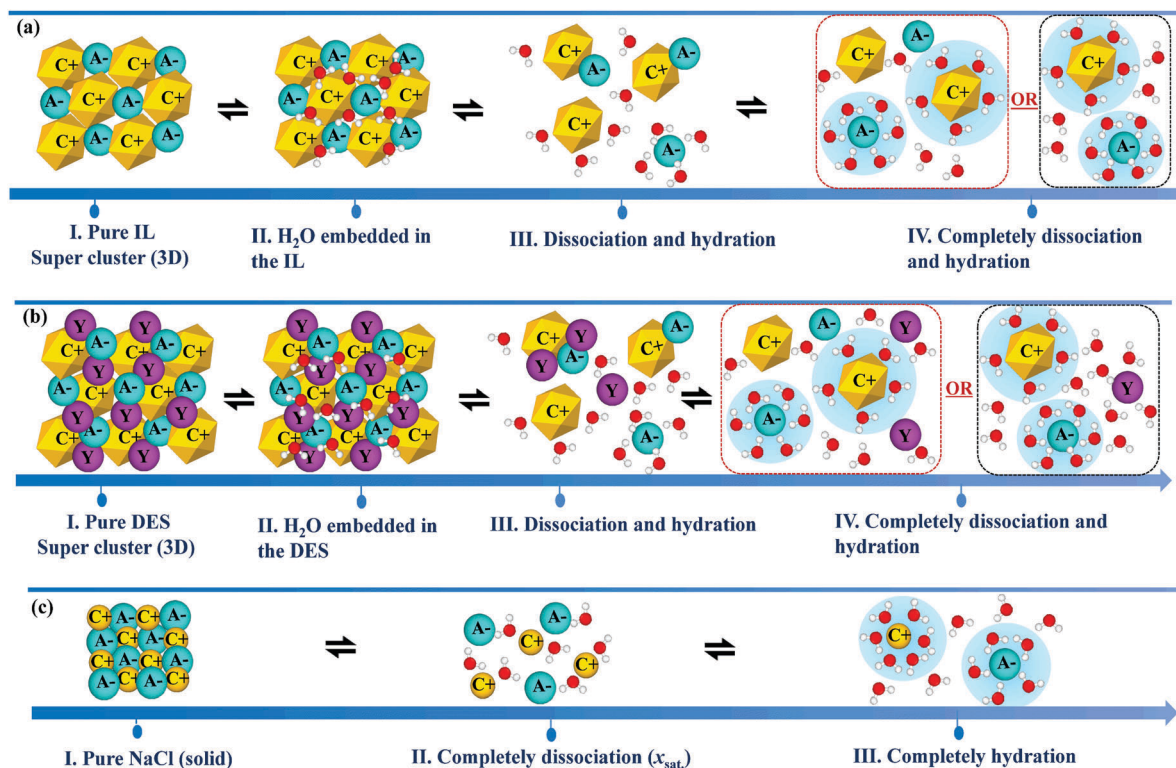

Fig. 6 The general schematic mechanism for (a) the conventional IL–H_2O systems (b) the typical DES–H_2O systems (c) NaCl–H_2O systems. Note: the yellow, blue, red and purple ones represent cation, anion, H_2O and HBD, respectively.

some large IL-ions can only be partially hydrated (Fig. 6a, region IV); for aqueous NaCl solutions, in a dilute solution, all the ions are fully hydrated (Fig. 6c, region III).

(c) For IL–H_2O systems, in general, the hydration of the IL–anions is more pronounced compared with the IL-cations; for aqueous NaCl solutions, the hydration of the cation is more pronounced compared with the anion.

(d) For IL–H_2O systems, the association is dominant even the concentration of IL is not so high; for aqueous NaCl solutions, NaCl is dissociated completely.

Even though DES is widely identified as either a new class of ILs or IL analogues, IL and DES are distinctly different as a solvent system. ILs are usually described as a general formula of CA. While for DES, the general formula is CA·nY, where Y and n refer to the HBD and the number of Y molecules interacting with the anion, respectively. As we can see from Fig. 6b, for the DES–H_2O system, the mechanism is similar to that for IL–H_2O (Fig. 6a), while it becomes more complex due to the presence of a neutral compound (Y or HBD), besides cation and anion for DES itself. In addition, the comparison of the differences between water solutions of DES and individual components from DES with water is an interesting topic. However, more work needs to be carried out to collect sufficient information for a through and comprehensive review in this topic.

4. Further analysis of IL/DES–H_2O binary systems

There have been many studies based on determining the physico-chemical properties of IL/DES–H_2O binary systems and the mechanistic analyses summarized in Sections 2 and 3. The conventional ILs, TSILs and DESs were primarily studied and the focus is on physicochemical properties while detailed mechanistic studies over varied concentration intervals are limited. Based on the summary of the experimental data (Section 2) and mechanistic studies (Section 3), six typical and widely-studied IL/DES–H_2O binary systems ([Bmim][I]–H_2O, [Bmim][BF$_4$]–H_2O, [Emim][BF$_4$]–H_2O, [Emim][EtSO$_4$])–H_2O, ChCl/urea (1:2)–H_2O, and ChCl/Gly (1:2)–H_2O were chosen to map the key experimental observations to the corresponding results obtained from mechanistic studies (Table 7).

Fig. 7 shows the comparison of the macroscopic-properties of these 6 IL–H_2O binary systems. For [Bmim][I], some research work has shown a complete hydration of [I]$^-$ in the infinitely

dilute IL solution.[147,165,260] MD simulations show that when the mole fraction of water is above 0.25, the ion–H_2O interactions are stronger than those between cation–anion. This can be reflected by the rapid increase of Λ (Fig. 7a). When the mole fraction of IL is 0.12, the association degree is only 0.075, which corresponds to the peak of the electrical conductivity as we can see from Fig. 7a. [Emim][BF$_4$] or [Bmim][BF$_4$] is a typical type of IL with large anions, and it cannot be completely dissociated even when the mole fraction of water is up to 0.9. This can be seen from Fig. 7b that the peak of Λ is located at around 0.95. This observation agrees well with the results from the simulation and thermodynamic analysis that [BF$_4$]$^-$ is not hydrated or partially hydrated in the dilute IL solutions.[210] For the [BF$_4$]-based ILs, when the cation is changed from [Bmim]$^+$ to [Emim]$^+$, the peak of Λ will be shifted to left (IL-rich region), which means that the maximum Λ appears at a lower mole fraction of water. This implies that the cation will also affect the association of IL. This observation agrees with the results from the QC calculations that an increase of the molar volume of the ions may result in a decrease of the ability to form H-bonds.[232] In addition, the maximum Λ of [Emim][BF$_4$] is found in the solution at a low mole fraction of water around 0.86, and this is in line with the results from the mechanistic analysis that the intruding water cannot completely dissociate ILs into ions even when the mole fraction of water is up to 0.9. Based on the above analysis, we can conclude that Λ can establish a link between the macroscopic-properties and the microstructure of IL–H_2O systems.

We have also compared other properties of these 6 systems. For [Bmim][BF$_4$]–H_2O and [Bmim][I]–H_2O, the shapes and values of V^E do not vary much. This is because the effective molar volume of [I]$^-$ (48.7 cm^3 mol^{-1}) is almost the same as that of [BF$_4$]$^-$ (53.4 cm^3 mol^{-1}),[275] while there is a negative region for [Bmim][I]–H_2O when the mole fraction of water is between 0.9 to 1. This phenomenon may be the reflection from the hydration of [I]$^-$. Meanwhile, for the ILs with a same anion (e.g. [BF$_4$]$^-$), when the cation is changed from [Bmim]$^+$ to [Emim]$^+$, the values of η^E, V^E and H_m also change greatly. This implies that the type of cation also affects the properties of IL–H_2O binary systems because of the relative competition between cation–H_2O and cation–anion interactions.

MD simulations show that for a very dilute IL solution ($x_{water} = 0.996$), 60% [Emim][EtSO$_4$] molecules can be dissociated into isolated ions, and water clearly decreases the electrostatic interaction energy between the cation and anion by shielding. Therefore, we can conclude that when the IL is infinitely diluted,

Table 7 Six typical IL/DES–H_2O systems for further study

ILs & DESs	Experimental data				Mechanistic study		
	V^E	η^E	Λ	H_m	MD/MC	QC	Advanced experiments
[Bmim][BF$_4$]	144	145	161	194 and 197	210	—	237 and 244
[Bmim][I]	269	147	147 and 165	—	147 and 165	—	244
[Emim][BF$_4$]	270	—	161, 167, 271 and 272	190	—	227 and 228	235 and 273
[Emim][EtSO$_4$]	134 and 274	134	161	187 and 188	209	—	—
ChCl/urea (1:2)	71	71	79	184	79	—	249, 251 and 252
ChCl/Gly (1:2)	77 and 85	85	—	183	—	—	249 and 251

This journal is © The Royal Society of Chemistry 2018
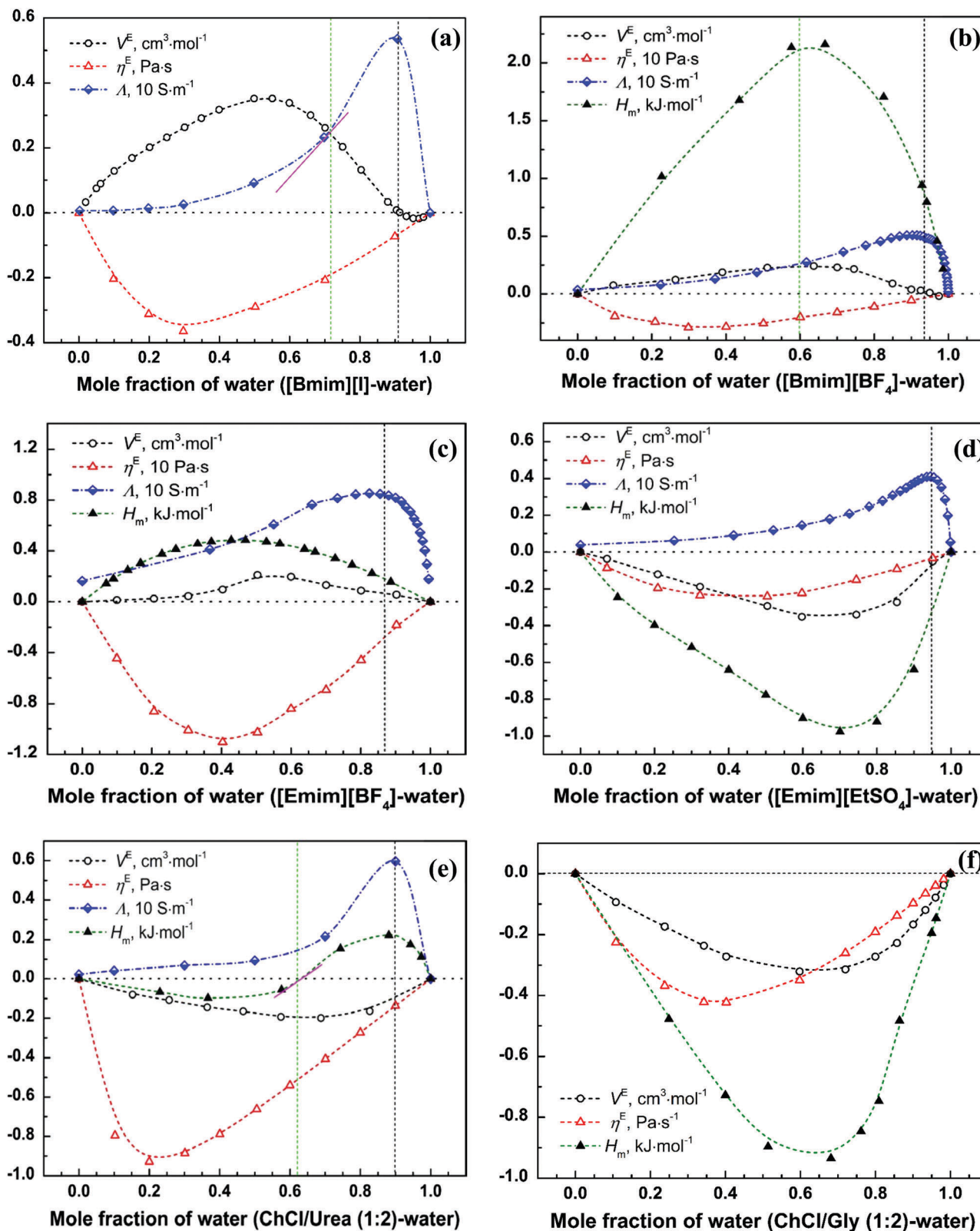
Chem. Soc. Rev., 2018, 47, 8685–8720 | 8707

Fig. 7 The physicochemical properties of 6 typical IL–H$_2$O binary systems. (a) [Bmim][I]; (b) [Bmim][BF$_4$]; (c) [Emim][BF$_4$]; (d) [Emim][EtSO$_4$]; (e) ChCl/urea (1 : 2); (f) ChCl/Gly (1 : 2).

the dissociated ions will be hydrated. The MD simulations also proposed two percolation limits: 0.8 and 0.95 of water in mole fraction,[209] and these two percolation limits can reflect the minimum points of V^E and H_m, respectively.

For the two chosen DESs, both of them contain $[Cl]^-$ which is usually hydrated in aqueous solutions. The simulations show that at a low water fraction (mass fraction of 0.1 or mole fraction of 0.33), $[Cl]^-$ prefers H_2O more than urea, and thus urea molecules tend to associate together. The typical macroscopic-property, *i.e.* the enthalpy of mixing, also shows a maximum energy release at the mole fraction of water around 0.35. In addition, the mass fraction of water at around 0.25 (mole fraction around 0.6) is a turnover point, where the DES (*i.e.* ChCl/urea $(1:2)$) is sufficiently dissociated and hydrated, and the enthalpy of mixing H_m changes from exothermic to endothermic. When urea is replaced by glycerol, the H-bonding between water and DES changes, which is reflected by the values of V^E, η^E and H_m. However, the mole fraction of water at around 0.6 is still a typical turnover point at where the mixture behaviour of DESs in water changes. Based on the mechanistic study from Hammond *et al.*,[252] they concluded that when $x_{water} = 0.833$, the DES components are preferable to be fully hydrated, and the nanostructure of this system changes from mixed-solvents to aqueous "electrolyte" solutions. This turning point may reflect the maximum points of Λ and H_m.

As we can see from Fig. 7, for each IL or DES, the excess or mixing properties are quite complex, and their shapes and values show that these binary systems are far different from ordinary binary solvent mixtures. For different properties, the dominant factors may be different, and thus the minimum or maximum positions in composition are quite different. For example, the minimum or maximum position in composition for excess viscosity is in the IL/DES-rich region, while that for excess volume is in the water-rich region. Some researchers interpreted that the positive excess volume is due to the breaking of the cation–anion network structure by the anion-hydration effect.[165] This explanation may be somewhat unreasonable. For example, the V^E values for $[Bmim][BF_4]$ and $[Emim][BF_4]$ are positive, however, the anions in these two ILs cannot be hydrated or can only be partially hydrated at the dilute solutions, therefore, the anion-hydration is only one of the reasons, while the structure and size of the anion can also be the reasons to affect the volumetric properties. If we further compare the experimental V^E in Fig. 8 for the ILs with the anions of $[I]^-$, $[Br]^-$ and $[Cl]^-$, it follows the order: $[I]^- > [Br]^- > [Cl]^-$. Since all these anions will be hydrated, it is reasonable to conclude that the anion-hydration has a negative effect on the value of V^E. In addition, the size of the cation also has an effect on the value of V^E, the larger the size, the higher the V^E value, as we can see from the V^E values of $[Bmim][I]$ and $[Hmim][I]$ (Fig. 8).

The electrical conductivity Λ can reflect both the dissocia-tion and association of ILs/DESs. According to the experimental results, we can find that the maximum Λ is always for the solutions with water at around 0.9 to 1 (mole fraction). In this water-rich region, IL/DES is highly dissociated, and isolated ions are formed. Compared the ILs that can be fully hydrated (*e.g.* $[Bmim][I]$) with those ILs cannot completely hydrated (*e.g.* $[Bmim][BF_4]$), the curves of electrical conductivity Λ do not have a noticeable difference. This means that, based on the electrical conductivity Λ, we can only get an indication of possible
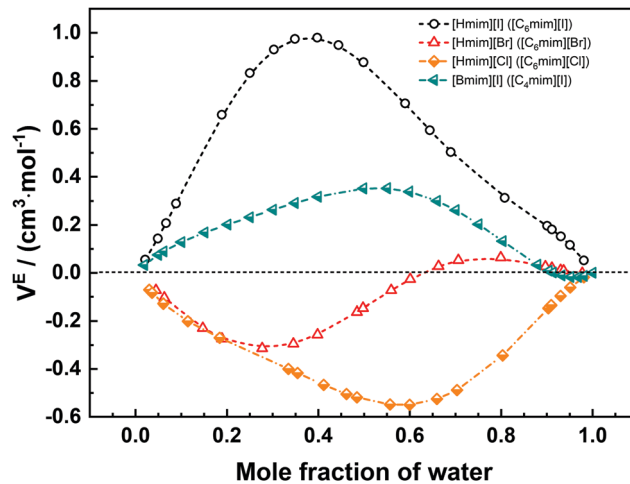

Fig. 8 The effect of anion or cation on the value of V^E.

association/dissociation, while it is difficult to tell that the dissociated ions will be fully or partially hydrated or show no hydration at all. In this case, molecular simulations are needed in order to obtain the threshold and hydration numbers.

In summary, to some extent, η^E, V^E, H_m, and Λ can reflect the complex interaction in IL/DES–H_2O binary systems, however, in order to develop a model to describe the dissociation and hydration of IL in water, Λ is more important. To get the threshold of complete dissociation and the hydration numbers of IL in water, MD or MC simulations are needed.

5. Modelling of IL–H₂O binary systems based on molecular thermodynamics

Thermodynamic models have been developed to describe the properties of pure ILs, treating the ILs as either neutral molecules or completely dissociated ions.[276–280] In the case of aqueous electrolyte solutions, two types of models have typically been developed: the excess Gibbs energy (G^E) and equation of state (EoS) models. The G^E models are used to describe the excess properties of mixtures in the liquid phase, and seldom consider pressure. The EoS approach can be used to describe the proper-ties of pure components as well as the excess properties of mixtures in both vapor (or gas) and liquid phases, and does take pressure into consideration.

IL/DES–H_2O binary systems resemble aqueous electrolyte solutions, however, there has been minimal thermodynamic modelling of such systems because of their complexity. Most of the models developed to date are for aqueous IL solutions (*i.e.* the concentration of IL is from infinitely dilute to a certain concentration) and are primarily based on EoS models. Typical examples include the perturbed chain-statistical associating fluid theory (PC-SAFT), the binding mean spherical approximation (BiMSA), hetero-segmented SAFT and non-random hydrogen-bonding (NRHB). Only one work, conducted by Simoni *et al.*,[281] was based on the electrolyte non-random two-liquid (eNRTL) approach, which is a G^E model.

5.1 Aqueous ILs

The model developed by Mahato et al.[282] is based on PC-SAFT, in which the IL was modelled as a molecule without ionic interactions, and the model parameters were fitted to the density of the pure ILs and the vapor pressure of IL–H_2O mixtures. The studied ILs are $[C_n mim][NTf_2]$ (n = 2 to 8). In the model developed by Papaiconomou et al.[283] based on the BiMSA, the IL was described as being weakly associated, the association constant was set as an adjustable parameter, and the osmotic coefficient was used in parameter fitting. The studied ILs are $[C_n mim]^+$ with the anions of $[Cl]^-$, $[Br]^-$, $[MeSO_4]^-$ and $[EtSO_4]^-$ and n is from 2 to 8. The hetero-segmented SAFT,[279,284,285] in which the IL was completely dissociated into cations and anions, was extended to describe the properties of aqueous ILs by using temperature-dependent segment energy of the cation head. The studied ILs are $[C_n mim][Cl]$ and $[C_n mim][Br]$. Based on PC-SAFT, Shahriari et al.[286] studied the thermodynamic properties of aqueous ILs involving ions of $[C_n mim]^+$, $[(CH_3)_4N]^+$, $[(C_2H_5)_4N]^+$, $[Cl]^-$, $[Br]^-$, $[MeSO_4]^-$, $[EtSO_4]^-$ and $[BF_4]^-$. In modelling, the IL was completely dissociated into cations and anions, and the mean spherical approximation (MSA) was used to describe the long-range ion–ion interactions. The association interaction was used to account for the formation of ion-pairs. In the square-well chain fluid with variable range (SWCF-VR) model proposed by Li et al.,[287] it was assumed that ion-pairs as well as free cations and anions can coexist in the solution, and both the short-range and long-range interactions were considered in the model. The long-range electrostatic interactions between ions were described by MSA model. The model parameters were fitted to the properties of aqueous ILs, rather than those

for pure ILs. A non-electrolyte equation of state model, the NRHB model, was used to describe the phase behaviour of $[C_n mim][NTf_2]$–H_2O system, in which the IL was modeled as a neutral molecule without long-range ionic interactions.[288]

5.2 IL–H_2O with a wide compositional range

Models have been developed to study the properties of IL–H_2O binary system in its whole compositional range. One is based on eNRTL conducted by Simoni et al.[281] In their modelling, IL was completely dissociated into cation and anion, and the studied ILs include $[Emim][EtSO_4]$, $[Emim][OTf]$, and $[Emim][TFA]$. eNRTL belongs to G^E model, and the properties of pure ILs cannot be obtained. The other model is based on the COSMO model where the IL was modelled as both in the ionic state and in the ion-pair state with a degree of dissociation parameter α.[289] The properties of vapor pressure, activity coefficients, and osmotic coefficients for the IL–H_2O binary systems based on the ILs with $[C_n mim]^+$ were studied, but not for other thermodynamic properties, such as mixing enthalpy, excess volume, etc.

5.3 New framework for modelling IL/DES–H_2O binary systems

IL/DES–H_2O binary systems are unique compared with either mixed solvents or aqueous electrolyte solutions. This makes it essential to develop a new model for IL/DES–H_2O systems instead of using the model for aqueous electrolyte solutions or for the common mixed solvents directly. The incorporation of association and hydration is important in a new model development. Based on the mechanistic studies, we propose a framework to model the IL/DES–H_2O systems (Fig. 9).
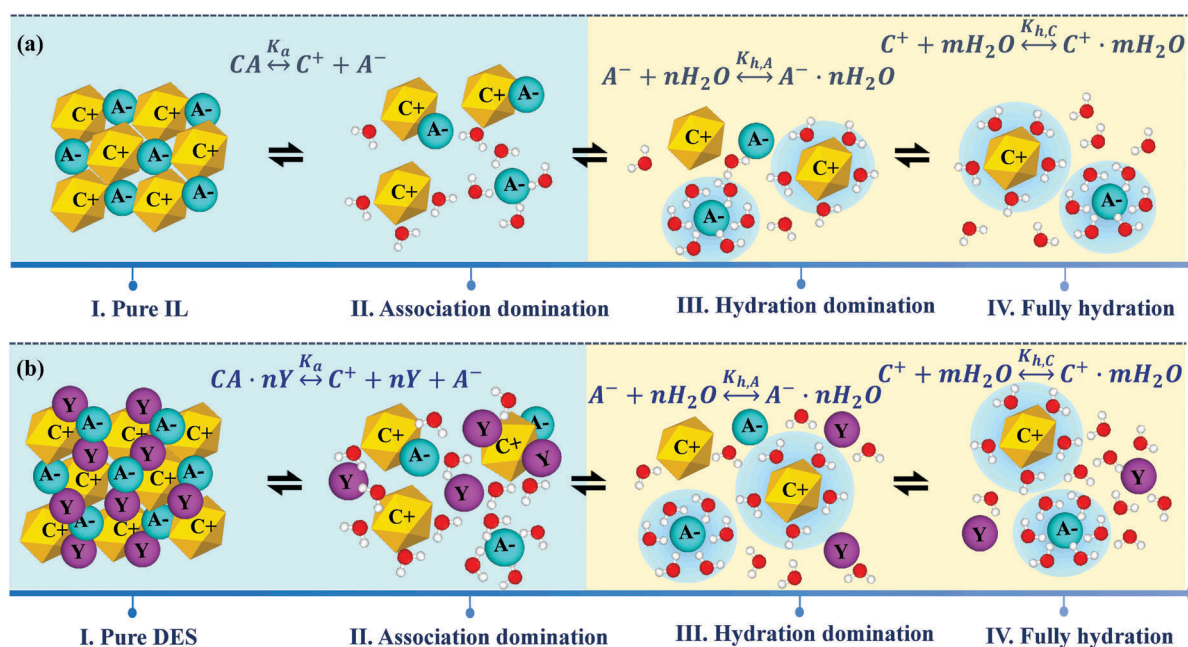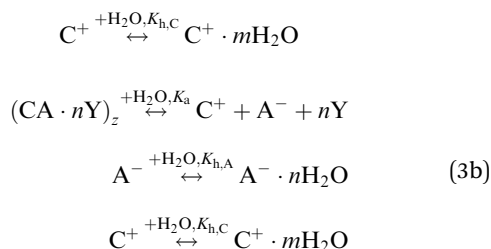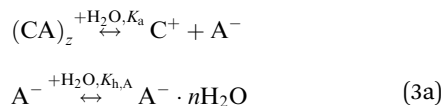

Fig. 9 Conceptual scheme and framework to model (a) the IL–H_2O system (b) the DES–H_2O system. Note: the yellow, blue, red and purple ones represent cation, anion, H_2O and HBD, respectively.

8710 | Chem. Soc. Rev., 2018, 47, 8685–8720

This journal is © The Royal Society of Chemistry 2018

Both the association equilibrium and hydration equilibrium exist in IL–H_2O (eqn (3a)) and DES–H_2O (eqn (3b)) systems

$$(CA)_z \overset{+H_2O, K_a}{\longleftrightarrow} C^+ + A^-$$

$$A^- \overset{+H_2O, K_{h,A}}{\longleftrightarrow} A^- \cdot nH_2O \qquad (3a)$$

$$C^+ \overset{+H_2O, K_{h,C}}{\longleftrightarrow} C^+ \cdot mH_2O$$

$$(CA \cdot nY)_z \overset{+H_2O, K_a}{\longleftrightarrow} C^+ + A^- + nY$$

$$A^- \overset{+H_2O, K_{h,A}}{\longleftrightarrow} A^- \cdot nH_2O \qquad (3b)$$

$$C^+ \overset{+H_2O, K_{h,C}}{\longleftrightarrow} C^+ \cdot mH_2O$$

where CA and CA·nY represent the neutral IL and DES, respectively, C^+ and A^- are the cation and anion of the IL/DES, respectively, Y and n refer to the HBD and the number of Y molecules that interacts with the anion, respectively, K_a, $K_{h,A}$ and $K_{h,C}$ are the equilibrium constants for association, anion hydration and cation hydration, respectively, and $C^+ \cdot mH_2O$ and $A^- \cdot nH_2O$ are the hydrated cation and hydrated anion, respectively.

The framework to model the IL/DES–H_2O system includes 4 regions: pure IL/DES (I), association domination (II), hydration domination (III) and fully hydration (IV).

In region II, there is either a neutral CA or CA·nY in the system, and some of the dissociated ions are hydrated. Both the association and hydration equilibria exist. However, association is dominating.

In region III, almost all the ILs/DESs are completely dissociated and the dissociated ions are completely or partially hydrated. Both association and hydration equilibria exist. However, the hydration is dominating.

In region IV, almost all the cations and anions are hydrated. There are only hydration equilibria. In addition, the hydration of cation may be ignored according to the mechanistic study.

For clarity, only a few IL/DES and water molecules are shown in Fig. 9 to introduce the concept. As we mentioned above, each cation is represented as an asymmetric particle concerning the large size and asymmetry, but each anion is represented as a spherical particle (Fig. 9). For a DES–H_2O system, the framework is similar to that for IL–H_2O, while the model is more complex due to the existence of another neutral compound besides cation and anion for DES itself.

6. Conclusions and perspectives

A comprehensive review of IL/DES–H_2O binary systems has been presented. The available experimental data of physicochemical properties, including density, viscosity, electrical conductivity and enthalpy of mixing, was compiled, analyzed and discussed. Density and viscosity are the most widely measured properties. The electrical conductivity and excess/mixing enthalpy have also been attracted a lot attention but the number of investigated ILs is still limited. Surface and interfacial tensions over a whole compositional range at different temperatures are

still scarce. The shapes and magnitudes of the excess volume, excess viscosity and enthalpy of mixing used to study the non-ideal behaviour have been quantitatively summarized. These characteristic shapes can be qualitatively described as single hump, positive double hump, negative double hump or S-shape depending on the interaction landscape and changes in solution structures upon varying the water concentration. The shapes of these excess properties for IL/DES–H_2O binary systems and the magnitudes (amplitudes) of these shapes are modified with variations in the size and type of cation or anion, and with changes in physical parameters, i.e. temperature and pressure. This implies that the properties of the mixtures are unique and at the same time largely unpredictable. In addition, the electrical conductivity values of IL/DES–H_2O binary systems over a wide compositional range generally exhibit a maximum value at a relatively low IL concentration, which is unique, compared with other solutions, such as aqueous electrolyte solutions and mixed organic solvents.

Mechanistic studies of IL/DES–H_2O systems based on MD/MC simulations, QC calculations, advanced experimental techniques and thermodynamic analyses were also surveyed, to better understand the manner in which H_2O interacts with ILs/DESs. Various structure-forming mechanisms were identified on this basis. Specifically, pure ILs are evidently composed of heterogeneous super-clusters having 3D network structures. The addition of H_2O drastically modifies this microstructure. Both dissociation and hydration should be considered when modelling such systems and, in the case of an infinitely dilute IL/DES solution, the IL/DES can be assumed to be completely dissociated. According to the sizes of the IL/DES ions, they may be fully or partially hydrated.

Six typical IL/DES–H_2O systems were chosen to further study the link between the macro-properties (as indicated by experimental results) and the microstructures of molecules (as determined by mechanistic studies). This examination demonstrates that the values of η^E, V^E, H_m and Λ all reflect the complex interactions in IL/DES–H_2O systems to some extent, and that Λ is the most important variable in terms of developing a reliable model considering the dissociation and hydration of such systems. In addition, MD/MC simulations are required to obtain parameters for the complete dissociation thresholds and the hydration numbers of IL/DES-ions in water.

Thermodynamic models, developed to describe the properties of IL/DES–H_2O systems, were also reviewed. An IL/DES is assumed to be a "neutral molecule" or to be composed of completely dissociated ions in the currently developed thermodynamic models. The majority of these models are for aqueous IL/DES solutions (i.e. the concentration of IL/DES from infinitely dilute to a certain concentration) and are typically based on an equation of state approach. The dissociation of the IL/DES is sometimes considered, but ion hydration is seldom taken into account. Based on the mechanistic studies reviewed herein, we have suggested a new conceptual framework including the dissociation of the IL/DES and ion hydration for the modeling of IL/DES–H_2O systems ranging from a pure IL/DES to infinitely dilute IL/DES solutions.

In the future, the thermodynamic modelling based on this proposed conceptual framework by combining the molecular interaction from MD/MC simulations with experimental data including density, viscosity, electrical conductivity and enthalpy of mixing, *etc.* will be of great interest and meaningful to the many practical applications of IL/DES-based technology. Compared with IL–H_2O binary system, the DES–H_2O binary systems are more complex and more work needs to be carried out to reveal the differences between water solutions of DES and individual components from DES with water.

Abbreviations

ILs & DESs

DESs

ChCl/EG (1 : 2)	Choline chloride : ethylene glycol (1 : 2)
ChCl/Gluc (2 : 1)	Choline chloride : glucose (2 : 1)
ChCl/Gly (1 : 2)	Choline chloride : glycerol (1 : 2)
ChCl/LA (1 : 2)	Choline chloride : lactic acid (1 : 2)
ChCl/MA (1 : 1)	Choline chloride : malonic acid (1 : 2)
ChCl/TG (1 : 2)	Choline chloride : triethylene glycol (1 : 2)
ChCl/urea (1 : 2)	Choline chloride : urea (1 : 2)
$CrCl_3$/ChCl (1 : 2)	Chromium(III) chloride : Choline chloride (1 : 2)
$CrCl_3$/ChCl (1 : 2.5)	Chromium(III) chloride : Choline chloride (1 : 2.5)
DEAC/EG (1 : 2)	*N,N*-Diethylethanol ammonium chloride : ethylene glycol (1 : 2)
DEAC/Gly (1 : 2)	*N,N*-Diethylethanol ammonium chloride : glycerol (1 : 2)
ATPPB/DEG (1 : 4)	Allyltriphenyl phosphonium bromide-diethylene glycol (1 : 4)
ATPPB/DEG (1 : 10)	Allyltriphenyl phosphonium bromide-diethylene glycol (1 : 10)
ATPPB/DEG (1 : 16)	Allyltriphenyl phosphonium bromide-diethylene glycol (1 : 16)

Imidazolium-based ILs

[Amim][Cl]	1-Allyl-3-methyl-imidazolium chloride
[BDBU][IM]	8-Butyl-1,8-diazabicyclo[5,4,0]-undec-7-enium imidazolide
[Bdmim][BF_4]	1-Butyl-2,3-dimethylimidazolium tetrafluoroborate
[Bmim][Ac]	1-Butyl-3-methylimidazolium acetate
[Bmim][BF_4]	1-Butyl-3-methylimidazolium tetrafluoroborate
[Bmim][Br]	1-Butyl-3-methylimidazolium bromide
[Bmim][Cl]	1-Butyl-3-methylimidazolium chloride
[Bmim][DCA]	1-Butyl-3-methylimidazolium dicyanamide
[Bmim][DMP]	1-Butyl-3-methylimidazolium dimethylphosphate
[Bmim][Ac]	1-Butyl-3-methylimidazolium acetate
[Bmim][HCOO]	1-Butyl-3-methylimidazolium formate
[Bmim][HSO_4]	1-Butyl-3-methylimidazolium hydrogensulfate

[Bmim][I]	1-Butyl-3-methylimidazolium iodide
[Bmim][L-lactate]	1-Butyl-3-methylimidazolium L-lactate
[Bmim][EtCOO]	1-Butyl-3-methylimidazolium propionate
[Bmim][$MeSO_3$]	1-Butyl-3-methylimidazolium methanesulfonate
[Bmim][$MeSO_4$]	1-Butyl-3-methylimidazolium methylsulphate
[Bmim][TCM]	1-Butyl-3-methylimidazolium tricyanomethanide
[Bmim][OTf]	1-Butyl-3-methylimidazolium trifluoromethanesulfonate
[Bmim][TOS]	1-Butyl-3-methylimidazolium tosylate
[Bmim][PF_6]	1-Butyl-3-methylimidazolium hexafluorophosphate
[Bmim][SCN]	1-Butyl-3-methylimidazolium thiocyanate
[Bmim][NTf_2]	1-Butyl-3-methylimidazolium bis(trifluoromethane sulfonyl)imide
[Bmim][TCB]	1-Butyl-3-methylimidazolium tetracyanoborate
[C_4C_2im][Br]	1-Butyl-3-ethylimidazolium bromide
[C_4C_1mim][Cl]	1-Butyl-2,3-dimethylimidazolium chloride
[Mim][Cl]	1-Methylimidazolium chloride
[Emim][Ac]	1-Ethyl-3-methylimidazolium acetate
[Emim][BF_4]	1-Ethyl-3-methyl imidazolium tetrafluoroborate
[Emim][$BuSO_4$]	1-Ethyl-3-methylimidazolium butylsulphate
[Emim][DCA]	1-Ethyl-3-methylimidazolium dicyanamide
[Emim][DEP]	1-Ethyl-3-methylimidazolium diethylphosphate
[Emim][DMP]	1-Ethyl-3-methylimidazolium dimethylphosphate
[Emim][$EtSO_4$]	1-Ethyl-3-methylimidazolium ethylsulphate
[Emim][$HexSO_4$]	1-Ethyl-3-methylimidazolium hexylsulphate
[Emim][HSO_4]	1-Ethyl-3-methylimidazolium hydrogensulfate
[Emim][L-lactate]	1-Ethyl-3-methylimidazolium L-lactate
[Emim][$MeSO_3$]	1-Ethyl-3-methylimidazolium methanesulfonate
[Emim][$MeSO_4$]	1-Ethyl-3-methylimidazolium methylsulphate
[Emim][$OcSO_4$]	1-Ethyl-3-methylimidazolium octylsulphate
[Emim][OTf]	1-Ethyl-3-methylimidazolium trifluoromethanesulfonate
[Emim][PF_6]	1-Ethyl-3-methylimidazolium hexafluorophosphate
[Emim][SCN]	1-Ethyl-3-methylimidazolium thiocyanate
[Emim][TCM]	1-Ethyl-3-methylimidazolium tricyanomethanide

[Emim][NTf$_2$]	1-Ethyl-3-methylimidazolium bis(trifluoromethanesulfonyl)imide
[Emim][TFA]	1-Ethyl-3-methylimidazolium trifluoroacetate
[Emim][Glyci]	1-Ethyl-3-methylimidazolium,glycinate
[Emim][Et$_2$PO$_4$]	1-Ethyl-3-methylimidazolium diethylphosphate
[Emim][Br]	1-Ethyl-3-methylimidazolium bromide
[Emim][Cl]	1-Ethyl-3-methylimidazolium chloride
[HDBU][IM]	8-Hydrogen-1,8-diazabicyclo[5,4,0]-undec-7-enium imidazolide
[Hmim][Br]	1-Hexyl-3-methyl imidazolium bromide
[Hmim][BF$_4$]	1-Hexyl-3-methyl imidazolium tetrafluoroborate
[Hmim][Br]	1-Hexyl-3-methyl imidazolium bromide
[Hmim][Cl]	1-Hexyl-3-methyl imidazolium chloride
[Hmim][I]	1-Hexyl-3-methyl imidazolium iodide
[Hmim][OTf]	1-Hexyl-3-methyl imidazolium trifluoromethanesulfonate
[Mmim][Cl]	1,3-Dimethylimidazolium chloride
[Mmim][DMP]	1,3-Dimethylimidazolium dimethylphosphate
[Mmim][MeSO$_4$]	1,3-Dimethylimidazolium methylsulphate
[Mmim][PF$_6$]	1,3-Dimethylimidazolium hexafluorophosphate
[OHemim][TFA]	1-(2-Hydroxyethyl)-3-methylimidazolium trifluoroacetate
[Omim][BF$_4$]	1-Octyl-3-methyl imidazolium tetrafluoroborate
[Omim][Br]	1-Octyl-3-methylimidazolium bromide
[Omim][Cl]	1-Octyl-3-methylimidazolium chloride
[Omim][NO$_3$]	1-Octyl-3-methylimidazolium nitrate
[Pmim][Cl]	1-Pentyl-3-methylimidazolium chloride
[C$_7$mim][Cl]	1-Heptyl-3-methylimidazolium chloride
[C$_{10}$mim][Br]	1-Decyl-3-methylimidazolium bromide
[C$_{10}$mim][Cl]	1-Decyl-3-methylimidazolium chloride
[C$_{12}$mim][Br]	1-Dodecyl-3-methylimidazolium bromide
[TMG][IM]	1,1,3,3-Tetramethylguanidine imidazolide
[C$_{20}$H$_{28}$N$_3$O$_3$][Br]	L-Histidine derived imidazolium bromide
[C$_{20}$H$_{28}$N$_3$O$_3$][NTf$_2$]	L-Histidine derived imidazolium bis(trifluoromethanesulfonyl)imide

Pyridinium-based ILs

[B$_2$mPy][BF$_4$]	1-Butyl-2-methylpyridinium tetrafluoroborate
[B$_2$mPy][Cl]	1-Butyl-2-methylpyridinium chloride
[B$_3$mPy][BF$_4$]	1-Butyl-3-methylpyridinium tetrafluoroborate
[B$_3$mPy][Cl]	1-Butyl-3-methylpyridinium chloride
[B$_4$mPy][BF$_4$]	1-Butyl-4-methylpyridinium tetrafluoroborate
[B$_4$mPy][Cl]	1-Butyl-4-methylpyridinium chloride
[B$_4$mPy][SCN]	1-Butyl-4-methylpyridinium thiocyanate
[BPy][BF$_4$]	1-Butylpyridinium tetrafluoroborate
[BPy][Cl]	1-Butylpyridinium chloride
[OcPy][BF$_4$]	1-Octylpyridinium tetrafluoroborate
[PPy][BF$_4$]	1-Propylpyridinium tetrafluoroborate
[EPy][MeSO$_3$]	1-Ethylpyridinium methanesulfonate

Pyrrolidinium-based ILs

[BmPyr][DCA]	1-Butyl-1-methylpyrrolidinium dicyanamide
[Bmpyr][Cl]	1-Butyl-1-methylpyrrolidinium chloride
[BmPyr][SCN]	1-Butyl-1-methylpyrrolidinium thiocyanate
[B$_4$mPyr][Br]	1-Butyl-4-methylpyrrolidinium bromide
[Empyr][EtSO$_4$]	1-Ethyl-1-methylpyrrolidinium ethylsulfate
[Empyr][Ac]	1-Ethyl-1-methylpyrrolidinium acetate
[Empyr][Glyc]	1-Ethyl-1-methylpyrrolidinium glycolate
[Epmpyr][Cl]	N-Methyl-N-(2′,3′-epoxypropyl)-2-oxopyrrolidinium chloride
[Epmpyr][Ac]	N-Methyl-N-(2′,3′-epoxypropyl)-2-oxopyrrolidinium acetate
[Epmpyr][SAL]	N-(2′,3′-Epoxypropyl)-N-methyl-2-oxopyrrolidinium salicylate
[Pe$_5$myrr][Br]	1-Pentyl-5-methylpyrrolidinium bromide
[Pyrr][C$_7$CO$_2$]	Pyrrolidinium octanoate
[Pyrr][HCOO]	Pyrrolidinium formate
[Pyrr][HSO$_4$]	Pyrrolidinium hydrogensulfate
[Pyrr][NO$_3$]	Pyrrolidinium nitrate
[P$_3$myrr][Br]	1-Propyl-3-methylpyrrolidinium bromide
[C$_3$C$_1$pyr][PF$_6$]	1-Methyl-1-propylpyrrolidinium hexafluorophosphate

Piperidinium-based ILs

[Empip][EtSO$_4$]	1-Ethyl-1-methyl-piperidiniumethylsulfate
[Bmpip][Cl]	1-Butyl-1-methylpiperidinium chloride
[Bmpip][SCN]	1-Butyl-1-methylpiperidinium thiocyanate
[Bmpip][DCA]	1-Butyl-1-methylpiperidinium dicyanamide
[C$_3$C$_1$pyr][PF$_6$]	1-Methyl-1-propylpiperidinium Hexafluorophosphate

Piperazinium-based ILs

| [(OH)$_2$C$_2$pi][EtCOO] | N-(2-Hydroxyethyl)piperazinium Propionate |
| [MP][Glyci] | Methyl-piperazinium glycinate |

Guanidinium-based ILs

[(C$_2$)$_{22}$(C$_1$)$_2$(C$_1$)$_{23}$gu][EtSO$_4$]	2,2-diethyl-1,1,3,3-tetramethylguanidinium ethylsulfate
[TMG][BEN]	Tetramethylguanidinium benzoate
[TMG][SAL]	Tetramethylguanidinium salicylate
[TMG][Lac]	1,1,3,3-Tetramethylguanidinium Lactate

Morpholinium-based ILs

| [Emmor][EtSO$_4$] | 1-Ethyl-1-methylmorpholinium ethylsulfate |

[Emmor][Ac]	1-Ethyl-1-methyl-morpholinium acetate
[Emmor][Pro]	1-Ethyl-1-methylmorpholinium propionate
[Emmor][Glyc]	1-Ethyl-1-methylmorpholinium glycolate

Collidinium-based ILs

| [Col][HCOO] | Collidinium formate |

Cholinium-based ILs

[Cho][Lac]	Choline lactate
[Cho][Prop]	Choline propanoate
[Cho][Mal]	Choline malonate
[Cho][Glyc]	Choline glycolate
[Cho][NTf$_2$]	Cholinium bis(trifluoromethanesulfonyl)imide
[Cho][Glyci]	Cholinium glycinate
[Cho][H$_2$Prop]	Choline dihydrogen phosphate

Ammonium-based ILs

[BA][Ac]	N-Butylammonium acetate
[BA][NO$_3$]	N-Butylammonium nitrate
[DEMA][MeSO$_3$]	Diethylmethylammonium methanesulfonate
[DEMA][OTf]	Diethylmethylammonium trifluoromethanesulfonate
[TEA][MeSO$_3$]	Triethylammonium methanesulfonate
[DIPEA][HCOO]	Diisopropyl-ethylammonium formate
[DEME][BF$_4$]	N,N-Diethyl-N-methyl-N-(2-methoxyethyl) ammonium tetrafluoroborate
[DEME][I]	N,N-Diethyl-N-methyl-N-(2-methoxyethyl) ammonium iodide
[EA][NO$_3$]	Ethylammonium nitrate
[MTEOA][MeSO$_4$]	Tris(2-hydroxyethyl) methylammonium methylsulfate
[PA][NO$_3$]	Propylammonium nitrate
EAB/[N$_{0002}$][C$_3$CO$_2$]	Ethylammonium butanoate
2-HDEAH	2-Hydroxy diethylammonium hexanoate
2-HEAB	2-Hydroxy ethylammonium butanoate
2-HEAH	2-Hydroxy ethylammonium hexanoate
2-HEAP	2-Hydroxy ethylammonium pentanoate
3HPAAc	3-Hydroxypropylammonium acetate
3HPAF	3-Hydroxypropylammonium formate
3HPATFAc	3-Hydroxypropylammonium trifluoroacetate
BHEAC	Bis(2-hydroxyethyl)ammonium acetate
CPL-TBABr	Caprolactam tetrabutyl ammonium bromide
CPL-TBACl	Caprolactam tetrabutyl ammonium chloride
CPL-TBAF	Caprolactam tetrabutyl ammonium fluorine
M2HEAPr	N-Methyl-2-hydroxyethylammonium propionate
PAAc	Propylammonium acetate
PAF	Propylammonium fromate
TMEAC	Tris(monoethanolamine) citrate

[N$_{4444}$][PF$_6$]	Tetrabutylammonium hexafluorophosphate
[DMEtA][Pr]	N,N-Dimethylethanolammonium propionate
[DMEtA][NTf$_2$]	N,N-Dimethylethanolammonium bis(trifluoromethanesulfonyl)imide
[CyN$_{1,1}$PrSO$_3$H][Tos]	N,N-Dimethyl-N-(3-sulfopropyl)-cyclohexylammonium tosylate

Phosphonium-based ILs

[aP$_{4443}$][Ala]	(3-Aminopropyl) tributylphosphonium L-α-aminopropionic acid salt
[aP$_{4443}$][Val]	(3-Aminopropyl) tributylphosphonium L-α-aminoisovaleric acid salt
[aP$_{4443}$][Leu]	(3-Aminopropyl) tributylphosphonium L-α-amino-4-methylvaleric acid salt
[P$_{6,6,6,14}$][BOB]	Trihexyltetradecylphosphonium bis(oxalato)-borate
[P$_{2444}$][DEP]	Ethyl(tributyl)phosphonium diethylphosphate
[P$_{4444}$][PF$_6$]	Tetrabutylphosphonium hexafluorophosphate

Quinolinium-based ILs

| [HiQuin][SCN] | N-Hexylisoquinolinium thiocyanate |
| [C$_8$iQuin][SCN] | N-Octylisoquinolinium Thiocyanate |

Advanced experimental methods

IR	Infrared
NMR	Nuclear magnetic resonance
FTIR	Fourier-transform infrared spectroscopy
ATR-IR	Attenuated total reflection and transmission infra-red
PGSE	Pulsed gradient spin-echo
FIR	Far-infrared
UV	Ultraviolet
PFG	Pulsed field gradient

Conflicts of interest

There are no conflicts to declare.

Acknowledgements

8714 | Chem. Soc. Rev., 2018, 47, 8685–8720

This journal is © The Royal Society of Chemistry 2018

References

1 K. Binnemans, *Chem. Rev.*, 2007, **107**, 2592–2614.

2 Z. Lei, B. Chen, Y.-M. Koo and D. R. MacFarlane, *Chem. Rev.*, 2017, **117**, 6633–6635.

3 E. L. Smith, A. P. Abbott and K. S. Ryder, *Chem. Rev.*, 2014, **114**, 11060–11082.

4 L. A. Blanchard, D. Hancu, E. J. Beckman and J. F. Brennecke, *Nature*, 1999, **399**, 28–29.

5 X. Zhang, X. Zhang, H. Dong, Z. Zhao, S. Zhang and Y. Huang, *Energy Environ. Sci.*, 2012, **5**, 6668–6681.

6 X. Zhang, L. Bai, S. Zeng, H. Gao, S. Zhang and M. Fan, in *Energy Efficient Solvents for CO₂ Capture by Gas-Liquid Absorption: Compounds, Blends and Advanced Solvent Systems*, ed. W. M. Budzianowski, Springer International Publishing, Cham, 2017, pp. 153–176.

7 C. Ye, W. Liu, Y. Chen and L. Yu, *Chem. Commun.*, 2001, 2244–2245.

8 I. Minami, *Molecules*, 2009, **14**, 2286.

9 F. Zhou, Y. Liang and W. Liu, *Chem. Soc. Rev.*, 2009, **38**, 2590–2599.

10 R. P. Swatloski, S. K. Spear, J. D. Holbrey and R. D. Rogers, *J. Am. Chem. Soc.*, 2002, **124**, 4974–4975.

11 S. P. Magalhaes da Silva, A. M. da Costa Lopes, L. B. Roseiro and R. Bogel-Lukasik, *RSC Adv.*, 2013, **3**, 16040–16050.

12 J. A. Sirviö, M. Visanko and H. Liimatainen, *Biomacromolecules*, 2016, **17**, 3025–3032.

13 M. Pan, G. Zhao, C. Ding, B. Wu, Z. Lian and H. Lian, *Carbohydr. Polym.*, 2017, **176**, 307–314.

14 Y.-L. Loow, T. Y. Wu, G. H. Yang, L. Y. Ang, E. K. New, L. F. Siow, J. Md. Jahim, A. W. Mohammad and W. H. Teoh, *Bioresour. Technol.*, 2018, **249**, 818–825.

15 W. Xing, G. Xu, J. Dong, R. Han and Y. Ni, *Chem. Eng. J.*, 2018, **333**, 712–720.

16 D. J. G. P. van Osch, L. J. B. M. Kollau, A. van den Bruinhorst, S. Asikainen, M. A. A. Rocha and M. C. Kroon, *Phys. Chem. Chem. Phys.*, 2017, **19**, 2636–2665.

17 X. Zhang and D. Hu, *Appl. Therm. Eng.*, 2012, **37**, 129–135.

18 E.-S. Abumandour, F. Mutelet and D. Alonso, *Appl. Therm. Eng.*, 2016, **94**, 579–589.

19 E. D. Bates, R. D. Mayton, I. Ntai and J. H. Davis, *J. Am. Chem. Soc.*, 2002, **124**, 926–927.

20 G. Cui, J. Wang and S. Zhang, *Chem. Soc. Rev.*, 2016, **45**, 4307–4339.

21 X. Li, M. Hou, B. Han, X. Wang and L. Zou, *J. Chem. Eng. Data*, 2008, **53**, 548–550.

22 S. Sarmad, J.-P. Mikkola and X. Ji, *ChemSusChem*, 2017, **10**, 324–352.

23 S. Sarmad, Y. Xie, J.-P. Mikkola and X. Ji, *New J. Chem.*, 2017, **41**, 290–301.

24 E. I. Ahmed, A. P. Abbott and K. S. Ryder, *AIP Conf. Proc.*, 2017, **1888**, 020006.

25 A. P. Abbott, E. I. Ahmed, R. C. Harris and K. S. Ryder, *Green Chem.*, 2014, **16**, 4156–4161.

26 K.-S. Kim, B.-K. Shin, H. Lee and F. Ziegler, *Fluid Phase Equilib.*, 2004, **218**, 215–220.

27 D. Zheng, L. Dong, W. Huang, X. Wu and N. Nie, *Renewable Sustainable Energy Rev.*, 2014, **37**, 47–68.

28 R. Abedin, S. Heidarian, J. C. Flake and F. R. Hung, *Langmuir*, 2017, **33**, 11611–11625.

29 L. Chen, M. Sharifzadeh, N. Mac Dowell, T. Welton, N. Shah and J. P. Hallett, *Green Chem.*, 2014, **16**, 3098–3106.

30 M. C. C. Ribeiro, *J. Phys. Chem. B*, 2012, **116**, 7281–7290.

31 P. Cozma, W. Wukovits, I. Mămăligă, A. Friedl and M. Gavrilescu, *Clean Technol. Environ. Policy*, 2015, **17**, 373–391.

32 S. Xia, G. A. Baker, H. Li, S. Ravula and H. Zhao, *RSC Adv.*, 2014, **4**, 10586–10596.

33 C. J. de la Parra, J. R. Zambrano, M. D. Bermejo, A. Martin, J. J. Segovia and M. J. Cocero, *J. Chem. Thermodyn.*, 2015, **91**, 8–16.

34 A. Podgoršek, J. Jacquemin, A. Pádua and M. Costa Gomes, *Chem. Rev.*, 2016, **116**, 6075–6106.

35 I. Bahadur, T. M. Letcher, S. Singh, G. G. Redhi, P. Venkatesu and D. Ramjugernath, *J. Chem. Thermodyn.*, 2015, **82**, 34–46.

36 Q. Cao, X. X. Lu, X. Wu, Y. S. Guo, L. Xu and W. J. Fang, *J. Chem. Eng. Data*, 2015, **60**, 455–463.

37 C. G. Hanke and R. M. Lynden-Bell, *J. Phys. Chem. B*, 2003, **107**, 10873–10878.

38 C. G. Hanke, N. A. Atamas and R. M. Lynden-Bell, *Green Chem.*, 2002, **4**, 107–111.

39 A. S. Amarasekara, *Chem. Rev.*, 2016, **116**, 6133–6183.

40 C. Dai, J. Zhang, C. Huang and Z. Lei, *Chem. Rev.*, 2017, **117**, 6929–6983.

41 K. Dong, X. Liu, H. Dong, X. Zhang and S. Zhang, *Chem. Rev.*, 2017, **117**, 6636–6695.

42 K. S. Egorova, E. G. Gordeev and V. P. Ananikov, *Chem. Rev.*, 2017, **117**, 7132–7189.

43 T. L. Greaves and C. J. Drummond, *Chem. Rev.*, 2008, **108**, 206–237.

44 J. P. Hallett and T. Welton, *Chem. Rev.*, 2011, **111**, 3508–3576.

45 P. Hapiot and C. Lagrost, *Chem. Rev.*, 2008, **108**, 2238–2264.

46 Z. Lei, C. Dai and B. Chen, *Chem. Rev.*, 2014, **114**, 1289–1326.

47 V. H. Paschoal, L. F. O. Faria and M. C. C. Ribeiro, *Chem. Rev.*, 2017, **117**, 7053–7112.

48 A. Podgoršek, J. Jacquemin, A. A. H. Pádua and M. F. Costa Gomes, *Chem. Rev.*, 2016, **116**, 6075–6106.

49 B. Wang, L. Qin, T. Mu, Z. Xue and G. Gao, *Chem. Rev.*, 2017, **117**, 7113–7131.

50 S. Zeng, X. Zhang, L. Bai, X. Zhang, H. Wang, J. Wang, D. Bao, M. Li, X. Liu and S. Zhang, *Chem. Rev.*, 2017, **117**, 9625–9673.

51 Q. Zhang and J. N. M. Shreeve, *Chem. Rev.*, 2014, **114**, 10527–10574.

52 S. Zhang, J. Zhang, Y. Zhang and Y. Deng, *Chem. Rev.*, 2017, **117**, 6755–6833.

53 D. Carriazo, M. Concepcion Serrano, M. Concepcion Gutierrez, M. Luisa Ferrer and F. del Monte, *Chem. Soc. Rev.*, 2012, **41**, 4996–5014.

54 Q. Zhang, K. D. O. Vigier, S. Royer and F. Jerome, *Chem. Soc. Rev.*, 2012, **41**, 7108–7146.

This journal is © The Royal Society of Chemistry 2018

Chem. Soc. Rev., 2018, **47**, 8685–8720 | 8715

55 Y. Dai, J. van Spronsen, G.-J. Witkamp, R. Verpoorte and Y. H. Choi, *J. Nat. Prod.*, 2013, **76**, 2162–2173.

56 E. Durand, J. Lecomte and P. Villeneuve, *Eur. J. Lipid Sci. Technol.*, 2013, **115**, 379–385.

57 B. Tang and K. H. Row, *Monatsh. Chem.*, 2013, **144**, 1427–1454.

58 A. Paiva, R. Craveiro, I. Aroso, M. Martins, R. L. Reis and A. R. C. Duarte, *ACS Sustainable Chem. Eng.*, 2014, **2**, 1063–1071.

59 D. V. Wagle, H. Zhao and G. A. Baker, *Acc. Chem. Res.*, 2014, **47**, 2299–2308.

60 D. A. Alonso, A. Baeza, R. Chinchilla, G. Guillena, I. M. Pastor and D. J. Ramon, *Eur. J. Org. Chem.*, 2016, 612–632.

61 S. Sarmad, Y. Xie, J.-P. Mikkola and X. Ji, *New J. Chem.*, 2017, **41**, 290–301.

62 M. Tariq, M. G. Freire, B. Saramago, J. A. P. Coutinho, J. N. C. Lopes and L. P. N. Rebelo, *Chem. Soc. Rev.*, 2012, **41**, 829–868.

63 M. Tariq, F. Moscoso, F. J. Deive, A. Rodriguez, M. A. Sanromán, J. M. S. S. Esperança, J. N. Canongia Lopes and L. P. N. Rebelo, *J. Chem. Thermodyn.*, 2013, **59**, 43–48.

64 T. Singh and A. Kumar, *J. Chem. Thermodyn.*, 2011, **43**, 958–965.

65 J. Jacquemin, P. Husson, A. A. H. Padua and V. Majer, *Green Chem.*, 2006, **8**, 172–180.

66 J. Skowronek, M. Geppert-Rybczyńska, J. Jacquemin, P. Goodrich, J. A. Vicente, M. Chorążewski, S. Jeżak, M. Zorębski, E. Zorębski, M. Żarska, W. Kaca, P. Berdyczko and M. Dzida, *J. Solution Chem.*, 2015, **44**, 824–837.

67 K. Oster, P. Goodrich, J. Jacquemin, C. Hardacre, A. P. C. Ribeiro and A. Elsinawi, *J. Chem. Thermodyn.*, 2018, **121**, 97–111.

68 M. Anouti, M. Caillon-Caravanier, Y. Dridi, J. Jacquemin, C. Hardacre and D. Lemordant, *J. Chem. Thermodyn.*, 2009, **41**, 799–808.

69 S. Porcedda, B. Marongiu, M. Schirru, D. Falconieri and A. Piras, *J. Therm. Anal. Calorim.*, 2011, **103**, 29–33.

70 U. Dománska and M. Królikowska, *J. Solution Chem.*, 2012, **41**, 1422–1445.

71 Y. Xie, H. Dong, S. Zhang, X. Lu and X. Ji, *J. Chem. Eng. Data*, 2014, **59**, 3344–3352.

72 J. G. Li, Y. F. Hu, S. F. Sun, Y. S. Liu and Z. C. Liu, *J. Chem. Thermodyn.*, 2010, **42**, 904–908.

73 F. S. Mjalli and O. Ahmad, *Thermochim. Acta*, 2017, **647**, 8–14.

74 R. Zarrougui, M. Dhahbi and D. Lemordant, *J. Solution Chem.*, 2015, **44**, 686–702.

75 R. B. Leron and M.-H. Li, *J. Chem. Thermodyn.*, 2012, **54**, 293–301.

76 R. B. Leron and M.-H. Li, *Thermochim. Acta*, 2012, **546**, 54–60.

77 R. B. Leron, D. S. H. Wong and M.-H. Li, *Fluid Phase Equilib.*, 2012, **335**, 32–38.

78 A. Yadav and S. Pandey, *J. Chem. Eng. Data*, 2014, **59**, 2221–2229.

79 D. Shah and F. S. Mjalli, *Phys. Chem. Chem. Phys.*, 2014, **16**, 23900–23907.

80 H. Shekaari, M. T. Zafarani-Moattar and B. Mohammadi, *J. Mol. Liq.*, 2017, **243**, 451–461.

81 A. Yadav, J. R. Kar, M. Verma, S. Naqvi and S. Pandey, *Thermochim. Acta*, 2015, **600**, 95–101.

82 R. B. Leron, A. N. Soriano and M.-H. Li, *J. Taiwan Inst. Chem. Eng.*, 2012, **43**, 551–557.

83 Y. P. Hsieh, R. B. Leron, A. N. Soriano, A. R. Caparanga and M. H. Li, *J. Chem. Eng. Jpn.*, 2012, **45**, 939–947.

84 C. M. Lin, R. B. Leron, A. R. Caparanga and M. H. Li, *J. Chem. Thermodyn.*, 2014, **68**, 216–220.

85 A. Yadav, S. Trivedi, R. Rai and S. Pandey, *Fluid Phase Equilib.*, 2014, **367**, 135–142.

86 K.-S. Kim and B. H. Park, *J. Mol. Liq.*, 2018, **254**, 272–279.

87 M. Francisco, A. van den Bruinhorst, L. F. Zubeir, C. J. Peters and M. C. Kroon, *Fluid Phase Equilib.*, 2013, **340**, 77–84.

88 V. S. Protsenko, L. S. Bobrova and F. I. Danilov, *Ionics*, 2017, **23**, 637–643.

89 L. S. Bobrova, F. I. Danilov and V. S. Protsenko, *J. Mol. Liq.*, 2016, **223**, 48–53.

90 K. R. Siongco, R. B. Leron and M. H. Li, *J. Chem. Thermodyn.*, 2013, **65**, 65–72.

91 H. Ghaedi, M. Ayoub, S. Sufian, A. M. Shariff, G. Murshid, S. M. Hailegiorgis and S. N. Khan, *J. Mol. Liq.*, 2017, **248**, 378–390.

92 S. Dožić, N. Zec, A. Tot, S. Papović, K. Pavlović, S. Gadžurić and M. Vraneš, *J. Chem. Thermodyn.*, 2016, **93**, 52–59.

93 Z. He, Z. Zhao, X. Zhang and H. Feng, *Fluid Phase Equilib.*, 2010, **298**, 83–91.

94 E. Gómez, B. González, N. Calvar and Á. Domínguez, *J. Chem. Thermodyn.*, 2008, **40**, 1208–1216.

95 E. Rilo, L. M. Varea and O. Cabeza, *J. Chem. Eng. Data*, 2012, **57**, 2136–2142.

96 H. Rodríguez and J. F. Brennecke, *J. Chem. Eng. Data*, 2006, **51**, 2145–2155.

97 E. Vataščin and V. Dohnal, *J. Chem. Thermodyn.*, 2015, **89**, 169–176.

98 E. Quijada-Maldonado, S. van der Boogaart, J. H. Lijbers, G. W. Meindersma and A. B. de Haan, *J. Chem. Thermodyn.*, 2012, **51**, 51–58.

99 C. Romich, N. C. Merkel, A. Valbonesi, K. Schaber, S. Sauer and T. J. S. Schubert, *J. Chem. Eng. Data*, 2012, **57**, 2258–2264.

100 J.-y. Wang, H.-c. Jiang, Y.-m. Liu and Y.-q. Hu, *J. Chem. Thermodyn.*, 2011, **43**, 800–804.

101 C. Herrera, L. T. Costa, M. Atilhan and S. Aparicio, *J. Mol. Liq.*, 2017, **236**, 81–92.

102 Y. H. Gong, C. Shen, Y. Z. Lu, H. Meng and C. X. Li, *J. Chem. Eng. Data*, 2012, **57**, 33–39.

103 L. de Pablo, J. J. Segovia Puras, C. Martín and M. D. Bermejo, *J. Chem. Eng. Data*, 2018, **63**, 1053–1064.

104 H. C. Jiang, Y. Zhao, J. Y. Wang, F. Y. Zhao, R. J. Liu and Y. Q. Hu, *J. Chem. Thermodyn.*, 2013, **64**, 1–13.

8716 | *Chem. Soc. Rev.*, 2018, **47**, 8685–8720

This journal is © The Royal Society of Chemistry 2018

105 L. X. Chen, J. Y. Chen, Z. H. Song, G. K. Cui, Y. J. Xu, X. H. Wang and J. Liu, *J. Chem. Thermodyn.*, 2015, **91**, 292–300.

106 F. Ye, J. Zhu, K. Yu, R. Zhu, Y. Xu, J. Chen and L. Chen, *J. Chem. Thermodyn.*, 2016, **97**, 39–47.

107 D. Wu, B. Wu, Y. M. Zhang and H. P. Wang, *J. Chem. Eng. Data*, 2010, **55**, 621–624.

108 M. Krolikowska, P. Lipinski and D. Maik, *Thermochim. Acta*, 2014, **582**, 1–9.

109 A. Vasanthakumar, I. Bahadur, G. G. Redhi, R. M. Gengan and K. Anand, *J. Mol. Liq.*, 2016, **219**, 685–693.

110 V. Arumugam, G. G. Redhi and R. M. Gengan, *J. Mol. Liq.*, 2017, **242**, 1215–1227.

111 A. Vasanthakumar, I. Bahadur, G. Redhi and R. M. Gengan, *RSC Adv.*, 2016, **6**, 61566–61575.

112 M. Królikowska, M. Zawadzki, U. Domańska, D. Ramjugernath and P. Naidoo, *J. Chem. Thermodyn.*, 2017, **109**, 71–81.

113 L. F. Zhang, X. X. Lu, D. F. Ye, Y. S. Guo and W. J. Fang, *J. Chem. Eng. Data*, 2016, **61**, 1023–1031.

114 A. P. Singh, R. L. Gardas and S. Senapati, *Phys. Chem. Chem. Phys.*, 2015, **17**, 25037–25048.

115 S. Tian, S. Ren, Y. Hou, W. Wu and W. Peng, *J. Chem. Eng. Data*, 2013, **58**, 1885–1892.

116 M. Krolikowska and M. Zawadzki, *J. Mol. Liq.*, 2018, **251**, 358–368.

117 D. J. S. Patinha, L. C. Tome, H. Garcia, R. Ferreira, C. S. Pereira, L. P. N. Rebelo and I. M. Marrucho, *J. Chem. Thermodyn.*, 2015, **84**, 93–100.

118 H. Zhang, C.-T. Lu, J.-G. Lu, L. Gao, G.-P. Hai, Y.-Q. Tang, L.-X. Chen, A.-C. Hua and L.-J. Wang, *J. Solution Chem.*, 2014, **43**, 2117–2132.

119 N. C. Merkel, C. Römich, R. Bernewitz, H. Künemund, M. Gleiß, S. Sauer, T. J. S. Schubert, G. Guthausen and K. Schaber, *J. Chem. Eng. Data*, 2014, **59**, 560–570.

120 P. K. Chhotaray, S. Jella and R. L. Gardas, *J. Mol. Liq.*, 2016, **219**, 829–844.

121 R. R. Pinto, D. Santos, S. Mattedi and M. Aznar, *Braz. J. Chem. Eng.*, 2015, **32**, 671–682.

122 Y. Li, E. J. P. Figueiredo, M. Santos, J. B. Santos, N. M. C. Talavera-Prieto, P. J. Carvalho, A. G. M. Ferreira and S. Mattedi, *J. Chem. Thermodyn.*, 2015, **88**, 44–60.

123 M. M. Taib and T. Murugesan, *J. Chem. Eng. Data*, 2010, **55**, 5910–5913.

124 D. Cai, J. Yang, H. Da, L. Li, H. Wang and T. Qiu, *J. Mol. Liq.*, 2017, **229**, 389–395.

125 Z. X. Wang, L. Fu, H. Xu, Y. Shang, L. Zhang and J. M. Zhang, *J. Chem. Eng. Data*, 2012, **57**, 1057–1063.

126 M. Krolikowska and M. Zawadzki, *J. Mol. Liq.*, 2018, **249**, 153–159.

127 L. Labík, T. Moucha, R. Petříček, J. F. Rejl, L. Valenz and J. Haidl, *Chem. Eng. Sci.*, 2017, **170**, 451–463.

128 J. C. F. Diogo, F. J. P. Caetano, J. M. N. A. Fareleira and W. A. Wakeham, *Int. J. Thermophys.*, 2014, **35**, 1615–1635.

129 M. Królikowska, M. Zawadzki and M. Królikowski, *J. Chem. Thermodyn.*, 2014, **70**, 127–137.

130 B. Yoo, W. Afzal and J. M. Prausnitz, *Z. Phys. Chem.*, 2013, **227**, 157–165.

131 M. Krannich, F. Heym and A. Jess, *J. Chem. Eng. Data*, 2016, **61**, 1162–1176.

132 M. A. R. Martins, C. Neves, K. A. Kurnia, P. J. Carvalho, M. A. A. Rocha, L. Santos, S. P. Pinho and M. G. Freire, *Fluid Phase Equilib.*, 2016, **407**, 188–196.

133 J. S. Torrecilla, T. Rafione, J. Garcia and F. Rodriguez, *J. Chem. Eng. Data*, 2008, **53**, 923–928.

134 E. Gómez, B. González, N. Calvar, E. Tojo and Á. Domínguez, *J. Chem. Eng. Data*, 2006, **51**, 2096–2102.

135 A. Bhattacharjee, C. Varanda, M. G. Freire, S. Matted, L. M. N. B. F. Santos, I. M. Marrucho and J. A. P. Coutinho, *J. Chem. Eng. Data*, 2012, **57**, 3473–3482.

136 S. Fendt, S. Padmanabhan, H. W. Blanch and J. M. Prausnitz, *J. Chem. Eng. Data*, 2011, **56**, 31–34.

137 E. Vataščin and V. Dohnal, *J. Chem. Thermodyn.*, 2017, **106**, 262–275.

138 T. Chen, M. Chidambaram, Z. P. Liu, B. Smit and A. T. Bell, *J. Phys. Chem. B*, 2010, **114**, 5790–5794.

139 S. Pandey, K. A. Fletcher, S. N. Baker and G. A. Baker, *Analyst*, 2004, **129**, 569–573.

140 M. S. Kelkar and E. J. Maginn, *J. Phys. Chem. B*, 2007, **111**, 4867–4876.

141 A. Gutiérrez, M. Atilhan, R. Alcalde, J. L. Trenzado and S. Aparicio, *J. Mol. Liq.*, 2018, **255**, 199–207.

142 M. M. Hoffmann, E. D. Sylvester and J. W. Russo, *J. Mol. Liq.*, 2014, **199**, 175–183.

143 P. J. Carvalho, T. Regueira, L. Santos, J. Fernandez and J. A. P. Coutinho, *J. Chem. Eng. Data*, 2010, **55**, 645–652.

144 Q. Zhou, L.-S. Wang and H.-P. Chen, *J. Chem. Eng. Data*, 2006, **51**, 905–908.

145 I. B. Malham and M. Turmine, *J. Chem. Thermodyn.*, 2008, **40**, 718–723.

146 J. S. Gao and N. J. Wagner, *J. Mol. Liq.*, 2016, **223**, 678–686.

147 S. D. Nickerson, E. M. Nofen, H. B. Chen, M. Ngan, B. Shindel, H. Y. Yu and L. L. Dai, *J. Phys. Chem. B*, 2015, **119**, 8764–8772.

148 H. T. Xu, D. C. Zhao, P. Xu, F. Q. Liu and G. Gao, *J. Chem. Eng. Data*, 2005, **50**, 133–135.

149 E. Gómez, B. González, Á. Domínguez, E. Tojo and J. Tojo, *J. Chem. Eng. Data*, 2006, **51**, 696–701.

150 V. Antón, H. Artigas, J. Muñoz-Embid, M. Artal and C. Lafuente, *J. Chem. Thermodyn.*, 2016, **99**, 116–123.

151 B. Mokhtarani, A. Sharifi, H. R. Mortaheb, M. Mirzaei, M. Mafi and F. Sadeghian, *J. Chem. Thermodyn.*, 2009, **41**, 323–329.

152 D. Constantinescu, K. Schaber, F. Agel, M. H. Klingele and T. J. Schubert, *J. Chem. Eng. Data*, 2007, **52**, 1280–1285.

153 A. Arce, A. Soto, J. Ortega and G. Sabater, *J. Chem. Eng. Data*, 2008, **53**, 770–775.

154 Y. Xu, *J. Chem. Thermodyn.*, 2013, **64**, 126–133.

155 M. Anouti, A. Vigeant, J. Jacquemin, C. Brigouleix and D. Lemordant, *J. Chem. Thermodyn.*, 2010, **42**, 834–845.

156 M. Zawadzki, M. Królikowska and P. Lipiński, *Thermochim. Acta*, 2014, **589**, 148–157.

157 J. A. Widegren, E. M. Saurer, K. N. Marsh and J. W. Magee, *J. Chem. Thermodyn.*, 2005, **37**, 569–575.

This journal is © The Royal Society of Chemistry 2018

Chem. Soc. Rev., 2018, **47**, 8685–8720 | 8717

158 H. Wang, J. Wang, S. Zhang, Y. Pei and K. Zhuo, *ChemPhysChem*, 2009, **10**, 2516–2523.

159 H. Shekaari, Y. Mansoori and R. Sadeghi, *J. Chem. Thermodyn.*, 2008, **40**, 852–859.

160 J. M. Zhang, W. Z. Wu, T. Jiang, H. X. Gao, Z. M. Liu, J. He and B. X. Han, *J. Chem. Eng. Data*, 2003, **48**, 1315–1317.

161 C. E. Woodward and K. R. Harris, *Phys. Chem. Chem. Phys.*, 2010, **12**, 1172–1176.

162 W. Liu, L. Cheng, Y. Zhang, H. Wang and M. Yu, *J. Mol. Liq.*, 2008, **140**, 68–72.

163 G. R. Chaudhary, S. Bansal, S. K. Mehta and A. S. Ahluwalia, *J. Solution Chem.*, 2014, **43**, 340–359.

164 J. M. Andanson, M. Traikia and P. Husson, *J. Chem. Thermodyn.*, 2014, **77**, 214–221.

165 M. Sha, H. Dong, F. Luo, Z. Tang, G. Zhu and G. Wu, *J. Phys. Chem. Lett.*, 2015, **6**, 3713–3720.

166 Q. W. Yang, K. Yu, H. B. Xing, B. G. Su, Z. B. Bao, Y. W. Yang and Q. L. Ren, *J. Ind. Eng. Chem.*, 2013, **19**, 1708–1714.

167 J. Vila, P. Gines, E. Rilo, O. Cabeza and L. M. Varela, *Fluid Phase Equilib.*, 2006, **247**, 32–39.

168 E. Rilo, J. Vila, S. Garcia-Garabal, L. M. Varela and O. Cabeza, *J. Phys. Chem. B*, 2013, **117**, 1411–1418.

169 N. Yaghini, L. Nordstierna and A. Martinelli, *Phys. Chem. Chem. Phys.*, 2014, **16**, 9266–9275.

170 N. J. English, D. A. Mooney and S. W. O'Brien, *J. Mol. Liq.*, 2010, **157**, 163–167.

171 E. H. Duan, Y. N. Guan, B. Guo, M. M. Zhang, D. Yang and K. Yang, *J. Mol. Liq.*, 2013, **178**, 1–4.

172 P. B. Sanchez, J. Garcia, J. Salgado and E. Gonzalez-Romero, *ACS Sustainable Chem. Eng.*, 2016, **4**, 5068–5077.

173 K. R. Siongco, R. B. Leron, A. R. Caparanga and M.-H. Li, *Thermochim. Acta*, 2013, **566**, 50–56.

174 B. Wu, Y. M. Zhang and H. P. Wang, *J. Chem. Eng. Data*, 2009, **54**, 1430–1434.

175 C. L. Wong, A. N. Soriano and M. H. Li, *J. Taiwan Inst. Chem. Eng.*, 2009, **40**, 77–83.

176 M. Bester-Rogac, A. Stoppa, J. Hunger, G. Hefter and R. Buchner, *Phys. Chem. Chem. Phys.*, 2011, **13**, 17588–17598.

177 Y. J. Chen, X. P. Xuan, H. H. Zhang and K. L. Zhuo, *Fluid Phase Equilib.*, 2012, **316**, 164–171.

178 Y. J. Chen, M. Y. Fang, G. Y. Bai, K. L. Zhuo and C. L. Yan, *J. Chem. Eng. Data*, 2016, **61**, 3779–3787.

179 K. L. Zhuo, Y. J. Chen, J. Chen, G. Y. Bai and J. J. Wang, *Phys. Chem. Chem. Phys.*, 2011, **13**, 14542–14549.

180 M. Bester-Rogac, J. Hunger, A. Stoppa and R. Buchner, *J. Chem. Eng. Data*, 2011, **56**, 1261–1267.

181 R. Sadeghi and N. Ebrahimi, *J. Phys. Chem. B*, 2011, **115**, 13227–13240.

182 C. Neves, A. R. Rodrigues, K. A. Kurnia, J. Esperanca, M. G. Freire and J. A. P. Coutinho, *Fluid Phase Equilib.*, 2013, **358**, 50–55.

183 C. Ma, Y. Guo, D. Li, J. Zong, X. Ji and C. Liu, *J. Chem. Thermodyn.*, 2017, **105**, 30–36.

184 C. Ma, Y. Guo, D. Li, J. Zong, X. Ji, C. Liu and X. Lu, *J. Chem. Eng. Data*, 2016, **61**, 4172–4177.

185 L. E. Ficke, R. R. Novak and J. F. Brennecke, *J. Chem. Eng. Data*, 2010, **55**, 4946–4950.

186 L. E. Ficke and J. F. Brennecke, *J. Phys. Chem. B*, 2010, **114**, 10496–10501.

187 G. García-Miaja, J. Troncoso and L. Romaní, *J. Chem. Thermodyn.*, 2009, **41**, 161–166.

188 L. E. Ficke, H. c. Rodríguez and J. F. Brennecke, *J. Chem. Eng. Data*, 2008, **53**, 2112–2119.

189 M. Leskiv, C. E. S. Bernardes, M. E. Minas da Piedade and J. N. Canongia Lopes, *J. Phys. Chem. B*, 2010, **114**, 13179–13188.

190 V. K. Sharma, S. Bhagour, S. Solanki, Sheetal and S. K. Jangra, *J. Chem. Thermodyn.*, 2014, **68**, 235–243.

191 T. Hector and J. Gmehling, *Fluid Phase Equilib.*, 2014, **371**, 82–92.

192 J. Ren, Z. Zhao and X. Zhang, *J. Chem. Thermodyn.*, 2011, **43**, 576–583.

193 X. Zhang, D. Hu and Z. Zhao, *J. Chem. Eng. Data*, 2014, **59**, 205–211.

194 L. P. N. Rebelo, V. Najdanovic-Visak, Z. P. Visak, M. Nunes da Ponte, J. Szydlowski, C. A. Cerdeirina, J. Troncoso, L. Romani, J. M. S. S. Esperanca, H. J. R. Guedes and H. C. de Sousa, *Green Chem.*, 2004, **6**, 369–381.

195 M. Teodorescu and V. T. Popa, *Rev. Roum. Chim.*, 2016, **61**, 525–530.

196 W. Hermann, *Angew. Chem., Int. Ed.*, 2008, **47**, 654–670.

197 J. Ortega, R. Vreekamp, E. Marrero and E. Penco, *J. Chem. Eng. Data*, 2007, **52**, 2269–2276.

198 J. Ortega, R. Vreekamp, E. Penco and E. Marrero, *J. Chem. Thermodyn.*, 2008, **40**, 1087–1094.

199 R. Vreekamp, D. Castellano, J. Palomar, J. Ortega, F. Espiau, L. Fernández and E. Penco, *J. Phys. Chem. B*, 2011, **115**, 8763–8774.

200 A. Navas, J. Ortega, R. Vreekamp, E. Marrero and J. Palomar, *Ind. Eng. Chem. Res.*, 2009, **48**, 2678–2690.

201 M. Królikowska, K. Paduszyński, M. Królikowski, P. Lipiński and J. Antonowicz, *Ind. Eng. Chem. Res.*, 2014, **53**, 258–262.

202 M. Królikowska, K. Paduszyński, T. Hofman and J. Antonowicz, *J. Chem. Thermodyn.*, 2012, **55**, 144–150.

203 M. Królikowska, K. Paduszyński and M. Zawadzki, *J. Chem. Eng. Data*, 2013, **58**, 285–293.

204 O. Cabeza, in *Ionic Liquids in Separation Technology*, ed. F. J. H. Fernández, Elsevier, Amsterdam, 2014, pp. 1–93.

205 J.-Y. Wang, X.-J. Zhang, Y.-M. Liu and Y.-Q. Hu, *J. Chem. Eng. Data*, 2011, **56**, 3734–3737.

206 C. Spickermann, J. Thar, S. B. C. Lehmann, S. Zahn, J. Hunger, R. Buchner, P. A. Hunt, T. Welton and B. Kirchner, *J. Chem. Phys.*, 2008, **129**, 104505.

207 R. C. Remsing, Z. W. Liu, I. Sergeyev and G. Moyna, *J. Phys. Chem. B*, 2008, **112**, 7363–7369.

208 P. D'Angelo, A. Serva, G. Aquilanti, S. Pascarelli and V. Migliorati, *J. Phys. Chem. B*, 2015, **119**, 14515–14526.

209 C. E. S. Bernardes, M. E. M. da Piedade and J. N. C. Lopes, *J. Phys. Chem. B*, 2011, **115**, 2067–2074.

210 X. J. Zhong, Z. Fan, Z. P. Liu and D. P. Cao, *J. Phys. Chem. B*, 2012, **116**, 3249–3263.

8718 | *Chem. Soc. Rev.*, 2018, **47**, 8685–8720

This journal is © The Royal Society of Chemistry 2018

211 S. V. J. Yuvaraj, R. K. Zhdanov, R. V. Belosludov, V. R. Belosludov, O. S. Subbotin, K. Kanie, K. Funaki, A. Muramatsu, T. Nakamura and Y. Kawazoe, *J. Phys. Chem. B*, 2015, **119**, 12894–12904.

212 T. M. Chang, L. X. Dang, R. Devanathan and M. Dupuis, *J. Phys. Chem. A*, 2010, **114**, 12764–12774.

213 T. Zhekenov, N. Toksanbayev, Z. Kazakbayeva, D. Shah and F. S. Mjalli, *Fluid Phase Equilib.*, 2017, **441**, 43–48.

214 E. O. Fetisov, D. B. Harwood, I. F. W. Kuo, S. E. E. Warrag, M. C. Kroon, C. J. Peters and J. I. Siepmann, *J. Phys. Chem. B*, 2018, **122**, 1245–1254.

215 Q. Gao, Y. Zhu, X. Ji, W. Zhu, L. Lu and X. Lu, *Fluid Phase Equilib.*, 2018, **470**, 134–139.

216 R. Ahmadi, B. Hemmateenejad, A. Safavi, Z. Shojaeifard, A. Shahsavar, A. Mohajeri, M. Heydari Dokoohaki and A. R. Zolghadr, *Phys. Chem. Chem. Phys.*, 2018, **20**, 18463–18473.

217 W. Jiang, Y. T. Wang and G. A. Voth, *J. Phys. Chem. B*, 2007, **111**, 4812–4818.

218 S. Feng and G. A. Voth, *Fluid Phase Equilib.*, 2010, **294**, 148–156.

219 A. A. Niazi, B. D. Rabideau and A. E. Ismail, *J. Phys. Chem. B*, 2013, **117**, 1378–1388.

220 Y. L. Wang, M. R. Shimpi, S. Sarman, O. N. Antzutkin, S. Glavatskih, L. Kloo and A. Laaksonen, *J. Phys. Chem. B*, 2016, **120**, 7446–7455.

221 Y.-L. Wang, S. Sarman, S. Glavatskih, O. N. Antzutkin, M. W. Rutland and A. Laaksonen, *J. Phys. Chem. B*, 2015, **119**, 5251–5264.

222 X. Wu, Z. Liu, S. Huang and W. Wang, *Phys. Chem. Chem. Phys.*, 2005, **7**, 2771–2779.

223 M. S. Kelkar, W. Shi and E. J. Maginn, *Ind. Eng. Chem. Res.*, 2008, **47**, 9115–9126.

224 S. L. Perkins, P. Painter and C. M. Colina, *J. Phys. Chem. B*, 2013, **117**, 10250–10260.

225 T. G. A. Youngs and C. Hardacre, *ChemPhysChem*, 2008, **9**, 1548–1558.

226 R. Ishizuka and N. Matubayasi, *J. Chem. Theory Comput.*, 2016, **12**, 804–811.

227 Y. Wang, H. Li and S. Han, *J. Phys. Chem. B*, 2006, **110**, 24646–24651.

228 M. L. S. Batista, K. A. Kurnia, S. P. Pinho, J. R. B. Gomes and J. A. P. Coutinho, *J. Phys. Chem. B*, 2015, **119**, 1567–1578.

229 I. Khan, M. Taha, S. P. Pinho and J. A. P. Coutinho, *Fluid Phase Equilib.*, 2016, **414**, 93–100.

230 I. Khan, K. A. Kurnia, T. E. Sintra, J. A. Saraiva, S. P. Pinho and J. A. P. Coutinho, *Fluid Phase Equilib.*, 2014, **361**, 16–22.

231 I. Khan, K. A. Kurnia, F. Mutelet, S. P. Pinho and J. A. P. Coutinho, *J. Phys. Chem. B*, 2014, **118**, 1848–1860.

232 I. Khan, M. Taha, P. Ribeiro-Claro, S. P. Pinho and J. A. P. Coutinho, *J. Phys. Chem. B*, 2014, **118**, 10503–10514.

233 X. Y. Zhu and H. Q. Ai, *J. Mol. Model.*, 2016, 22.

234 D. V. Wagle, C. A. Deakyne and G. A. Baker, *J. Phys. Chem. B*, 2016, **120**, 6739–6746.

235 L. Zhang, Z. Xu, Y. Wang and H. Li, *J. Phys. Chem. B*, 2008, **112**, 6411–6419.

236 A. Mele, C. D. Tran and S. H. De Paoli Lacerda, *Angew. Chem., Int. Ed.*, 2003, **115**, 4500–4502.

237 L. Almásy, M. Turmine and A. Perera, *J. Phys. Chem. B*, 2008, **112**, 2382–2387.

238 T. Toshiyuki, H. Yusuke, F. Kenta and K. Shigeharu, *Anal. Sci.*, 2008, **24**, 1285–1290.

239 H. Zhang, H. Liang, J. Wang and K. Li, *Z. Phys. Chem.*, 2007, **221**, 1061.

240 L. Cammarata, S. G. Kazarian, P. A. Salter and T. Welton, *Phys. Chem. Chem. Phys.*, 2001, **3**, 5192–5200.

241 P. A. Bergstroem, J. Lindgren and O. Kristiansson, *J. Phys. Chem.*, 1991, **95**, 8575–8580.

242 A.-L. Rollet, P. Porion, M. Vaultier, I. Billard, M. Deschamps, C. Bessada and L. Jouvensal, *J. Phys. Chem. B*, 2007, **111**, 11888–11891.

243 T. Köddermann, C. Wertz, A. Heintz and R. Ludwig, *Angew. Chem., Int. Ed.*, 2006, **45**, 3697–3702.

244 D. K. Singh, S. Cha, D. Nam, H. Cheong, S. W. Joo and D. Kim, *ChemPhysChem*, 2016, **17**, 3040–3046.

245 N.-N. Wang, Q.-G. Zhang, F.-G. Wu, Q.-Z. Li and Z.-W. Yu, *J. Phys. Chem. B*, 2010, **114**, 8689–8700.

246 D. J. S. Patinha, L. C. Tomé, H. Garcia, R. Ferreira, C. S. Pereira, L. P. N. Rebelo and I. M. Marrucho, *J. Chem. Thermodyn.*, 2015, **84**, 93–100.

247 S. Peter, F. Koichi and L. Ralf, *Angew. Chem., Int. Ed.*, 2013, **52**, 2990–2994.

248 U. Salma, N. V. Plechkova, R. Caminiti and L. Gontrani, *J. Phys. Chem. B*, 2017, **121**, 6399–6407.

249 A. Pandey and S. Pandey, *J. Phys. Chem. B*, 2014, **118**, 14652–14661.

250 O. S. Hammond, D. T. Bowron and K. J. Edler, *Green Chem.*, 2016, **18**, 2736–2744.

251 C. D'Agostino, L. F. Gladden, M. D. Mantle, A. P. Abbott, E. I. Ahmed, A. Y. M. Al-Murshedi and R. C. Harris, *Phys. Chem. Chem. Phys.*, 2015, **17**, 15297–15304.

252 O. S. Hammond, D. T. Bowron and K. J. Edler, *Angew. Chem., Int. Ed.*, 2017, **56**, 9782–9785.

253 D. Xiao, J. R. Rajian, A. Cady, S. Li, R. A. Bartsch and E. L. Quitevis, *J. Phys. Chem. B*, 2007, **111**, 4669–4677.

254 G. Raabe and J. Köhler, *J. Chem. Phys.*, 2008, **128**, 154509.

255 Y. Imai, H. Abe, T. Miyashita, T. Goto, H. Matsumoto and Y. Yoshimura, *Chem. Phys. Lett.*, 2010, **486**, 37–39.

256 Y. Imai, H. Abe, H. Matsumoto, O. Shimada, T. Hanasaki and Y. Yoshimura, *J. Chem. Thermodyn.*, 2011, **43**, 319–322.

257 Y. Yoshimura, H. Kimura, C. Okamoto, T. Miyashita, Y. Imai and H. Abe, *J. Chem. Thermodyn.*, 2011, **43**, 410–412.

258 P. Sippel, V. Dietrich, D. Reuter, M. Aumüller, P. Lunkenheimer, A. Loidl and S. Krohns, *J. Mol. Liq.*, 2016, **223**, 635–642.

259 N. Yaghini, M. N. Garaga and A. Martinelli, *Fuel Cells*, 2016, **16**, 46–54.

260 H. Katayanagi, K. Nishikawa, H. Shimozaki, K. Miki, P. Westh and Y. Koga, *J. Phys. Chem. B*, 2004, **108**, 19451–19457.

261 K. Miki, P. Westh, K. Nishikawa and Y. Koga, *J. Phys. Chem. B*, 2005, **109**, 9014–9019.

262 K. R. Seddon, A. Stark and M.-J. Torres, *Pure Appl. Chem.*, 2000, **72**, 2275–2287.

263 M. Abraham and M.-C. Abraham, *Electrochim. Acta*, 1986, **31**, 821–829.

264 R. L. Gardas, D. H. Dagade, J. A. P. Coutinho and K. J. Patil, *J. Phys. Chem. B*, 2008, **112**, 3380–3389.

265 S. Panda, V. Singh, N. Islam and R. L. Gardas, *Fluid Phase Equilib.*, 2017, **445**, 35–44.

266 M. Rumyantsev, S. Rumyantsev and I. Y. Kalagaev, *J. Phys. Chem. B*, 2018, **122**, 5951–5960.

267 J. E. S. J. Reid, R. J. Gammons, J. M. Slattery, A. J. Walker and S. Shimizu, *J. Phys. Chem. B*, 2017, **121**, 599–609.

268 M.-M. Huang, Y. Jiang, P. Sasisanker, G. W. Driver and H. Weingärtner, *J. Chem. Eng. Data*, 2011, **56**, 1494–1499.

269 N. V. Sastry, N. M. Vaghela and P. M. Macwan, *J. Mol. Liq.*, 2013, **180**, 12–18.

270 S. Zhang, X. Li, H. Chen, J. Wang, J. Zhang and M. Zhang, *J. Chem. Eng. Data*, 2004, **49**, 760–764.

271 E. Rilo, J. Vila, J. Pico, S. García-Garabal, L. Segade, L. M. Varela and O. Cabeza, *J. Chem. Eng. Data*, 2010, **55**, 639–644.

272 E. Rilo, J. Vila, M. García, L. M. Varela and O. Cabeza, *J. Chem. Eng. Data*, 2010, **55**, 5156–5163.

273 L. Q. Zhang, Z. Xu, Y. Wang and H. R. Li, *J. Phys. Chem. B*, 2008, **112**, 6411–6419.

274 J. Lehmann, M. H. Rausch, A. Leipertz and A. P. Fröba, *J. Chem. Eng. Data*, 2010, **55**, 4068–4074.

275 B. Lal, M. Sahin and E. Ayranci, *J. Chem. Thermodyn.*, 2012, **54**, 142–147.

276 U. Domańska and K. Paduszyński, *J. Phys. Chem. B*, 2008, **112**, 11054–11059.

277 S. Nebig and J. Gmehling, *Fluid Phase Equilib.*, 2011, **302**, 220–225.

278 K. Paduszyński and U. Domańska, *J. Phys. Chem. B*, 2012, **116**, 5002–5018.

279 G. Shen, C. Held, X. Lu and X. Ji, *Fluid Phase Equilib.*, 2015, **405**, 73–82.

280 X. Xu, C. Peng, H. Liu and Y. Hu, *Ind. Eng. Chem. Res.*, 2009, **48**, 11189–11201.

281 L. D. Simoni, L. E. Ficke, C. A. Lambert, M. A. Stadtherr and J. F. Brennecke, *Ind. Eng. Chem. Res.*, 2010, **49**, 3893–3901.

282 S. Mahato, A. Kumar and T. Banerjee, *J. Taiwan Inst. Chem. Eng.*, 2016, **59**, 69–78.

283 N. Papaiconomou, J.-P. Simonin and O. Bernard, *J. Chem. Thermodyn.*, 2015, **91**, 445–451.

284 X. Ji and C. Held, *Fluid Phase Equilib.*, 2016, **410**, 9–22.

285 G. Shen, C. Held, X. Lu and X. Ji, *Mol. Phys.*, 2016, **114**, 2492–2499.

286 R. Shahriari, M. R. Dehghani and B. Behzadi, *Ind. Eng. Chem. Res.*, 2012, **51**, 10274–10282.

287 J. Li, C. He, C. Peng, H. Liu, Y. Hu and P. Paricaud, *Ind. Eng. Chem. Res.*, 2011, **50**, 7027–7040.

288 C. Tsioptsias, I. Tsivintzelis and C. Panayiotou, *Phys. Chem. Chem. Phys.*, 2010, **12**, 4843–4851.

289 B.-S. Lee and S.-T. Lin, *Fluid Phase Equilib.*, 2013, **356**, 309–320.

8720 | *Chem. Soc. Rev.*, 2018, **47**, 8685–8720

This journal is © The Royal Society of Chemistry 2018